The Optimization of the Processing of Low Carbon Reinforcing Steel Bars

Composed by

Yuthika Nehro Murilal (302829)

Submitted to

School of Chemical and Metallurgical Engineering, Faculty of Engineering and the Built Environment, University of the Witwatersrand, Johannesburg, South Africa

In partial fulfillment of

MSc (Materials and Metallurgical Engineering), (50/50)

Supervisor: Prof C.S. Kucukkaragoz

October, 2015

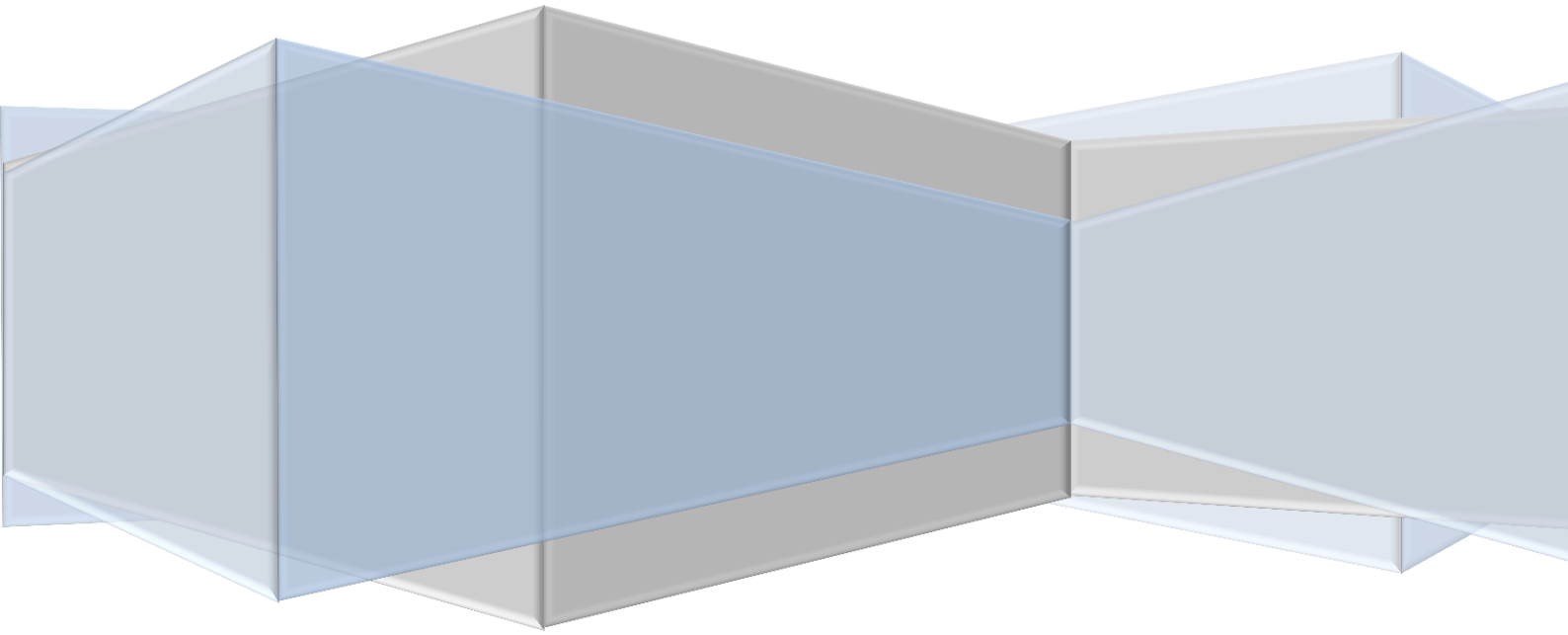

Table of Contents

DECLARATION

This thesis is a presentation of my original research work. Where sources have been used they have been referenced. This thesis is submitted in partial fulfillment for the 50/50 Master of Science in Engineering (Metallurgy and Materials Engineering) at the University of the Witwatersrand. This work has not been submitted before for any degree or examination at any other institution.

Y Murilal Date

ABSTRACT

Reinforcing bars produced at ArcelorMittal via the Electric Arc Furnace (EAF) process route and the Rod Mill are breaking during application. This is due to the high residual content of the material, which produces an excessively high tensile strength and reduces its ductility. This work aims to develop a cooling program at Rod Mill to process the high residual material and to optimize the chemistry at the EAF to compensate for the high residuals in order to achieve a maximum tensile strength of 600MPa, which has sufficient ductility for downstream processing.

Less severe cooling conditions were imposed at the Rod Mill on the high residual material and lower tensile strength and higher ductility were achieved. The C and Mn contents of the material were decreased at the EAF and lower tensile strength and increased ductility were achieved.

ACKNOWLEDGEMENTS

Prof C.S. Kucukkaragoz for supervision.

ArcelorMittal Newcastle Works & Vereeniging Works for the use of facilities and resources required for this study.

Mr. E. Khumalo for guidance and technical assistance provided.

LIST OF FIGURES

LIST OF TABLES

NOMENCLATURE

Aluminium	Al
Basic Oxygen Furnace	BOF
Breaking elongation	%A
Carbon	C
Carbon Equivalent	CE
Chromium	Cr
Copper	Cu
Ductile to brittle transition temperature	DBTT
Electric Arc Furnace	EAF
Hydrogen Induced Cold Cracking	HICC
Isothermal Transformation	I-T
Manganese	Mn
Megapascals	MPa
Molybdenum	Mo
Newcastle	NC
Nickel	Ni
Niobium	Nb
Nitrogen	N
Phosphorous	P
Reinforcing bar	Rebar
Silicon	Si
Sulphur	S
Total uniform elongation	% Agt
Ultimate Tensile Strength	UTS
Vanadium	V
Vereeniging	VRN
Yield Strength	YS

1. INTRODUCTION

Reinforcing bar, commonly known as 'rebar', is used in worldwide structural applications especially in the construction sector. The construction sector has a direct impact on job creation, economic growth and sustainability. According to the South African National Budget of 2013, the government has budgeted R827 billion on Infrastructure projects encompassing power generation, transport, schools, hospitals and clinics.

Although a large demand for structural steel exists, the steel industry has taken a downturn during recent years. Due to the difficult financial conditions, manufacturers are competitive, striving to produce steel of a superior quality at a lower cost.

At ArcelorMittal Newcastle works, a significant portion of the steel dispatched are reinforcing bars. This product proves to be a major source of income. Customers are complaining of rebar-breaks during applications such as bending and forming. The rebar breaks during application are due to the excessively high yield strength, which results in a loss of ductility. Customer dissatisfaction in this economic downturn is of the ultimate detriment as customers can easily be lost to one of the competitors.

Reinforcing bars are a type of a High Strength Low Alloy Steel (HSLA), which has a low alloying element content, but has a high strength. This reinforcing bar complies with the international specification BS 4449: 1997 460B. According to this specification the minimum yield strength required is 460 MPa.

Traditionally this material is produced at ArcelorMittal Newcastle Works via the Basic Oxygen Furnace (BOF) process route. The material is rolled into an intermediate billet and it is then rolled into reinforcing bars at the Rod Mill. Due to economic and process considerations this material is sourced from ArcelorMittal Vereeniging (VRN) Works in the form of billets. These billets are then further processed at the Rod Mill.

At ArcelorMittal VRN Works, these blooms are manufactured at the steel plant via the Electric Arc Furnace (EAF) process route. Because of the high content of alloying elements in the scrap material charged into the EAF, the final billet product has a higher residual content (Cu, Ni, Cr) as compared to the Basic Oxygen Furnace process route. This results in the final rebar product having a high yield strength in the range of 600-900 MPa. Although attaining a high yield strength may seem advantageous, in this case it is detrimental because the material endures a loss in ductility which causes it to break during bending. This also proves to be problematic during the mechanical straightening of the material when producing rebar lengths from coil form. This situation cannot be tolerated as it will result in a loss of customers.

The high tensile strength of the material can be remedied by improving the chemical composition and or the cooling parameters at the rod mill. There are currently 1000 tons of billets from VRN in stock that need to be further processed. Since the material is already produced, the chemical composition cannot be altered. The processing of the stock at the rod mill is therefore the only process that can be adjusted. The cooling parameters at the rod mill can be further optimized to accommodate the high residual content of VRN material. Additional stock will be sourced from VRN in the future. The chemical composition of the future stock will be adjusted to result in a lower yield strength material.

In the field of High Strength Low Alloy (HSLA) steels, the knowledge base is well equipped with topics covering the alloy additions, cooling conditions and strengthening mechanisms. This study will contribute to this knowledge base and add a greater understanding to the effects of cooling and chemical parameters on the properties of structural steel. This will prove to be handy when handling feed material of varying composition. Instability in the supply of material is inevitable due to resources depleting over time.

Application of Rebar

Rebar is commonly used in bending applications. Since bending occurs at room temperature, the steel strain hardens during bending, due the bending force applied onto the work piece, resulting in deformation. Strain hardening results in a loss of ductility and this can lead to failure of the work piece. Figure 1-1 shows a reinforcing bar that has failed during application.

High yield strength is usually sought after in the construction industry but with increasing yield strength a loss of ductility will be incurred. A loss of ductility can be detrimental, depending on the application, for example, if rebar is used for bending applications, ductility will be critical but if rebar is used as fencing poles or for concrete reinforcement, ductility will not play a significant role.

According to the BS 4449: 1997 460B specification, the reinforcing bar is required to have a minimum yield strength of 460 MPa and the maximum yield strength is not specified. The rebar that is supplied by ArcelorMittal Newcastle Works is used for a variety of applications. When changes are made to the product, consideration for all applications should be taken in to account. A conservative safety factor of 30% was chosen in case of the event of overloading or excessive force application. This results in a maximum yield strength of 600 MPa.

2. PROBLEM STATEMENT

Reinforcing bars are manufactured at the steel plant via the Electric Arc Furnace Steel making route and are rolled into their final profile at the Rod Mill. The reinforcing bars produced at Newcastle works are failing during application due to the brittle nature of the material. This is a result of the high residual content of the material which originated from the high alloying element content of the scrap used as feed material to the electric arc.

The yield strength values of this material are exceedingly high causing a loss in ductility. The processing of this material at the Steel Plant and Rod Mill needs to be adjusted to produce a more ductile material that will not fail during application. This can be done by adjusting the chemical analysis of the reinforcing bar or improving the cooling process at the Rod Mill.

3. RESEARCH OBJECTIVES

- To adjust the cooling parameters of the rolling method to process existing stock of billets to obtain a maximum yield strength of 600 MPa*
- To revise the current chemical specification of the billets to produce a new chemical composition that will prompt a decrease in yield strength
- To adjust the cooling parameters of the rolling method to process the billets of optimized chemical composition to obtain a maximum yield strength of 600 MPa*

* A maximum value for yield strength is 600 MPa due to the 30 % safety factor (Discussed in Section 1).

4. HYPOTHESIS

1. Decreasing the C and Mn contents of the rebar will result in a yield strength below 600 MPa.
2. Decreasing the cooling rate of the rebar at Rod Mill will result in a yield strength below 600 MPa due to an increase in grain size and a decrease in % bainite in the microstructure.
3. The ductility of steel will increase with a decrease in yield strength.

5. LITERATURE REVIEW

5.1. HSLA Steels and Micro-alloying of Steels

In the field of High Strength Low Alloy (HSLA) steels the knowledge base is well equipped with topics covering the alloying additions, cooling conditions and strengthening mechanisms. A brief description of this information follows.

5.1.1. High Strength Low Alloy (HSLA) Structural Steels

HSLA steels are low carbon steels that are micro-alloyed with strong carbide forming elements such as V, Nb and Ti etc. as stated by Cabibbo et al (2008). Silvestre et al (2012) claims that the presence of the alloying elements plays a significant role in the strengthening mechanisms which results in the HSLA steel being 20-30% lighter in weight than a carbon steel with the same strength. Micro-alloy additions are advantageous as they also increase the weldability of steels by allowing a lower carbon content to be used which still produces a steel of high strength. According to Held and Lauer (1983), the relative effect of 0.01% addition of Mn, C and V on yield strength is 1-, 4-, 8-fold respectively. Micro-alloys also increase the strength of steel by the precipitation hardening mechanism (Silvestre et al, 2012). HSLA structural steels have a total micro-alloying content of 1%. The typical composition of HSLA structural steel is included in Table 5-1.

Table 5-1: Typical Composition of HSLA Structural Steel (Adapted from Buahombura P, 2009)

% C	% Mn	Total % Micro-alloying Content	Yield Strength (MPa)
0 - 0.25	1.6 max	1 max	250 - 700

The typical chemical analysis of steel that will be used in this work is presented in Table 5-2. The sum of the total micro-alloying content is 0.80%. It can be seen that this chemical composition fits within the HSLA Structural steel category.

Table 5-2: Typical Chemical Analysis of Steel obtained from VRN Works

C	Cr	Cu	Mn	Mo	Ni	S	P	Si	V
0.24	0.072	0.11	1.30	0.021	0.079	0.013	0.019	0.44	0.052

Microstructure of a HSLA Structural Steel during Hot Rolling

When steel is reheated to an austenizing temperature in the reheating furnace, it possesses a coarse grained austenitic structure. When steel passes through the rolls at a temperature below the recrystallization stop temperature, the coarse austenite grains are flattened into a pancake shape (Paules, 1991). These austenite grains recrystallize to form fine equiaxed grains as shown in Figure 5-1. If the rolling temperature at subsequent roll passes is above the recrystallization-stop temperature, which is the minimum temperature required for recrystallization, austenite grains will be further refined to even smaller grains producing a stronger, more ductile structure. (EVRAZ East Metals, 2013)

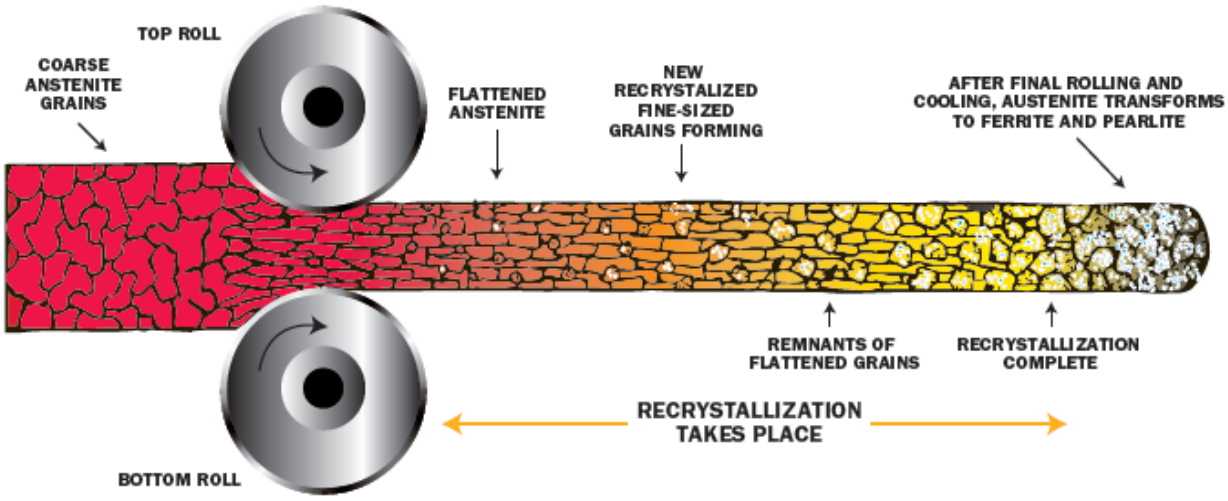

Figure 5-1: Recrystallization after Hot Rolling (EVRAZ East Metals, 2013)

5.1.2. Alloy Strengthening Mechanisms

Precipitation Strengthening

The precipitation strengthening mechanism usually takes place at elevated temperatures and this mechanism is based on the change in solubility of grain refining elements due to the exposure to high temperatures. These precipitates move to energy conserving sites which results in the impeding of dislocation movement.

When steel is subjected to high temperatures the grains tend to coarsen. When the steel is micro-alloyed with a grain refining alloying element e.g. Nb, it begins to precipitate along the grain boundaries during the high temperature exposure (Silvestre et al, 2012). This results in a `pinning effect`, where the edges of the grain boundary are pinned down and grain growth is retarded. This produces a finer grained microstructure which results in a steel of higher strength. As stated by Cline et al (1986), while precipitation strengthening may be advantageous it also leads to a loss in ductility and impact strength. The precipitation strengthening mechanism is depicted in Figure 5-2.

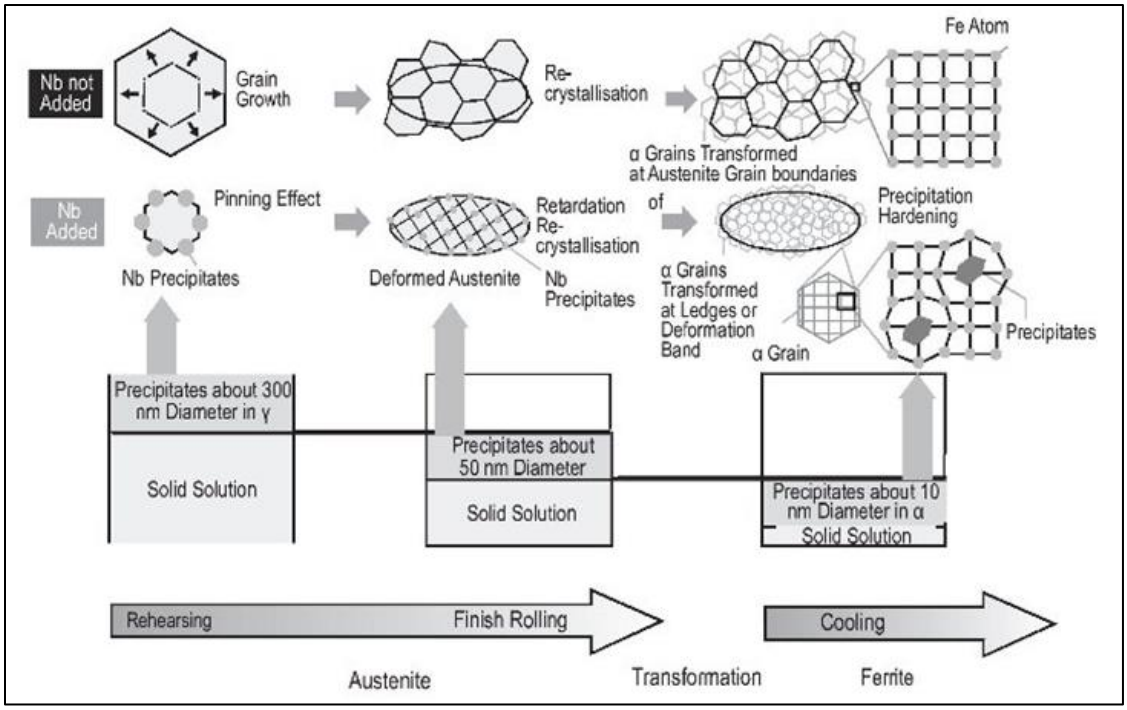

Figure 5-2: The Precipitation Strengthening Mechanism of Nb in Hot Rolled Steels (Yun-Chul Jung et al, 1998)

Strain Hardening

When stress is imposed onto a material, it deforms. The deformation is initially elastic, where the material returns to its original state after the stress is removed. The deformation transitions from elastic to plastic deformation once the stress exerted on the material exceeds the yield stress. Once the material begins to yield, it is strengthened by plastic deformation. This phenomenon is known as strain hardening, where there is an increase in dislocation movement causing an interaction between the dislocations. This interaction decreases the mobility of dislocations, thereby strengthening it. Strain hardening is also referred to as work hardening, cold working or cold reduction.

The degree of strain hardening is influenced by the alloying elements, carbon and nitrogen content of the material. Carbon, nitrogen or other alloying components tend to diffuse towards dislocations, causing an anchoring effect. The movement of dislocations in the metal is impeded, thereby strengthening the metal.

As stated by Reed-Hill, Nitrogen has a higher solubility and diffusion coefficient and produces less complete precipitation compared to other elements. Nitrogen therefore has a greater effect on the degree of strain hardening compared to other elements. In applications where strain hardening is detrimental, nitrogen scavengers such as vanadium, titanium, niobium etc. are added during steelmaking to consume the excess nitrogen and to produce precipitates which also strengthen the steel.

The effect of strain hardening or cold reduction, on the mechanical properties of steel is depicted in Figure 5-3. It can be seen that as the percentage of cold reduction increases, the yield strength and tensile strength increases but the elongation decreases. Elongation gives an indication of how ductile a particular steel is.

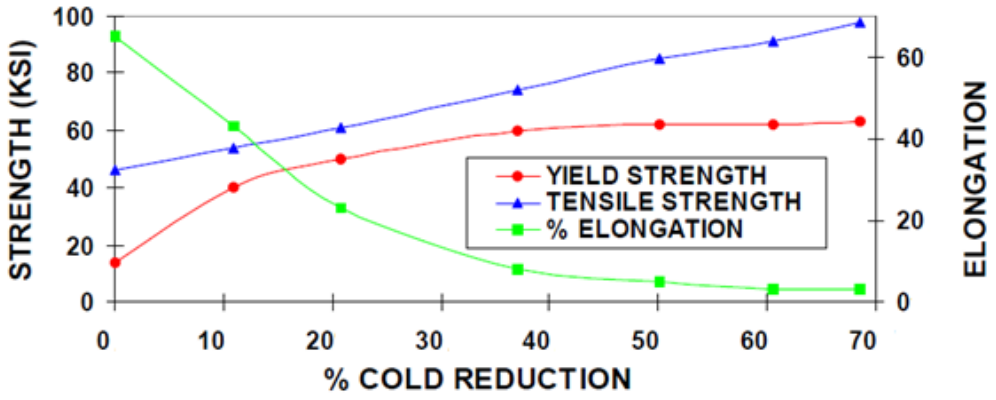

Figure 5-3: Effect of Cold Reduction on Mechanical Properties of Steel (*Strain Hardening & Strength*, 2010)

Solid-Solution Strengthening

When evaluating the hardness of metals, pure metals tend to be softer than their alloys. This is due to solid solution strengthening that occurs due to the presence of alloying elements, also termed the solute, in the matrix. When the alloying elements are in an interstitial or substitutional site in the matrix it causes the solid solution to increase in strength. The presence of the solute atoms causes a strain on the lattice which in turn anchors the dislocation. Figure 5-4 illustrates the strengthening mechanism of substitutional and interstitial atoms. Substitutional atoms replace the original atom that belongs to the matrix and an interstitial atom fits into the interstitial sites that exist between the atoms. Substitutional and interstitial atoms are not always the same size as the solvent atom or the interstitial site. If these atoms are larger in size, the strain induced onto the lattice will be greater.

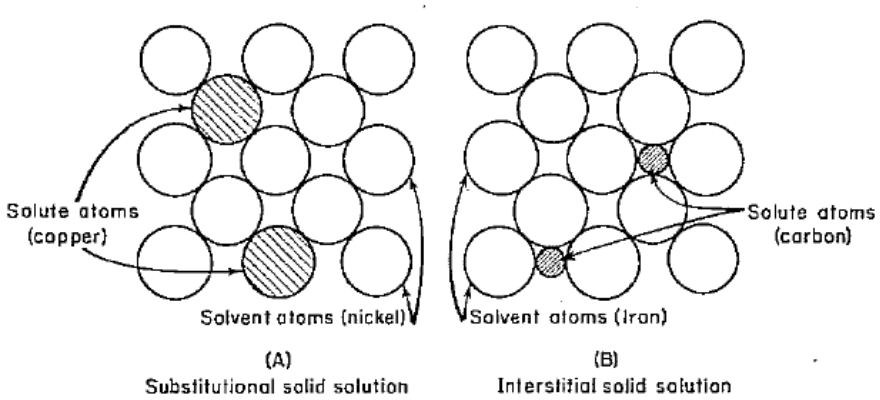

Figure 5-4: Substitutional and Interstitial Solid Solutions (Reed-Hill, 1973)

5.1.3. Effects of Alloy additions to steel

Alloy additions are usually added to structural steel to optimize the mechanical properties attained. Some alloying elements are added in relatively large amounts such as C, Mn and Si, whereas other alloying elements are added as micro-additions e.g. V, Cu and Ni. The effect of various alloying elements on steel will be discussed.

Carbon

Carbon increases the strength of iron by fitting into the interstitial sites of the body-centered cubic (BCC) lattice of iron atoms. The lattice becomes close packed, see Figure 5-5, and reduces the movement of dislocations. This causes an increase in the mechanical properties of steel.

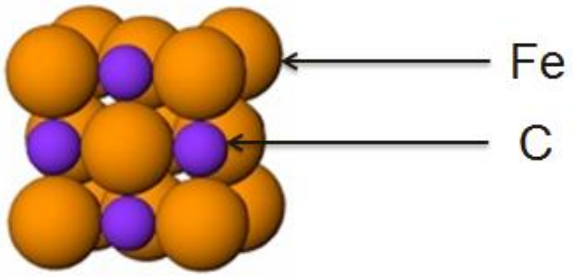

Figure 5-5: Close-packed BCC structure of Fe with C

The effect of carbon content on the mechanical properties of steel is depicted in Figure 5-6. It can be seen that as the carbon content increases the hardness, tensile strength and yield strength of the steel also increase. The effect of carbon on tensile strength and the yield strength begins to plateau at approximately 0.83 % carbon.

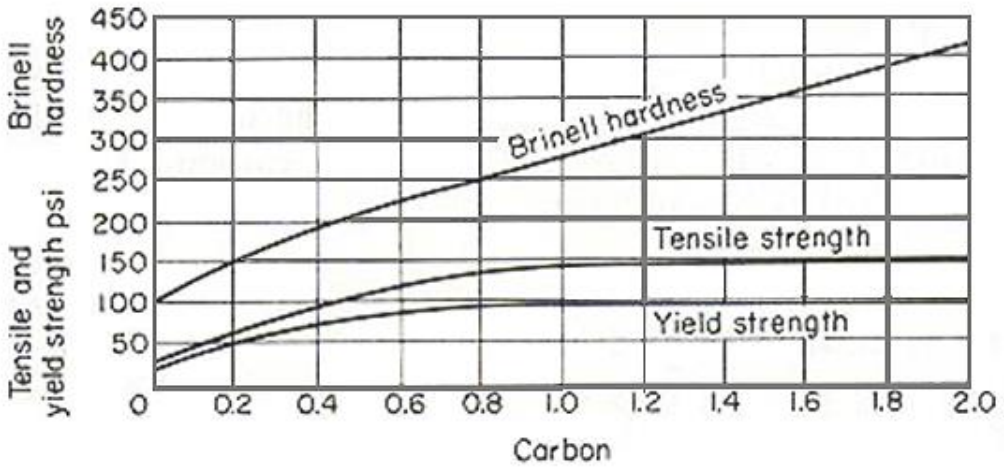

Figure 5-6: Effect of carbon on Mechanical Properties of steels (Attallah M. M., 2002)

Carbon plays a significant role on the microstructural constituents of steel. This is illustrated in the Fe- Fe_3C Phase Diagram presented in Figure 5-7. If the carbon content is below 2% it describes steel and if the C content exceeds 2% it describes cast iron. The eutectoid point of steel lies at 0.80 %C. This allows steels to be classified into hypo-eutectoid (%C <0.80) and hyper- eutectoid steels (%C >0.80). Hypo-eutectoid steels consist mainly of ferrite and pearlite and hyper-eutectoid consist mainly of cementite and pearlite. Carbon therefore has a prominent effect on the microstructure and heat treatment of steel.

Since carbon affects the microstructure, it is a significant component of the carbon equivalent (CE) of steels. CE takes into account all alloying elements that have a similar contribution as carbon. These contributions are weighted and summed up to produce a CE value, which gives an indication of how weldable a specific steel is. The carbon content affects the formation of martensite in welds which plays a crucial role in the occurrence of Hydrogen Induced Cold Cracking (HICC). Structural steel needs to have a CE < 0.51% to have acceptable weldability properties. The formula for calculating the CE for structural carbon steel is (Dearden & O'Neill, 1967):

$$CE = C + \frac{Mn}{6} + \frac{Cr + Mo + V}{5} + \frac{Ni + Cu}{15}$$

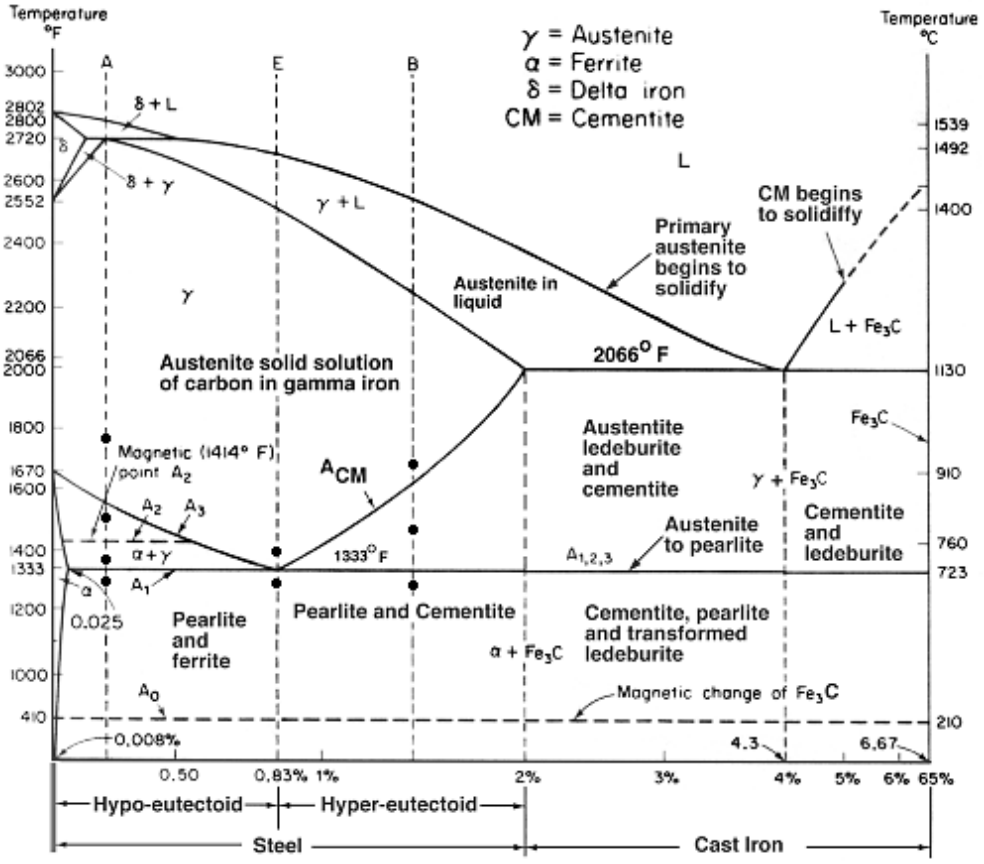

Figure 5-7: Fe- Fe_3C Phase Diagram (Pollack H., 1988)

Yan et al (1963) investigated the effects of the rolling process on the microstructure and mechanical properties for low carbon V-N steels with varying carbon contents. The tensile strength and microstructural features of steels under various reductions were evaluated. It was found that an increase in carbon content and rolling reduction resulted in a smaller ferrite grain size which caused an increase in strength.

Manganese

Manganese (Mn) improves hardenability, ductility and wear resistance of steel. Manganese also eliminates the formation of harmful iron sulphides, increasing strength at high temperatures and improving its hot workability. The Mn/S ratio of steels needs to be at least 8 to avoid hot shortness, which is a phenomenon where steel becomes brittle at elevated temperatures. The MnS inclusions in steel are deformed during the rolling process to form elongated stringers, (Deeley P. D., 1981).

Manganese has a small effect on solid solution strengthening in austenite and a moderate effect in ferrite; however Mn exhibits a large effect during work hardening. It increases the work hardening rate in austenite and reduces it in ferrite. The overall effect of Mn is the steel having a greater resistance to deformation resulting in a stiffer stronger steel.

Excess manganese forms stable carbides (Mn_3C) which increases the mechanical properties of steel. The % Mn in α-Fe has an increasing effect on the hardness of steel as depicted in Figure 5-8. Mn also acts a de-oxidizer, removing excess oxygen from steel, which is detrimental to the integrity of the cast structure. Manganese is an austenite forming element and has a decreasing effect on the transformation temperature of steel.

Manganese is commonly added to structural steels, instead of carbon, to strengthen the steel and to achieve higher mechanical properties. This is done to ensure that the chemical composition of the steel complies with the maximum carbon equivalent (CE) set out in the specifications of structural steel. Manganese has one sixth of the influence of carbon on weldability.

Copper

When copper is added to steel it offers resistance to atmospheric corrosion. Cu increases the strength via the precipitation hardening mechanism if it exceeds levels of 0.75% (Deeley et al, 1981). Deeley et al stated that copper does not interact with carbon therefore Cu will be dissolved or precipitated in ferrite which will induce a hardening effect on the steel.

Silicon

Silicon (Si) is the first element that is removed during the oxidation process of steelmaking due to Si having a relatively low Gibb's free energy. Silicon is a de-oxidizing agent used during steel making and is usually added in conjunction with Mn which results in lower oxygen levels being achieved. Fully-killed steel contain Si in the range of 0.15 – 0.30 %, (Deeley P. D., 1981). Steel that has alloying additions such as V, Ti, B etc. for inclusion control, grain refinement or nitrogen scavengers, are first deoxidized with Si which results in more economic processing. The reason for this is because these alloying elements have a high affinity for oxygen and will be readily consumed by the free oxygen during steel making. This will result in these alloying elements not being able to form the required precipitates, thus being prevented from serving its intended purpose.

Steels that contain Si have a lower tendency to form scale at elevated temperatures. However this type of scale formation is more difficult to remove during pickling, which is a chemical process that removes scale.

Silicon strengthens ferrite by solid solution strengthening, described in section 5.3.2. With the increase in strength, a loss in ductility is incurred. Si increases the hardness of steel but results in a loss of toughness. The %Si in α-Fe has an increasing effect on the hardness of steel as depicted in Figure 5-8.

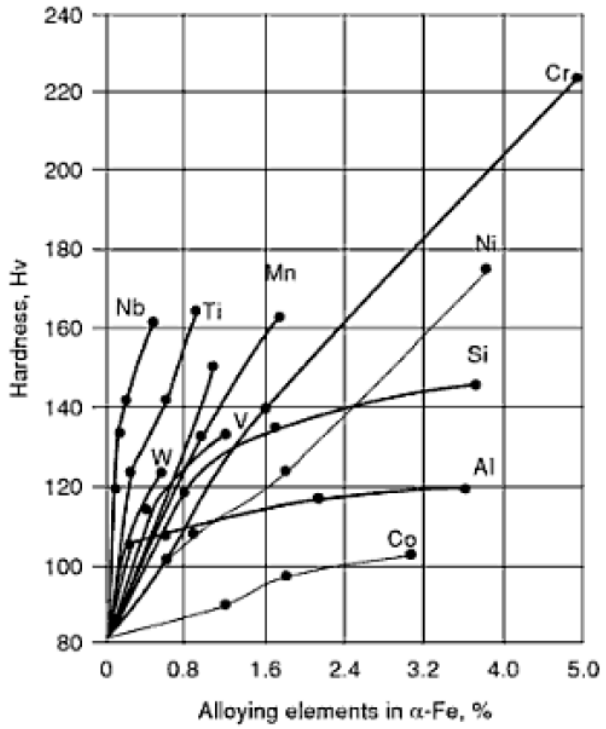

Figure 5-8: Effect of % Alloying element in α-Fe on Hardness. Totten, G. (2007) PM Steel, C= 0.8 %

Vanadium

Vanadium is commonly used as a micro-alloying element in rebar. It favourably affects grain refinement, wear resistance and hardenability of steels. Vanadium contributes to the strength of steel by forming V(C, N) (Klinkenberg C. 2005). These V(C, N) precipitates remain in solution during rolling and only come out of solution during cooling. Thus, the cooling rate has a significant effect on the strengthening provided by these precipitates. (Davis, 2001). Since vanadium does not increase the recrystallization stop temperature, it facilitates the rolling process by promoting repeated recrystallization between rolling passes. This process is known as recrystallization-controlled rolling. Fast cooling after rolling decreases the amount of austenite to ferrite transformation, retarding the growth of ferrite. This further increases the strength of the structure. Korchynsky M. (2001) has pointed out that vanadium not only contributes to grain refinement and precipitation hardening but it is also compatible with the nitrogen content of EAF steels and it contributes to cost saving due to its effect on reheating and finishing temperatures during hot rolling.

Role of Nitride-forming elements

All carbide formers are also nitride formers. In structural steels nitrogen is introduced into the steel by absorption from the atmosphere. When nitride forming elements such as Al, Ti, V, Cr and Mo react with nitrogen in steel, they form nitrides. These nitrides are situated at the grain boundaries and exhibit a pinning effect during grain growth upon exposure to high temperatures during hot rolling. This refines the grain size, producing a finer grained structure with superior mechanical properties. Nitride-forming elements are therefore known as grain refiners and cause strengthening in steel. The effect of the content of nitride-forming elements on the hardness of steel is depicted in Figure 5-9. It can be seen that Al, Ti, V, and Cr have an increasing effect on the hardness of steel. Mo has an increasing effect on the hardness up till an optimum concentration of 1.5%. When Mo has a concentration that exceeds 1.5%; it tends to exhibit a decreasing effect on the hardness of steel. The effect of Ni on the hardness of steel is negligible compared to the results obtained from the abovementioned Nitride-forming elements due to the fact that Ni is not a nitride-forming element.

Effect of Alloying Elements on Eutectoid Transformation Temperature

The effect of Alloying elements on Eutectoid Transformation Temperature is depicted in Figure 5-10. It can be seen that Ti, Mo, Si, W and Cr have an increasing effect on the eutectoid transformation temperature, with Ti having the most significant effect. This is due to the fact that the abovementioned alloying elements are ferrite stabilizers. Mn and Ni have a decreasing effect on the eutectoid transformation temperature since they are austenite stabilizers.

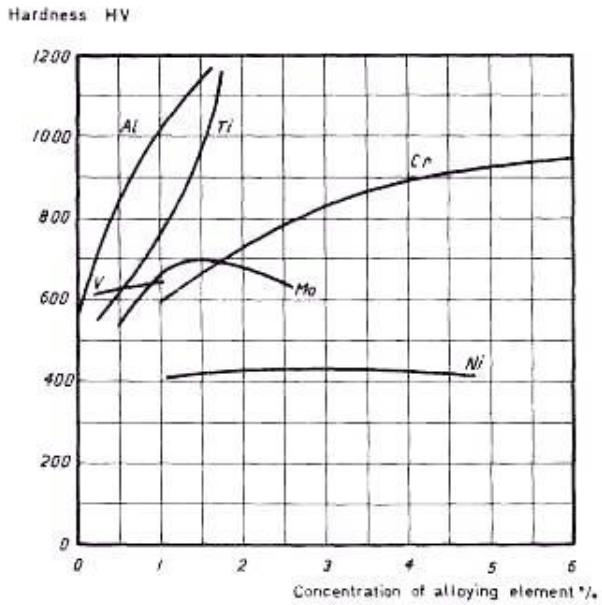

Figure 5-9: Effect of Nitride-forming elements on Hardness of steel.
Base composition: 0.25% C, 0.30% Si, 0.70% Mn (Key to Metals, 1999-2010)

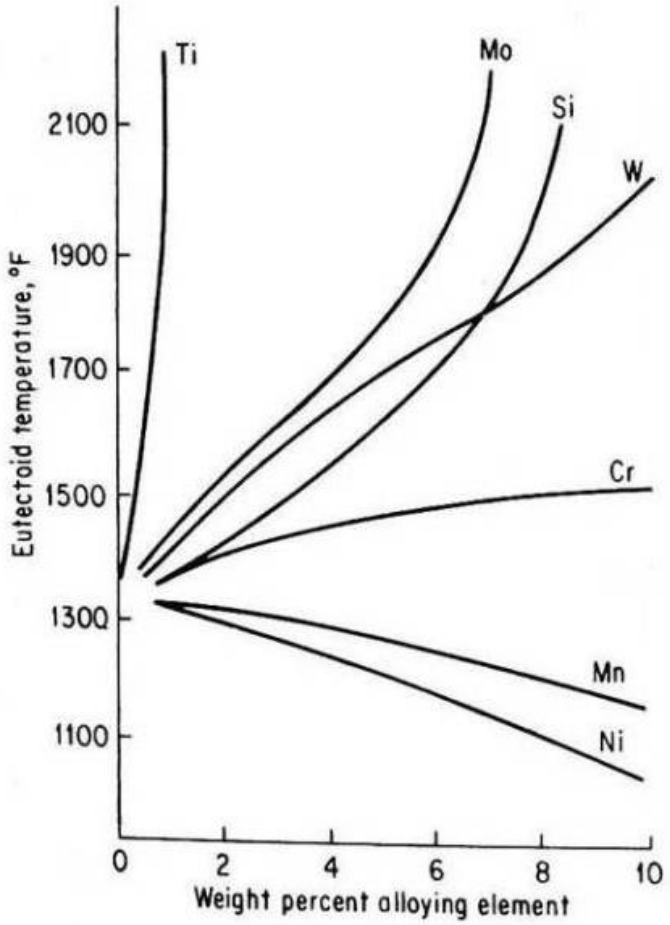

Figure 5-10: Effect of Alloying Elements on Eutectoid Transformation Temperature (Shah K. P., 2009)

5.2. Isothermal Transformation Diagrams

Isothermal Transformation (I-T) Diagrams also known as the Time- Temperature-Transformation diagrams are used to predict the microstructure of steel during non-equilibrium cooling conditions, unlike phase diagrams which predict the microstructure of steel during equilibrium cooling conditions.

The I-T diagram of steel is derived from plotting phases present in the microstructure at certain temperature versus the logarithm of time for a steel alloy with a fixed composition. This data is obtained from experiments where samples are austenitized and held at a constant subcritical temperature for varying time intervals. The samples are quenched and the hardness and microstructure are evaluated.

The most significant microstructures that are found in steel are:

Ferrite
Ferrite also known as α-ferrite is a solid solution of carbon in iron with a BCC crystal structure. The maximum solubility of carbon in ferrite is 0.02% at 723°C. Ferrite exhibits low hardness and tensile properties. When looking at ferrite under the microscope, ferrite has the appearance of irregular white grains. An example of how ferrite grains look is presented in Figure 5-11.

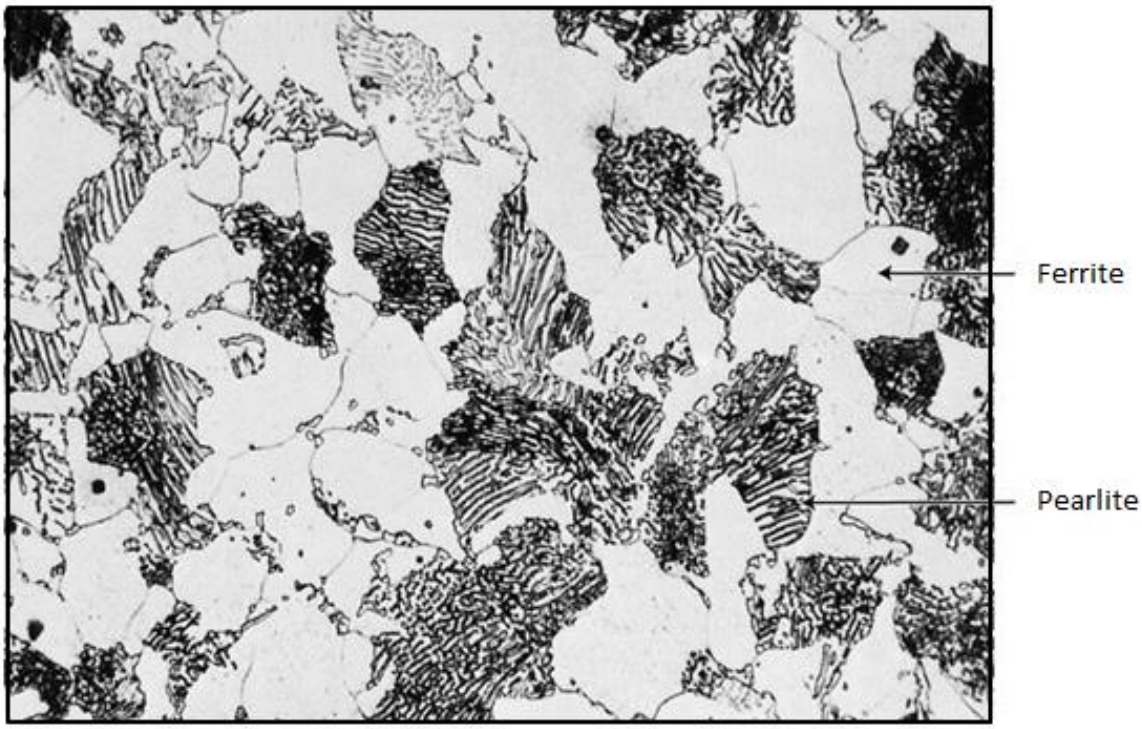

Figure 5-11: Microstructure of 0.2% C Steel

Pearlite

Pearlite is a lamellar structure composed of alternating layers of ferrite and cementite which be seen in Figure 5-11. Cementite is an intermetallic iron compound with a carbon content of 6.67 % C. Cementite has an orthorhombic crystal structure and is hard and brittle. Coarse, medium or fine pearlite can be formed depending on the cooling rate. The higher the cooling rate, the finer the structure and the higher the mechanical properties will be. Pearlite exhibits higher hardness and tensile properties compared to that of ferrite.

The effect of different speeds of nucleation and growth on formation of pearlite colonies is depicted in Figure 5-12 (a). At 700 °C the rate of nucleation is slow and then it increases drastically to form large pearlite colonies that cover the austenite grains. As the temperature decreases to 550 °C the nucleation and growth rate decreases and fine pearlite colonies are formed and a large number of nuclei precipitates on the austenite grain boundaries. Figure 5-12 (b) shows the nucleation mechanism of pearlite where a nucleus is formed and C diffuses out of the austenite matrix producing Fe_3C platelets. The carbon deficient areas on the sides of the Fe_3C platelets are ferrite. The alternating layers of Fe_3C and ferrite form pearlite. During side nucleation pearlite grains are formed on the side of the initial pearlite grain. Edge growth can also occur and this results in a different orientation of the pearlite grains (Rollason, E. C., 1961).

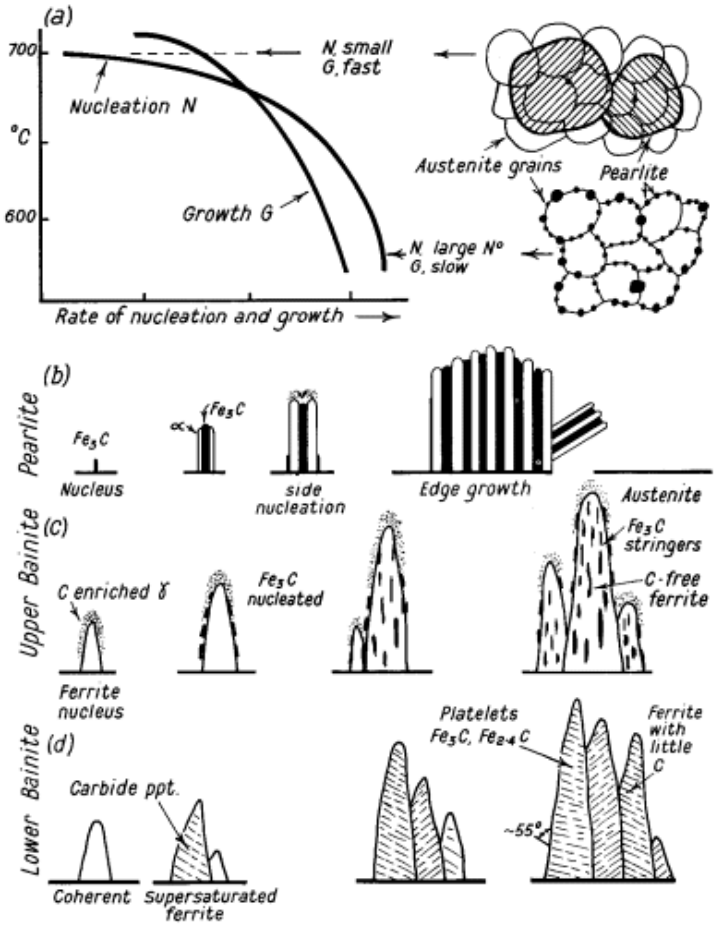

Figure 5-12: Formation of Pearlite, upper bainite and lower bainite (Rollason, E. C., 1961)

Bainite

Bainite, first discovered by Bain and Davenport, is composed of iron and iron-carbide constituents. Bainite forms by using a faster cooling rate than that of the formation of pearlite. Bainite commonly exists in 2 types, namely upper bainite and lower bainite. Upper bainite has a feathery structure which consists of small cementite platelets and ferrite needles oriented in a parallel manner. Lower bainite possesses thinner ferrite needles and smaller carbide platelets which are more closely spaced and has a structure similar to tempered martensite, as described by Bain. The ferrite needles and carbide platelets of lower bainite have a random orientation. Lower bainite is formed at a faster cooling rate compared to that of upper bainite. Micrographs of lower and upper bainite are presented in Figure 5-13. Bainite exhibits higher hardness and tensile properties compared to that of pearlite, with lower bainite being harder than upper bainite.

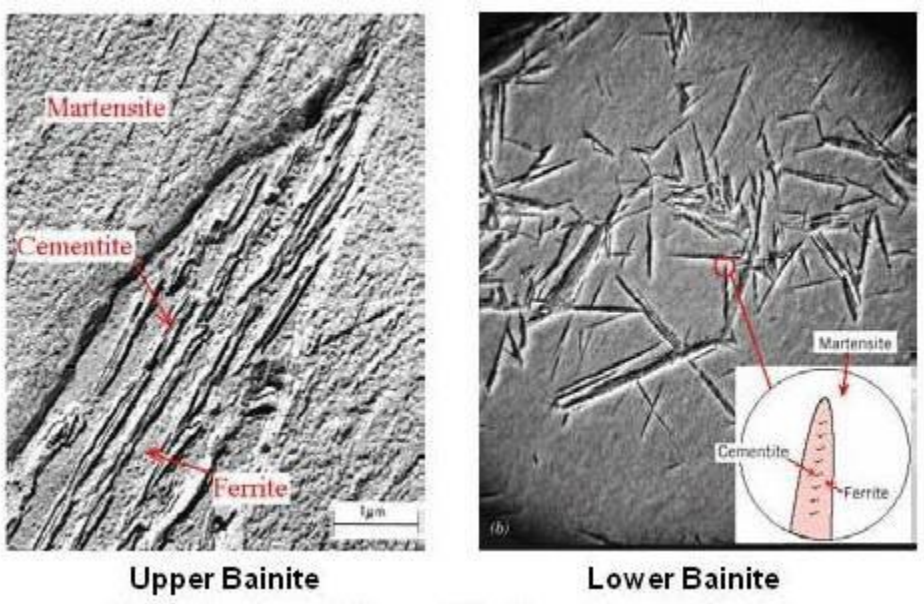

Figure 5-13: Microstructure of Upper and Lower Bainite (Shah K. P., 2009)

Formation of Upper and Lower Bainite

At temperatures ranging between 500 °C - 350 °C the initial nuclei is ferrite cementite precipitates from the carbon rich areas of the austenite matrix encouraging ferrite formation in the carbon depleted areas. The cementite precipitates lie parallel to the bainite needle and this gives the appearance of a feathery structure which is characteristic of upper bainite. This mechanism is depicted in Figure 5-12 (c) At temperatures below 350 °C the ferrite nuclei becomes supersaturated with C and carbides precipitate at an angle of 55° within the ferrite needle. This structure looks like a needle-like structure and is characteristic of lower bainite (Rollason, E. C., 1961). This mechanism is depicted in Figure 5-12 (d)

Martensite

During rapid cooling, austenite transforms into martensite, producing a distorted body-centered- tetragonal structure. The distortion is caused by trapped carbon atoms which has insufficient time to nucleate into cementite. Martensite is extremely hard and brittle and exhibits higher hardness and tensile properties compared to that of bainite. The microstructure of martensite consists of a needle-like structure which can be seen in Figure 5-14.

Figure 5-14: Microstructure of Martensite (Callister, W.D. Jr., 2003)

Summary of the relationship between cooling and microstructural constituents

A summary of the effect of cooling rate on the microstructural constituents formed is shown in Figure 5-15. The Rockwell C hardness values for eutectoid steel are presented in Figure 5-16.

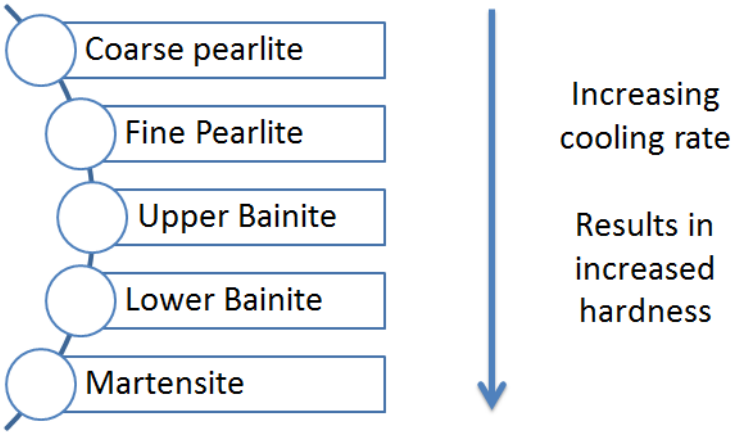

Figure 5-15: Summary of the relationship between cooling and microstructural constituents

An example of an I-T diagram of a hypothetical hypo-eutectoid steel is presented in Figure 5-16.

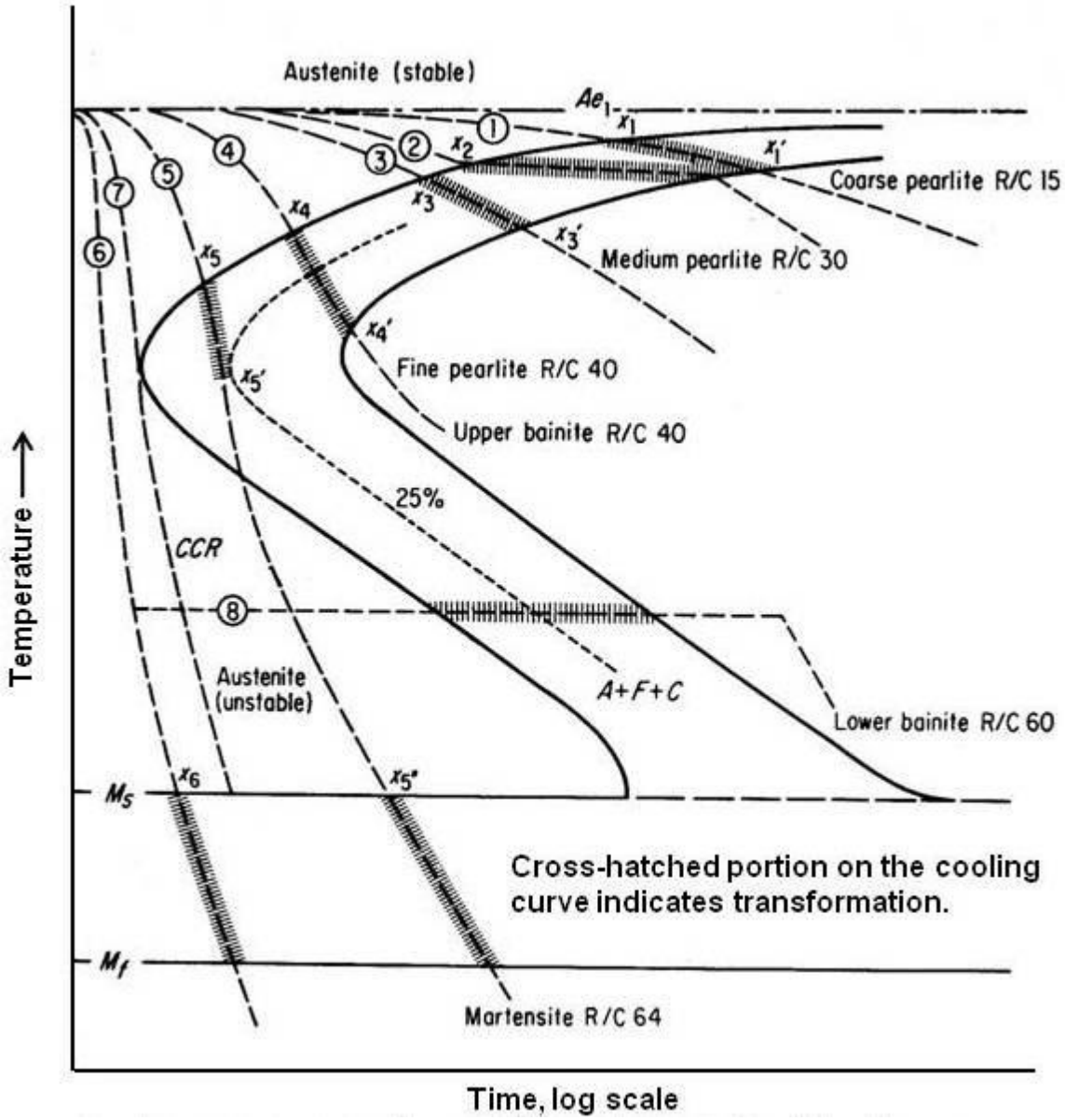

Figure 5-16: Hypothetical I-T Diagram for Eutectoid Steel (Avner, 1997)

Various cooling curves have been superimposed onto the I-T diagram ranging from cooling curve 1 to cooling curve 7. By considering the 2 extremes, cooling curve 1 exhibits a very slow cooling rate to produce a coarse Pearlitic structure and cooling curve 6 exhibits a very fast cooling rate to produce a fully martensitic structure. The microstructures of the remaining cooling curves are determined in a similar manner.

The I-T diagram of steel can be affected by the presence of alloying elements that have an effect on the transformation temperature, as discussed in section 5.1.3.

5.3. Grain size

Metals possess a polycrystalline structure that consist of grain boundaries which enclose grains. When metal is cooled during steel making or hot rolling practices, the grain size of the metal changes. Grain size has a significant effect on the mechanical properties of materials namely strength and toughness and has been studied in great depth by Hall (1951) and Petch (1953, 1986). The effects of grain size on tensile properties will be discussed in greater detail in section 5.4.1.

Due to the significance of grain size in metal properties, ASTM (American Society of Testing and Materials) have compiled a standard that governs the acceptable methods of grain size determination. There are many methods in ASTM E112 that can be used to calculate the average grain size of a sample i.e. the McQuaid-Ehn test, Shepherd Fracture Grain Size Method, Planimetric procedure and the Heyn Lineal Intercept Procedure.

The McQuaid-Ehn test compares the microstructure with a standard grain size chart which yields an ASTM grain size number (ASTM E112, 2004). The Shepherd Fracture Grain Size Method compares the grain size of the fracture of hardened steel with a set of standard fractures to produce a fracture size which can be converted to ASTM grain sizes (ASTM E112, 2004). The Planimetric (or Jeffries') Procedure involves the counting of grains inside an inscribed circle or rectangle as well as the grains intersected by the boundary of the area and calculations that use the Jefferies multiplier constant to produce the number of grains per mm^2 which can be used to calculate the ASTM grain size number(ASTM E112, 2004). The Heyn Lineal Intercept Procedure consists of counting the number of grains that are intersected by a number of lines with varying orientation and using this data to calculate the average grain size (ASTM E112, 2004).

The method that will be utilized for this work is the Heyn Lineal Intercept Procedure (ASTM E112, 2004). This method has been selected because it produces the average grain size instead of the ASTM grain size number and this test is more suited for analysis of non-equiaxed structures such as worked material due to the varying line orientation of this method which includes the 2 principal directions.

5.3.1. The Heyn Lineal Intercept Procedure

The Heyn Lineal Intercept Procedure consists of the following steps:

1. Determination of the number of grains intersected by the line segment
    - 4 lines of a known length are superimposed onto the microstructure of the test specimen as shown in Figure 17.
    - The number of grains intersected by each line segment is counted
2. Calculation of the average number of grain boundary intersections
    - The average number of grain boundary intersections is calculated by taking the average of the 4 values produced in step 1.
3. Calculation of the average line length intersected
    - The average number of grain boundary intersections is divided by the length of the line to produce the average line length intersected
4. Calculation of the average grain diameter, d
    - The average line length intersected is divided by the magnification to produce the average grain diameter, d.

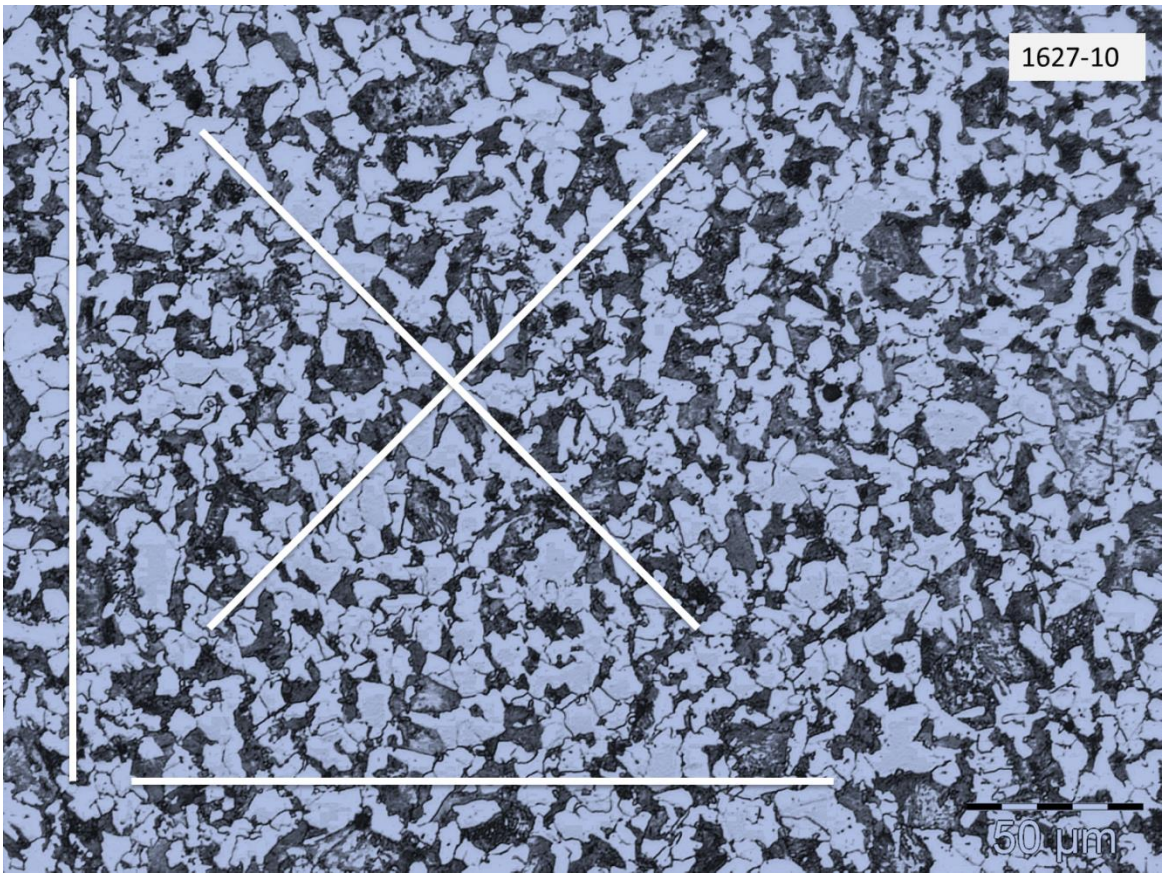

Figure 5-17: Example of microstructure with superimposed lines for average grain size calculation

5.4. Yield Strength

The yield strength of a material plays an integral role in engineering structural design. If a component that must support a load during application needs to be designed, it must be ensured that the component does not plastically deform. A material that has high yield strength must therefore be selected or the component should be large enough so that the applied force produces a stress that is below the yield strength.

The ductility of a sample is determined by conducting a tensile strength test. Samples of the material are placed in a tensile testing machine, gripped by the ends, and a vertical force is applied until they break. During the stretching process, the machine measures the load, the displacement of the sample and taking into consideration the original cross sectional area of the sample and the original length, an engineering stress-strain curve can be created. The standard for metal samples is ASTM E-8.

Typical tensile test
Figure 5-18 represents the typical result obtained from a tensile test. A detailed explanation follows.

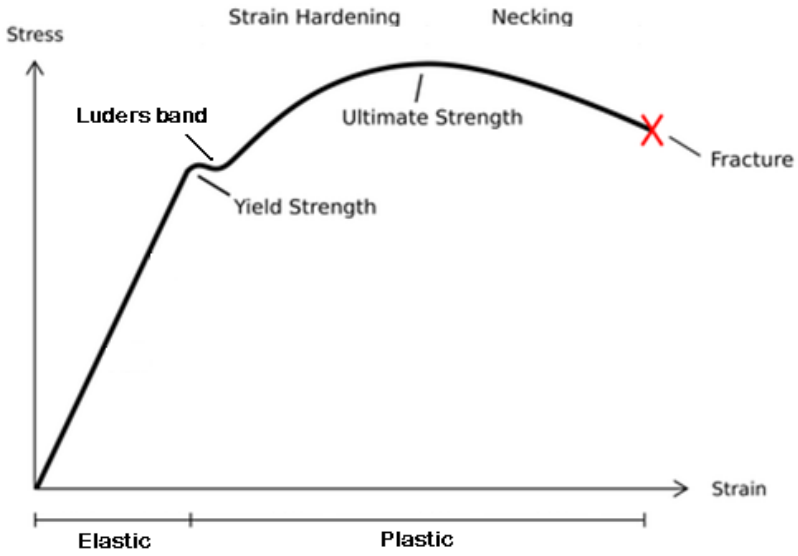

Figure 5-18: Typical tensile test stress-strain graph (Adapted from Resilience, 2014)

Elastic Behaviour
When the tensile force is applied to the specimen it begins to elongate. The material initially exhibits elastic behaviour i.e. the specimen returns to its original length when the load acting on it is removed. The Young's Modulus is the slope of the linear portion of the stress-strain curve. It is a constant that is usually specific to each material.

Plastic Behaviour
There is a slight increase in stress above the elastic limit which will result in permanent deformation when the load is removed.

Yielding
The material then begins to yield. The yield strength of the material is the value of stress at the point where the material begins to plastically deform.

Lüders Band
A Lüders band is a localized band of plastic deformation which occurs in certain materials before fracture. This is a brief stage of inhomogeneous deformation due to the pinning of dislocations. When dislocations meet obstacles, their movement is restricted for a short period of time. During this time solutes e.g. interstitial particles diffuse around the dislocations further strengthening the obstacles that impede the dislocation movement. Eventually these dislocations overcome these obstacles with sufficient energy and the process repeats itself.

Strain Hardening
Once the material begins to yield it is strengthened by plastic deformation. This phenomenon is known as strain hardening, where there is an increase in dislocation movement causing an interaction between the dislocations. This interaction decreases the mobility of dislocations, thereby strengthening it. The highest value of stress that is reached is termed the ultimate tensile strength (UTS). The higher the residual content of steel, the higher the strain hardening rate will be.

Necking
After reaching the UTS the cross-sectional area begins to decrease in a localized region of the specimen instead of over its entire length. A neck is formed as the specimen is elongated further, Stress-Strain Diagrams (1995-2014). Necking continues until failure of the component. The value of stress at the point of fracture is termed the fracture stress.

The variables that affect tensile strength will be explained in the subsequent sections.

Relationship between Yield Strength, Ultimate Tensile Strength and Ductility

The ductility of a material describes its ability to deform under tensile stress and is quantified by the amount of strain that a material can undergo. Ductility allows for the redistribution of stresses in material, especially at points where stress raisers such as inclusions, discontinuities and holes occur. As mentioned before, when a tensile stress, which is lower than the yield stress, is exerted onto steel, elastic behaviour is exhibited. This relationship between the stress and strain of a material during elastic deformation is described as the Young's Modulus Equation (Thomas Young):

$$E = \frac{Stress}{Strain} = \frac{\sigma}{\varepsilon} = \frac{F/A_O}{\Delta L/L_O}$$

Where:

E: Young's Modulus
F: Tensile Force exerted onto the specimen
A_O : Original Cross sectional Area of the specimen
ΔL: Change in length
L_O: Original length of the specimen

According to the Young's Modulus Equation, Yield strength is inversely proportional to elongation (ductility). Ductility is a direct indication of breaking elongation (%A), which is the elongation value that corresponds to the yield strength and total uniform elongation (% Agt), which is the elongation value that corresponds to the ultimate tensile strength. As can be seen in Figure 5-18, UTS will always exceed the yield strength. UTS is proportional to Yield stress

When the tensile stress exceeds the yield stress, plastic deformation occurs. Whilst the material is plastically deforming, it is also strengthened by the strain hardening mechanism, until it reaches its UTS.

5.4.1. Effect of Grain Size on Tensile Properties

The yield strength is inversely proportional to grain size. As the grain size decreases the metal becomes stronger and as the grain size increases the opposite effect on strength occurs. The difference in grain size is caused mainly by the heat-treating parameters and the chemical composition of the metal. The relationship between grain size and yield strength is shown in Figure 5-19.

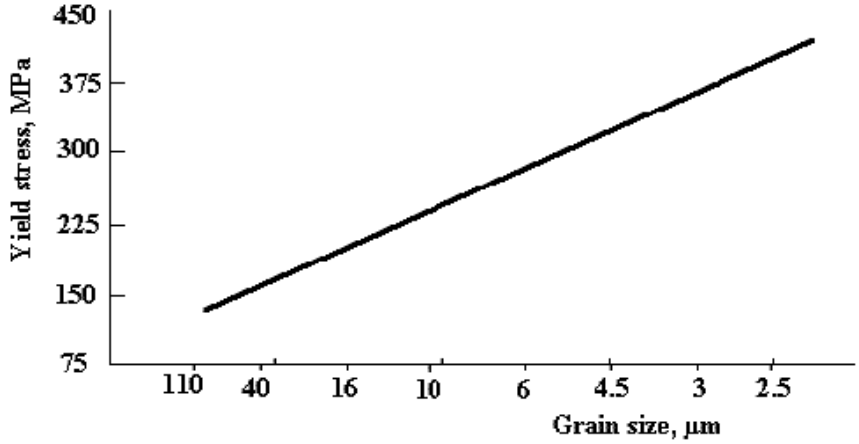

Figure 5-19: Effect of grain size on yield stress (TPP Information Centre, 2006)

The latter topic has been researched in great depth by Hall (1951) and Petch (1953, 1986). The effect of grain size on yield strength for structural steels is given by the Hall-Petch equation:

$$\sigma_y = \sigma_o + kd^{-1/2}$$

Where:

σ_y Yield Strength
σ_o Stress opposing dislocation movement
k Proportionality constant
d Ferrite grain size

The Hall-Petch relationship described above is depicted graphically in Figure 5-20. It is evident that the lower yield stress is proportional to $d^{-1/2}$. It can also be seen that lower yield stress is influenced by temperature. As the temperature increases the lower yield stress decreases and vice versa.

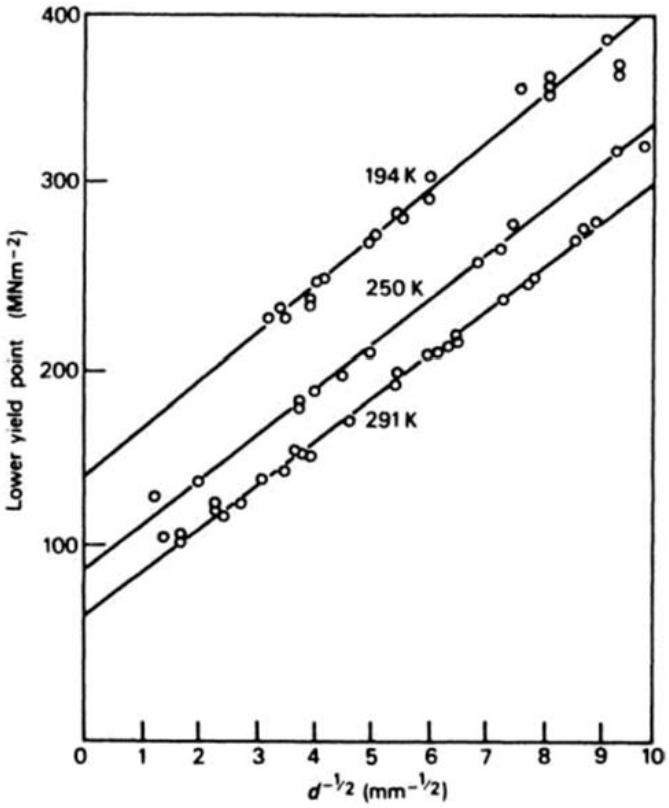

Figure 5-20: Dependence of lower yield stress on grain size (Petch N. J. 1959)

5.4.2. Effect of Cooling Rate on Tensile Properties

The cooling rate of steel after hot rolling plays a crucial role on the mechanical properties of steel. The cooling rate affects the microstructure as well as the grain size. A faster cooling rate promotes the formation of bainite (Avner, 1997; Shanmugam, 2007), which results in a higher yield strength (Niwa et al, 1981; Das et al, 2003). A high cooling rate also promotes finer grain structures which increases the strength of the steel.

Figure 5-21 shows the effect of furnace cooling vs. air cooling on the tensile strength of steel composed of 3 different carbon contents. Furnace cooling conditions represents a slow cooling rate whilst air cooling represents a faster cooling rate. The following deductions can be derived from Figure 5-21:

Furnace cooling:

- The higher the carbon content, the higher the tensile strength.
- An increasing Cr composition has a slightly increasing effect on tensile strength.
- Furnace cooling achieves a lower tensile strength compared to air cooling.

Air cooling:

- The higher the carbon content, the higher the tensile strength.
- An increasing Cr composition has an increasing effect on tensile strength.
- Air cooling achieves a higher tensile strength compared to furnace cooling.

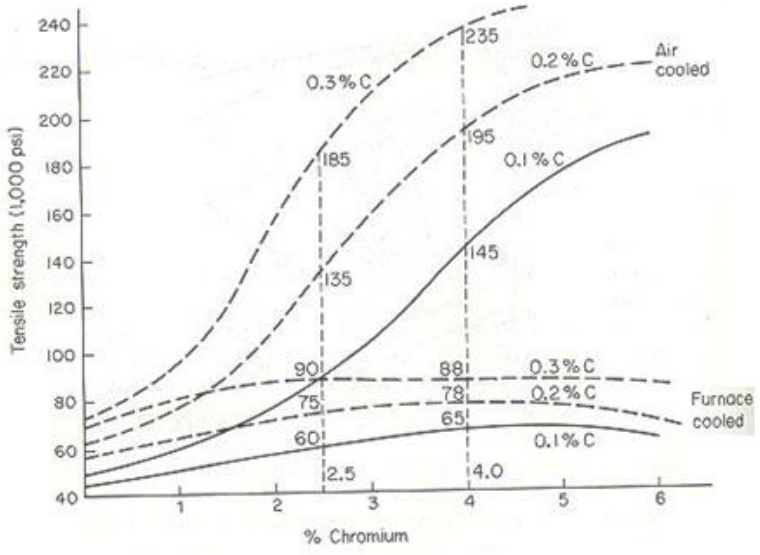

Figure 5-21: Effect of cooling and %Cr on tensile strength (Shah K. P., 2009)

A summary of the effect of cooling rate on the microstructural constituents formed is shown in Figure 5-15. As mentioned before the content of the microstructural constituents affects the hardness and tensile strength of steel.

The effect of cooling rate on the phase % present in the microstructure is shown in Table 5-3 (a). When the steel is water quenched the cooling rate is the highest. This cooling rate results in a smaller % Ferrite and a larger % Pearlite, Martensite and retained Austenite. Air cooling has a lower cooling rate compared to that of water quenched heat treatment. This cooling rate results in a lower % Ferrite and larger % Pearlite with no Martensite or retained Austenite for Steel A and the presence of martensite in Steel B and C. Steels B and C are more prone to martensite formation due to the higher C content. Furnace cooling has the lowest cooling rate which results in a larger % Ferrite and a lower % Pearlite. Çalik A, (2009).

The effect of cooling rate on the hardness is shown in Table 5-3 (b). The higher the cooling rate and % C the higher the hardness will be.

Table 5-3: The effect of Cooling Rate on the Phase % and Hardness, Çalik A, (2009).
Steel A: AISI 1020, 0.2 %C; Steel B: AISI 1040, 0.4 %C; Steel C: AISI 1060, 0.6 %C

(a)

Heat treatment	Steel type	Ferrite (%)	Pearlite (%)	Martensite (%)	Retained austenite (%)
Water-quenched	A	15	70	5	10
	B	20	60	20	-
	C	5	60	30	5
Air-cooled	A	45	55	-	-
	B	30	50	20	-
	C	30	65	5	-
Furnace- cooled	A	55	45	-	-
	B	50	40	-	10
	C	50	50	-	-

(b)

Steel type	Hardness ($HV_{0.1}$)		
	Water quenched	Air cooled	Furnace cooled
Steel A	476	149	125
Steel B	521	166	149
Steel C	610	203	167

5.4.3. Effect of Finish-rolling temperature on Tensile Properties

Mekkawy et al (1990) investigated the effect of finishing rolling temperature on microstructure and strength of V- and Ti- Micro-alloyed steels. It was found that a decrease in the finish-rolling temperature results in an increase in the ultimate tensile strength and a decrease ductility of steel due to the formation of bainite in the microstructure. Mekkawy et al also concluded that a lower finishing rolling temperature results in a loss of precipitation strengthening.

Chen et al (2013) have conducted a study investigating the effect of finishing rolling temperature during hot rolling on the microstructure and mechanical properties of stainless steel. Even though the study was based on stainless steel, the basis of metallurgy principals can be imposed onto structural steel. It was found that as the finishing rolling temperature

increased, the tensile strength decreased and the ductility increased. This relationship is depicted in Figure 5-22. Chen et al also stated that grain coarsening and α-fiber strengthening occur if the finishing rolling temperature is too high.

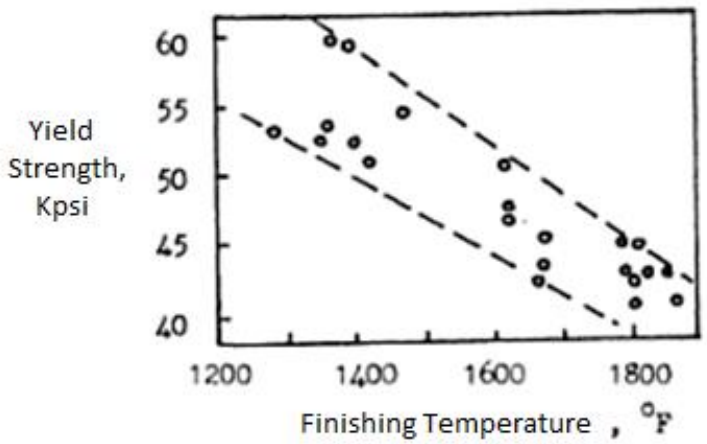

Figure 5-22: Effect of Finishing Temperature on Yield Strength (Adapted from Roberts W. L., 1983)

5.4.4. Effect of Transformation Temperature on Tensile Properties

The transformation temperature of a metal has a strong influence on the microstructure obtained after cooling the metal down to room temperature. The microstructure affects the magnitude of the mechanical properties of the metal.

For a steel of approximately 0.20 % C, the A1 transformation is most significant because this is where the following eutectoid reaction occurs:

Austenite → Pearlite + Ferrite

Figure 5-23 illustrates the relationship between transformation temperature, tensile strength, yield strength, elongation and reduction in area of Ni-Cr-Mo steel. The following is evident:

- A lower transformation temperature favours an increase in tensile strength
- A lower transformation temperature favours an increase in yield strength
- A lower transformation temperature favours a decrease in % elongation
- Transformation temperature yields optimum values for reduction of area at temperatures ranging between 300 °C - 400 °C and 750°C

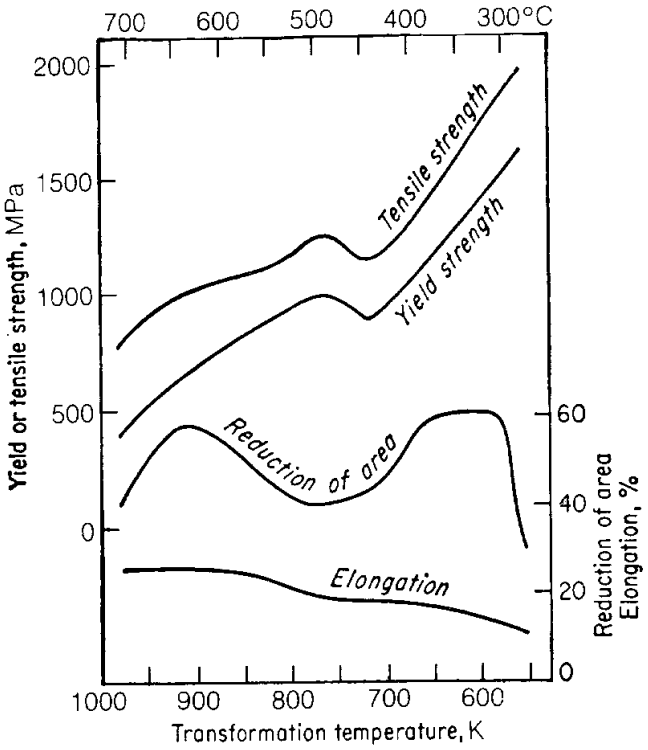

Figure 5-23: The effect of Transformation Temperature on Mechanical properties of Ni-Cr-Mo Steel. (Davenport E. S., 1961)

5.4.5. The Effect of Rolling Process on Properties of Steel

Mechanical properties:

During the hot rolling process steel is plastically deformed while it is above its recrystallization temperature (~ 1090 °C). The austenitized steel passes through a series of rolls through which it is deformed and stretched. Since the steel is being rolled above its recrystallization temperature, the material recrystallizes during deformation. This prevents the steel from strain hardening, which will produce a rolled product that has a lower yield strength with higher ductility.

If the steel is plastically deformed whilst being at a temperature lower than the recrystallization temperature, the steel will strain harden and the yield strength will increase resulting in a corresponding decrease in ductility.

Directional properties:

The input material to the hot rolling process is usually billets that are cast at a steel plant. The microstructure of a casted billet is not optimized with regards to the directional mechanical properties. Hot rolling improves the directional properties of the casted steel by creating an anisotropic microstructure which is comprised of fine spherical grains. This means that a specific physical property will have a different value when measured in different directions. This improved microstructure will improve the mechanical properties of the steel by increasing its strength, ductility and toughness.

Inclusions:

During hot rolling, the orientation of inclusions which originated from the steel making process is also improved. When the steel is cast, the inclusions are randomly orientated. If these inclusions are close to the surface, they can act as crack propagation points. When steel is hot rolled, the inclusions tend to flow with the contour of the surface, creating stringers. The stringers create a flow structure where the properties are anisotropic. When the stringers orientation is parallel to the surface it strengthens the material by acting as "crack-arrestor". The crack will want to propagate through the stringer and not along it, so the stringer will 'arrest' the crack.

5.5. Bend Test

Bend testing determines the ductility or the strength of a material by bending the material over a given radius. The bend test is conducted according the BS 4449: 1997 460B standard, which specifies that the specimen should be bent around a mandrel with a diameter of 4d (4 x diameter).

After the bend is conducted, the bent sample is inspected for cracks that could have occurred on the outer surface. If there are cracks that are found on the sample's surface, the sample would have failed the bend test and will be deemed as brittle. If there are no cracks that are found on the sample's surface, after the bend test, the sample would have passed the test and be considered to be a ductile material.

The tensile test is more commonly used to give an indication of the strength of a material because it quantifies the Yield strength, ultimate tensile strength, % elongation amongst other variables. The bend test does not quantify exactly how strong a material is, but will give an indication of its ductility. For example, two samples can have similar tensile strengths yet one sample could fail the bend test instead of the other sample. Factors that can affect the ductility of steel are the chemical composition and the microstructural constituents.

For the purposes of this project, a bend test will be conducted in conjunction with the tensile test for the purpose of ductility validation, because ductility cannot be determined by only evaluating the tensile properties.

A rebar sample that has undergone a bend test is shown in Figure 5-27. There are no cracks visible on the samples surface, thus this sample has passed the bend test.

Figure 5-24: Bend Test Specimen

6. METHODOLOGY

The methodology that will be carried out for this experimental work is depicted in Figure 6-1. A detailed description of each of these stages will follow.

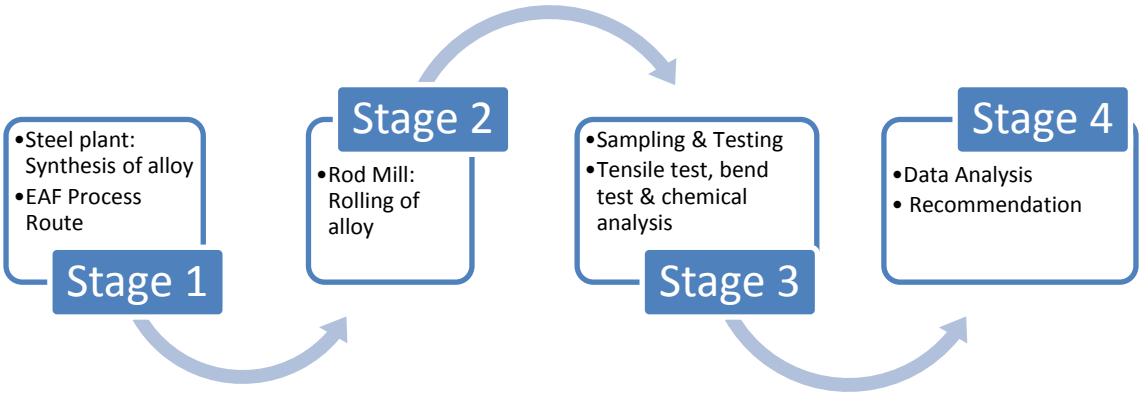

Figure 6-1: Methodology for Experimental Work

As listed before, the objectives of this experimental works are:

- To adjust the cooling parameters of the rolling method to process existing stock of billets to obtain a maximum yield strength of 600 MPa
- To revise the current chemical specification of the billets to produce a new chemical composition that will prompt a decrease in yield strength
- To adjust the cooling parameters of the rolling method to process the billets of optimized chemical composition to obtain a maximum yield strength of 600 MPa

Since there are 3 objectives and 2 parameters that will be changed i.e. chemical composition and rolling method, there will be a total of 6 trials conducted for this work. These trials will be grouped into 3 sets, with each set comprising of the use of 1 chemical composition and 2 cooling programs. The purpose of this is to have a control for each trial. A summary of the trials are present in Table 6-1. Detailed descriptions of these trials are given in sections 6.1 and 6.2.

Table 6-1: Trial Chemical Composition and Cooling program details

Trial	Chemical Composition	Cooling Program
1A	Original	CP 1
1B	Original	CP 2
2A	Original	CP 3
2B	Original	CP 4
3A	Optimized	CP 1
3B	Optimized	CP 5

6.1. Stage 1: Synthesis of alloy

One of the objectives of this work is to adjust the chemical composition of the billets to produce a new chemical composition that will prompt a decrease in yield strength. This will be done during the synthesis of the alloy in the steel making process.

The alloyed samples used for this experimental work will be synthesized at the steel plant with specially designed chemical analysis. Details of the steel making process and chemical composition will be discussed in sections 6.1.1 and 6.1.2.

6.1.1. Steel Making Process Routes

Traditionally, this material is produced at ArcelorMittal Newcastle Works via the Basic Oxygen Furnace (BOF) process route but due to economic and process considerations this material has to be sourced from ArcelorMittal Vereeniging Works, where the Electric Arc Furnace (EAF) Steel Making process is used. A description of the BOF and EAF Steel Making process routes follow in the subsequent sections.

6.1.1.1. Basic Oxygen Furnace Steel Making Process

The Basic Oxygen Furnace steel making process, which consists of a Basic Oxygen Furnace, Ladle Furnace and a Continuous Caster, is depicted in Figure 6-2.

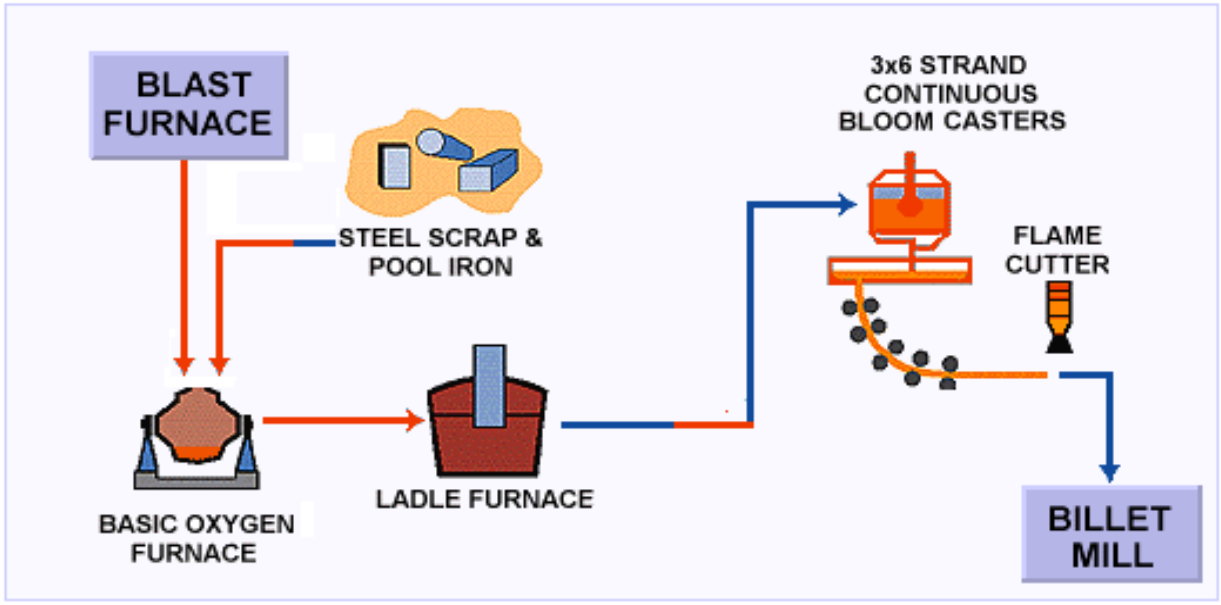

Figure 6-2: Basic Oxygen Furnace Steel Making Process (Source: ArcelorMittal Newcastle Works)

Basic Oxygen Furnace (BOF)

Hot metal, also known as pig iron, is produced at the blast furnace from iron ore. Hot metal and steel scrap are charged into the basic oxygen furnace. Fluxes such as lime and dolomite are added to the melt to form slag. Due to the low density of the slag, compared to the density of the molten steel, the slag floats on top of the molten steel forming a 'protective blanket'. The functions of slag are to absorb the impure oxides, thermally insulate the steel bath and to protect it from re-oxidation with the atmosphere.

Oxygen is injected into the BOF where elements such as C, Mn, P, S, and Si react exothermically with oxygen to form oxides. The energy that is liberated by these exothermic reactions is used to heat the steel bath to steelmaking temperatures of ~1500 $^{\circ}$C – 1600 $^{\circ}$C. The 'end of blow' is reached when the correct levels of P, S and C are attained.

The molten steel is then de-slagged and tapped from the BOF to a ladle. Alloying elements are also added during tapping to attain the target chemical composition. The ladle is then sent to the ladle furnace for further processing.

Secondary Metallurgy: Ladle Furnace

The ladle furnace is equipped with 3 graphite electrodes which are used to heat the steel. During 'arcing', electricity flows through the graphite electrodes producing heat energy which is transferred to the molten steel. This raises the temperature of the steel to the correct temperature that is required for casting. Alloying elements are added to the molten steel to attain the correct chemical composition. The ladle furnace is also equipped with argon bottom-stirring which is used to attain homogeneity of the molten steel with respect to both chemical composition and temperature. The ladle is then sent to Continuous Casting, the last stage of the steel making process.

Continuous Casting

The molten steel is transferred from the ladle through the ladle shroud into a tundish which is a temporary reservoir which ensures continuity during the casting process and allows the steel to be cast using a number of strands. The steel then flows from the tundish through the submerged entry nozzle into a copper mould. The steel is water cooled and the steel solidifies into a 260 mm x 260 mm bloom, which is the final product of the steel making process.

6.1.1.2. Electric Arc Furnace Steel Making Process

The Electric Arc Furnace steel making process is similar to the Basic Oxygen Furnace steel making process, with respect to Secondary metallurgy (Ladle furnace) and continuous casting. The Electric Arc Furnace steel making process is depicted in Figure 6-3:

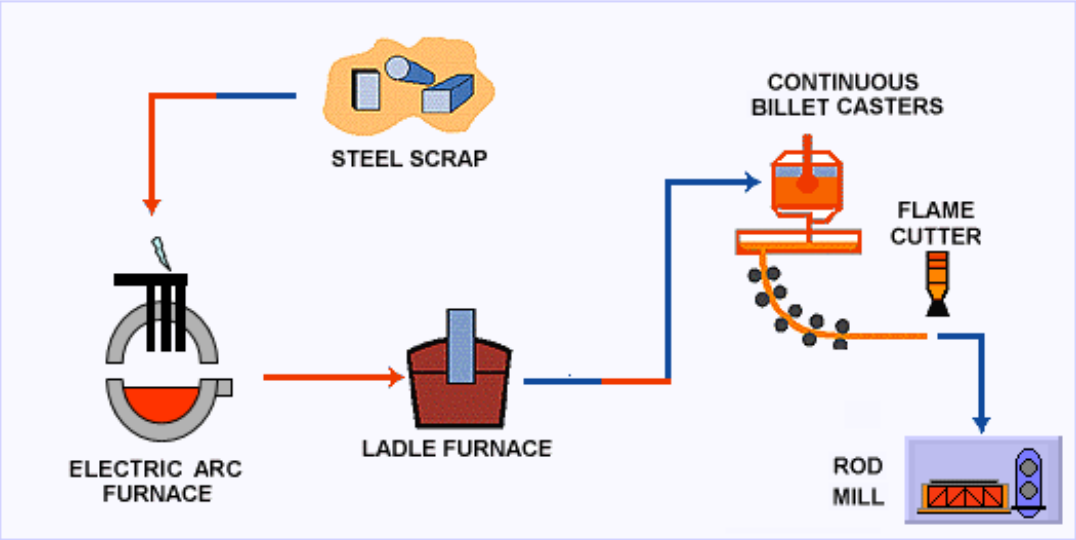

Figure 6-3: Electric Arc Furnace Steel Making Process (Source: ArcelorMittal Newcastle Works)

Electric arc furnace

The input material for the electric arc furnace steel making process is scrap, which is selected such that the process is optimized with respect to scrap melting and chemical composition. The scrap is charged into the furnace and is then melted using electrical and chemical energy. Electrical energy is passed through the graphite electrodes that the furnace is equipped with, and an arc is formed. The arc transfers the heat energy to the steel, thereby facilitating the melting process. (Jones J. A. T, 2013)

Chemical energy is supplied by a blend of oxygen and air. The presence of oxygen promotes certain exothermic reactions, which contribute to the energy required for scrap melting. During the refining stage, C is removed by oxidation, producing CO as a by-product. The evolution of CO assists with H and N removal. Harmful elements such as S and P are also removed. The steel is then de-slagged and tapped into a ladle, where it is transferred to the ladle furnace.

Secondary Metallurgy: Ladle furnace

The ladle furnace process is the same as that described in the basic oxygen furnace steel making process route. (Section 6.1.1.1.)

Continuous casting

The continuous casting process is similar to that described in the basic oxygen furnace steel making process route (Section 6.1.1.1.)The main difference is that in the EAF steel making process route, a billet caster is used instead of a bloom caster. The final product is a 140 mm x 140 mm billet.

High Residual Content of Steel Manufactured via EAF Process Route

The scrap used in this process has a high alloy content, which results in the final product having a high residual content. Parker (2003) defines residual elements as alloying elements that are present in the steel in small amounts but are not intentionally added as a part of the process. Examples of residual elements of this process are Cr, Cu, Ti, Mo, Ni, etc. The aforementioned residual elements enhance strengthening mechanisms in steel, which results in a final product with higher mechanical strength.

The increase in mechanical strength of rebar is detrimental to bending and forming applications as explained previously. A change in input scrap composition can remedy the increase in mechanical properties, however, economic constraints prevent this.

6.1.2. Chemical Composition

The chemical specification of the billets will be adjusted to produce a new chemical composition that will prompt a decrease in yield strength. This will be done by adjusting the 'original' rebar chemical composition to produce an 'optimized' chemical composition which will compensate for the high residual content.

Since C and Mn are the biggest contributors to the yield strength of steel, the C and Mn content will be reduced, such that the decrease in yield strength will compensate for the presence of residual elements. According to literature, residual elements such as Cr, Cu, Ni and Mo have an increasing effect on the yield strength of steel.

The 'original' chemical composition is the current chemical composition that is being used to produce reinforcing bars and the 'optimized' chemical composition is similar to the 'original' chemical composition, but has a lower C and Mn content. This is achieved by adding less C and Mn alloys during the steelmaking process.

The 'original' chemical composition and the 'optimized' chemical composition are presented in Table 6-2.

Table 6-2: Aim Specification of the chemical composition of Rebar at Newcastle Works (Mass %)

	C	Cr	Cu	Mn	Mo	N	Ni	P	Si	V
Original	***0.23 – 0.25***	0-0.25	0-0.25	***1.20 – 1.30***	0 -0.1	0.008-0.014	0-0.25	0 - 0.04	0.4-0.5	0.05-0.06
Optimized	***0.21 – 0.23***	0-0.25	0-0.25	***1.15 – 1.25***	0 -0.1	0.008-0.014	0-0.25	0 - 0.04	0.4-0.5	0.05-0.06

As mentioned before, there will be a total of 6 trials conducted. The allocation of the chemical composition that will be used is as follows:

- 'Original' chemical composition: Trial 1A, 1B, 2A and 2B
- 'Optimized' chemical composition: Trial 3A and 3B

6.1.3. Sample Details

The flow of samples during stage 1 is as follows:

- 3 casts will be produced via the EAF steel making process for the trial.
- Each cast produced in the EAF has a total weight of 50 tons. Due to budget constraints, 30 tons per cast is allocated for this trial.
- The weight of 1 billet is approximately 2 tons. A total weight of 30 tons will yield approximately 15 billets.
- Trial 1, 2 and 3 will therefore be comprised of 3 different casts weighting 30 tons each, which consists of ± 15 billets, which will be the input material for stage 2.

6.2. Stage 2: Rolling of alloy

The remaining objectives of this experimental work are:

- To adjust the cooling parameters of the rolling method to process existing stock of billets to obtain a maximum yield strength of 600 MPa;
- To adjust the cooling parameters of the rolling method to process the billets of optimized chemical composition to obtain a maximum yield strength of 600 MPa.

This will be done during the rolling process. The steel with the 'original' and 'optimized' chemical composition will be rolled at Rod Mill with a specially designed cooling program. Details of the Rod Mill rolling process and cooling parameters will be discussed in sections 6.2.1 and 6.2.2.

6.2.1. Rolling Process

The rod mill rolling process is a hot rolling process. Rolling occurs at austenizing temperatures, so that the steel is easily deformed due to the ductility and malleability that exists at these high temperature conditions. The rod mill rolling process is depicted in Figure 6-4.

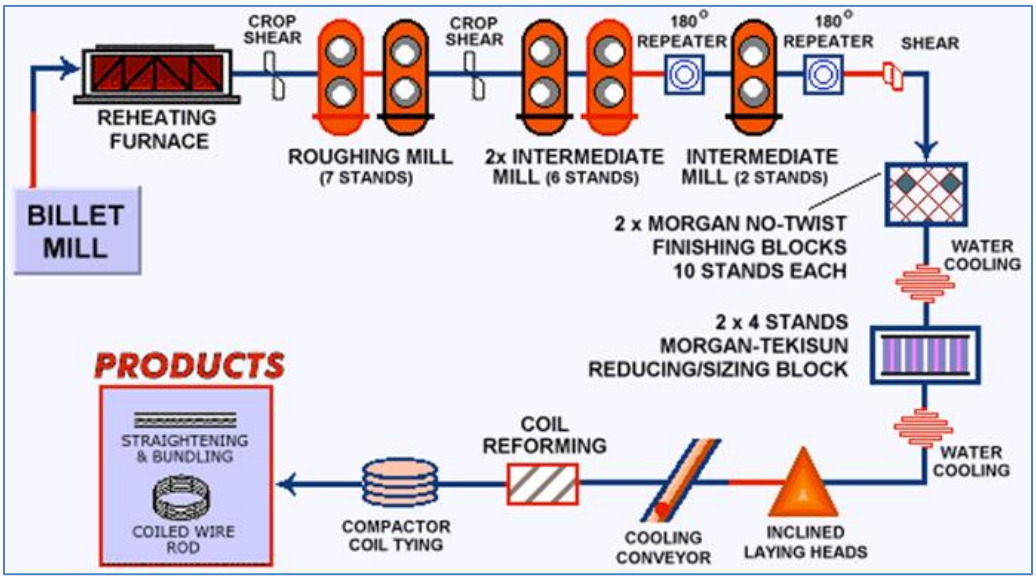

Figure 6-4: Rod Mill Roll Process (Source: ArcelorMittal Newcastle Works)

Re-heat furnace

Billets are the input material for the rod mill rolling process. These billets can consist of 3 sizes:

- 101 mm x 101mm, which is obtained from the billet mill (BOF process route)
- 131 mm x 131mm, which is obtained from the billet mill (BOF process route)
- 140 mm x 140mm, which is obtained from the billet caster (EAF process route)

The billets are weighed and fed into the reheating furnace where the billets are re-heated from room temperature to the required rolling temperature which ranges between 1100 °C – 1200°C. The heated billets are then fed into the roughing mill with a peel bar.

Roughing & Intermediate Mill

The initial size reduction occurs at the roughing mill, which consist of 7 Stands. The billet then goes through the intermediate mill, which consists of 8 stands, where it is reduced to a rod ranging from 6 mm - 14mm. Crop shears are used to cut off the heads of the rods and to remove rolling defects present at the head of the rod.

Finishing Mills

The rod then enters the No-Twist Morgan Finishing Block, where it is further reduced in size. It then enters water-box 1 where the rod is cooled using room temperature water (25 °C). The rod enters the Morgan Reducing/Sizing Block, where it is reduced to even smaller sizes and has an improved surface finish. It is then cooled with water-box 2.

Water Boxes and Temperature Control

An essential element of high speed rolling is the ability to control the temperature rise of the steel due to adiabatic heating and to reduce the temperature sufficiently when needed for further rolling or for coiling. Water-box 1 (WB1) is located after the No-Twist Morgan Finishing Block and water-box 2 (WB2) is located after the Morgan Reducing/Sizing Block. The temperature before the bar enters Water-box 1 is not measured or recorded.

Pinch Rolls and Laying Heads

The laying head and pinch roll system play a crucial role in the success of a high speed rod mill. It is a high speed operation which provides well-shaped rings that are correctly positioned on the Ashlow cooling conveyor. (Siemens AG, 2010).

Ashlow Cooling Conveyor

The cooling experienced by the rebar on the Ashlow cooling conveyor significantly affects its final mechanical properties. The cooling conditions affect the microstructure of the steel, which in turn affects the hardness and mechanical properties. The higher the cooling rate, the higher the mechanical properties the steel will have.

The cooling rate on the Ashlow cooling conveyor can be altered by changing the following variables:

- The speed of the conveyor;
- The speed of the fans that are under the conveyor;
- The use of cooling lids which cover the conveyor for slow cooling requirements.

The optimization of the cooling rates results in improved as-rolled rod properties. This enables the production of more grades in a directly usable condition, thus reducing or eliminating downstream processes, such as spheroidize annealing. (Siemens AG, 2010).

Reforming and Compacting
After the coils are cooled on the cooling conveyor and it enters the reform tub, where the coils are reformed to the correct coil shape. Samples are cut and inspected for quality control purposes. If the coil passes the inspection criteria, it is compacted and strapped.

The final product consists of rods which are dispatched as coils or are straightened and cut into lengths.

6.2.2. Rolling Parameters

In order to develop a rolling method to process existing stock of billets to obtain a maximum yield strength of 600 MPa and a rolling method to process the billets of optimized chemical composition to obtain a maximum yield strength of 600 MPa, the cooling parameters need to be optimized.

According to literature, a lower cooling rate will produce a material with a decreased yield strength. The cooling rate at Rod Mill can be decreased in the following ways:

- Increasing the temperatures of water box 1 (WB 1) and water box 2 (WB 2);
- Decreasing the utilization of the cooling fans ;
- Using cooling lids.

By varying the abovementioned parameters, 5 cooling programs were designed. The details of the cooling programs that will be used during the trials are presented in Table 6-3.

Table 6-3: Rod Mill Cooling Programs

Cooling Program	WB1 Temp Aim (°C)	WB2 Temp Aim (°C)	Cooling Fans	Lids
CP 1	970	950	100%	No
CP 2	990	970	50%	No
CP 3	1000	980	None	No
CP 4	1000	980	None	Yes
CP 5	970	950	50%	No

CP 1 is the current cooling practice and CP 2 - CP 5 are cooling programs that have been created to vary the cooling conditions by altering the temperatures of WB1 and WB2, utilization of the cooling fans and the implementation of cooling lids. WB1 and WB2 temperatures affect the finishing temperature. According to literature, if the finishing temperature is increased, it will produce a larger austenite grain and lower mechanical strength will be achieved. The use of 50% & 100% of the cooling fans was used to determine the effect of reduced cooling on the mechanical strength achieved. The use of lids was also enforced to lower the cooling rate further, to achieve lower mechanical properties.

6.2.3. Sample Details

The flow of samples during stage 2 is a follows:

- The input material for trial 1, 2 and 3 will be comprised of 3 different casts weighting 30 tons each, which consists of ± 15 billets;
- Each billet will be rolled via the rod mill rolling process to produce 1 coil each;
- 2 x 0.5m rod samples will be cut from each coil and be used in stage 3

6.3. Stage 3: Sampling and Testing

Samples obtained from stage 2 will undergo the following tests:

- Tensile test to determine the yield strength of the steel
  - Equipment: Messphysik Tensile tester
  - Aim: Yield strength < 600 MPa
- Bend test to determine whether the steel is ductile or brittle
  - Equipment: Uni bend tester
  - If the steel does not crack during the bend test, it will be considered to be ductile.
- Chemical analysis to determine the chemical composition of the final product
  - Equipment: Optical Emission Spectrometer (OES) and LECO Combustion analyser
  - Chemical analysis of the final product will be checked against the specification.
- Metallographic Analysis to examine microstructural changes
  - Equipment: Optical Microscope, analySIS docu software and SEM
  - Microstructure of samples will be analyzed
  - The % of each phase present in the microstructure will be determined
- Grain size test
  - Equipment: Optical Microscope
  - To determine the changes in grain size during each trial using Heyn Lineal Intercept Procedure (ASTM E112).

6.4. Stage 4: Data Analysis and recommendation

The data will be analyzed to check for the following:

- Yield strength < 600MPa
- Chemical analysis within aim specification
- Ductility (Bend test)
- Microstructural changes
- Grain size changes

Once the data is analysed, recommendations will be made, based on the results achieved.

7. FACILITIES USED

The following equipment will be used for this project:

Steel plant:

- Electric Arc furnace
- Ladle furnace
- Continuous Caster

The location of the abovementioned equipment is at ArcelorMittal Vereeniging Works.

Rod Mill

- Reheating furnace
- Roughing mill
- Intermediate mill
- Finishing mill
- Water boxes
- Ashlow cooling conveyor
- Cooling lids

Mechanical testing

- Messphysik Tensile tester
- Uni bend tester

Chemical testing

- Optical Emission Spectrometer (OES)
- LECO Combustion analyser

Metallurgical Testing:

- Optical microscope
- Scanning Electron Microscope (SEM)
- AnalySIS Docu software

The location of the abovementioned equipment is at ArcelorMittal Newcastle Works.

8. RESULTS

8.1. Trial 1

The input material for trial 1A and 1B consisted of billets, cast number 9311618, with the 'original' chemical composition described in Table 6-2. This material was rolled using 2 cooling programs, namely CP1 and CP2, described in Table 6-3. The use of the original chemical composition with cooling program CP1 and CP2, constituted Trial 1A and 1B respectively. The billets for trial 1 were rolled into 12mm reinforcing bars. A 12mm sized bar was selected as it is one of the larger sizes available at the rod mill and it would produce lower tensile properties compared to a small rod due to the strain hardening effects during rolling. A summary of trial 1 is presented in Table 8-1.

Table 8-1: Summary of Trial 1

Trial No	Chemical Composition	Cooling Program	Size (mm)	Cast No
1A	Original	CP 1	12	9311618
1B	Original	CP 2		

8.1.1. Chemical analysis

The chemical composition for Cast 9311618 was determined by using an Optical Emission Spectrometer (OES) and a LECO Combustion analyzer for C and S. The chemical composition of cast 9311618 is shown in Table 8-2.

Table 8-2: Chemical analysis (mass percent) of cast 9311618- Trial 1

C	Mn	P	S	Si	Cu	Ni	Cr	Mo	V	Al
0.24	1.34	0.022	0.013	0.43	0.11	0.10	0.09	0.02	0.05	0.005

The chemical analysis conforms to the BS 4449: 1997 460B specification; however it is out of the aim specification listed in Table 6-2. The Mn composition is 3.54 % higher than the specified maximum of 1.30%

The chemical analysis of trial 1A and 1B are presented in Table 8-3. The deviation of chemical composition amongst samples belonging to one cast can be attributed to experimental error or poor sampling and preparation methods during LECO and OES Analysis or segregation that occurred at the caster.

Table 8-3: Chemical Analysis (mass percent) for Trial 1A and 1B

Trial	Coil No	C*	Mn	P	S*	Si	Cu	Ni	Cr	Mo	V	Al	CE
1A	1	0.24	1.49	0.014	0.006	0.47	0.13	0.06	0.05	0.02	0.05	0.006	0.53
	2	0.23	1.54	0.015	0.006	0.47	0.13	0.06	0.05	0.02	0.05	0.006	0.53
	3	0.26	1.28	0.030	0.013	0.38	0.10	0.15	0.15	0.04	0.05	0.004	0.54
	4	0.25	1.36	0.015	0.012	0.44	0.12	0.05	0.05	0.01	0.05	0.005	0.51
	5	0.23	1.38	0.017	0.013	0.44	0.12	0.06	0.05	0.01	0.06	0.005	0.50
	6	0.24	1.36	0.015	0.013	0.44	0.12	0.05	0.05	0.01	0.05	0.005	0.50
	7	0.26	1.30	0.031	0.014	0.39	0.10	0.15	0.15	0.04	0.05	0.004	0.54
	8	0.26	1.29	0.030	0.014	0.40	0.10	0.15	0.14	0.04	0.05	0.004	0.54
1B	9	0.23	1.38	0.015	0.013	0.44	0.12	0.05	0.05	0.01	0.05	0.005	0.49
	10	0.26	1.31	0.031	0.014	0.40	0.10	0.15	0.15	0.04	0.05	0.004	0.54
	11	0.26	1.31	0.031	0.014	0.40	0.10	0.15	0.15	0.04	0.05	0.004	0.54
	12	0.25	1.31	0.019	0.013	0.43	0.10	0.13	0.08	0.03	0.06	0.005	0.52
	13	0.25	1.31	0.019	0.013	0.44	0.10	0.13	0.08	0.03	0.06	0.005	0.52
	14	0.23	1.30	0.015	0.020	0.48	0.11	0.06	0.04	0.01	0.05	0.005	0.48
	15	0.26	1.32	0.032	0.014	0.41	0.11	0.16	0.15	0.04	0.06	0.004	0.54
	16	0.24	1.31	0.020	0.021	0.48	0.12	0.05	0.04	0.01	0.05	0.005	0.49

*LECO Analysis

8.1.2. Rod Mill Cooling Data

The rod mill cooling data was obtained using a stationary pyrometer at the exit of the water boxes. The water box 1 and 2 (WB 1 & WB 2) temperatures indicate the temperature of the bar as it exits WB 1 and WB 2 respectively. The aim temperatures for WB1 and WB2 are 970℃ and 950℃ respectively with a tolerance of ± 20℃. Water box temperatures are important because they play a significant role on the final mechanical properties of the bar due to their influence of the cooling rates of the bar. The cooling data of WB 1 and WB 2 are presented in Table 8-4.

Table 8-4: Temperature Data for Trial 1A and 1B

Trial	Coil No	Actual WB Temperatures (°C)	
		WB1	WB2
1A	1	977	948
	2	969	931
	3	970	943
	4	992	955
	5	977	933
	6	1008	967
	7	996	948
	8	1008	967
1B	9	1028	975
	10	1019	972
	11	1040	991
	12	1038	982
	13	1021	972
	14	1039	987
	15	1019	973
	16	1039	985

The cooling data of WB 1 and WB 2 are depicted in Figures 8-1 and 8-2.

Water Box 1

The recommended WB 1 temperature for trial 1A and 1B were 970 ℃ and 990 ℃ respectively. During rolling, a 20 ℃ temperature tolerance is acceptable. This provides a temperature range with a maximum and minimum WB temperature. The temperature ranges for trial 1A and 1B are 990 ℃ – 950 ℃ and 1100 ℃ – 970 ℃ respectively.

From Figure 8-1, it can be seen that cooling temperatures for WB 1 were mostly within tolerance for trial 1A, with 3 coils having temperatures slightly higher than the maximum recommended temperature. The cooling temperatures for WB 1 for trial 1B were all above the maximum recommended temperature.

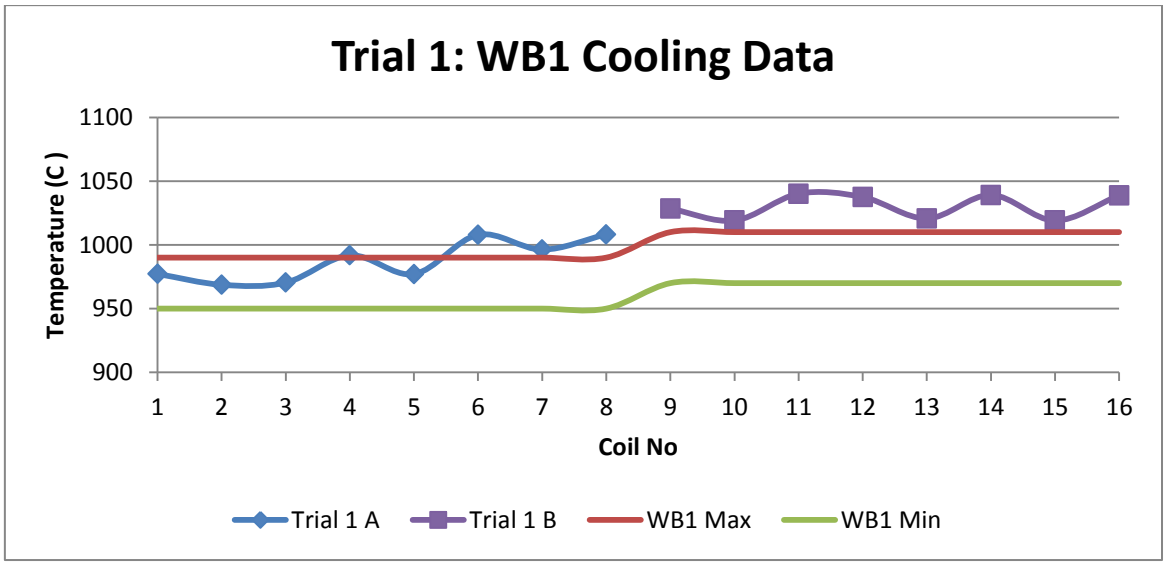

Figure 8-1: Trial 1 Water Box 1 Cooling Data

Water Box 2

The recommended WB2 temperature for trial 1A and 1B were 950 ℃ and 970 ℃ respectively. During rolling, a 20 ℃ temperature tolerance is acceptable. This provides a temperature range with a maximum and minimum WB temperature. The temperature ranges for trial 1A and 1B were 970 ℃ – 930 ℃ and 990 ℃ – 950 ℃ respectively.

From Figure 8-2, it can be seen that cooling temperatures for WB 2 were within tolerance for both trial 1A and 1B.

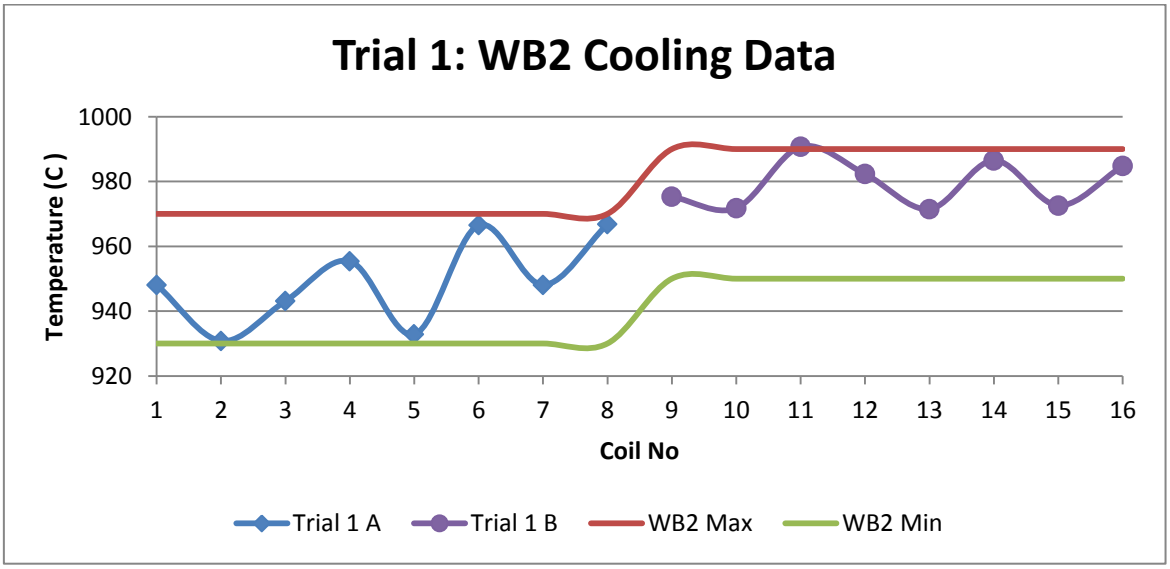

Figure 8-2: Trial 1 Water Box 2 Cooling Data

8.1.3. Mechanical Testing

8.1.3.1. Tensile Test

A tensile test, using a MESSPHYSIK tensile tester, was performed on the samples obtained during trial 1A and 1B. The tensile testing performed was in accordance to the BS 4449: 1997 460B specification. The yield strength results of trial 1A and 1B are presented in Table 8-5.

Table 8-5: Detailed Yield Strength Results for Trial 1A and 1B

Trial	Coil No	%A	% Agt	UTS (MPa)	YS (MPa)
1A	1	21.29	7.81	818.2	649.1
	2	20.93	5.64	854.4	683.0
	3	20.83	9.45	773.2	590.9
	4	20.98	9.98	750.2	553.2
	5	20.55	10.68	780.5	569.9
	6	20.69	8.07	770.5	588.3
	7	20.27	7.84	787.8	628.0
	8	20.43	9.04	805.8	646.1
1B	9	21.07	8.88	797.0	604.4
	10	21.18	9.95	793.3	611.3
	11	21.10	7.27	820.6	661.9
	12	20.95	10.22	769.7	572.7
	13	20.92	9.83	772.2	595.9
	14	20.26	10.22	782.5	580.9
	15	20.08	9.47	801.3	612.6
	16	20.59	11.76	750.1	563.6

The yield strength results for trial 1A and 1B are depicted in Figure 8-3. It can be seen that the yield strength of 4 samples (50%) from trial 1A and 4 samples from trial 1B were above the maximum yield strength of 600 MPa specified as an aim for this work.

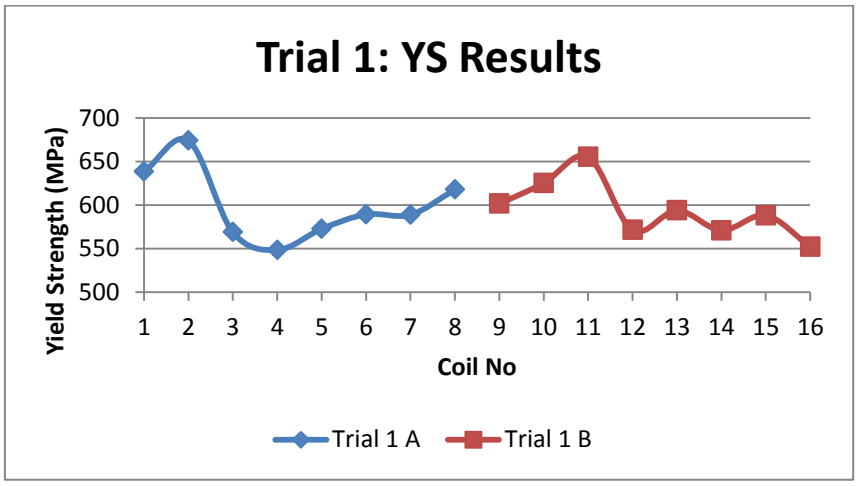

Figure 8-3: Yield Strength results for Trial 1

8.1.3.2. Bend Test

A bend test, using a Cannon Bend Tester, was performed on the samples obtained during trial 1A and 1B. The tensile testing performed was in accordance to the BS 4449: 1997 460B specification. The bend test results of trial 1A and 1B are presented in Table 8-6. It can be seen that in trial 1A, 75% (6 samples) of the coils passed the bend test and in trial 1B 100% (8 samples) of the coils passed the bend test.

Table 8-6: Bend Test Results for Trial 1A and 1B

Trial	Coil No	Sample 1	Sample 2
1A	1	Pass	Pass
	2	Pass	Fail
	3	Pass	Pass
	4	Pass	Pass
	5	Pass	Pass
	6	Pass	Pass
	7	Pass	Pass
	8	Fail	Fail
1B	9	Pass	Pass
	10	Pass	Pass
	11	Pass	Pass
	12	Pass	Pass
	13	Pass	Pass
	14	Pass	Pass
	15	Pass	Pass
	16	Pass	Pass

8.1.4. Metallurgical Testing

8.1.4.1. Microstructural Analysis

Transverse sections were cut from 4 random samples (Coils 2, 4, 10 & 14) for metallographic examination. A metallographic assessment was performed at x200 magnification using an optical microscope indicated by Figure 8-X* (a). Images at x200 magnification give an overview of the microstructure where some phases showing the characteristic traits of typical 0.2% C steel microstructures can be determined. Other phases need to be viewed at a higher magnification to be correctly identified.

A metallographic assessment was performed at x1000 and x5000 magnification using Scanning Electron Microscope (SEM), indicated by Figure 8-X* (b) and Figure 8-X* (c) respectively. At higher magnifications the characteristic traits of typical 0.2% C steel microstructures can be viewed and the microstructures can be correctly identified. The colours of the phases are inverted when using the SEM. The light phases appear to be dark and vice versa. The typical microstructure of a 0.2% C steel at equilibrium conditions is ferrite and pearlite as shown in Figure 5-11.

* Where "X" is the relevant figure number

Sample 2

Figure 8-4 (a) shows a lighter phase, which is ferrite which can be identified as the irregularly shaped white grains. A darker phase which could possibly be pearlite or bainite can also be seen. Figure 8-4 (b) shows a bainitic and ferritic phase. Figure 8-4 (c) shows upper bainite surrounded by the ferrite phase. The characteristic bainite islands can be seen from the small cementite platelets and ferrite needles that are oriented in a parallel manner. Ferrite which is the softer phase is etched more easily and is shown as the darker phase under the SEM.

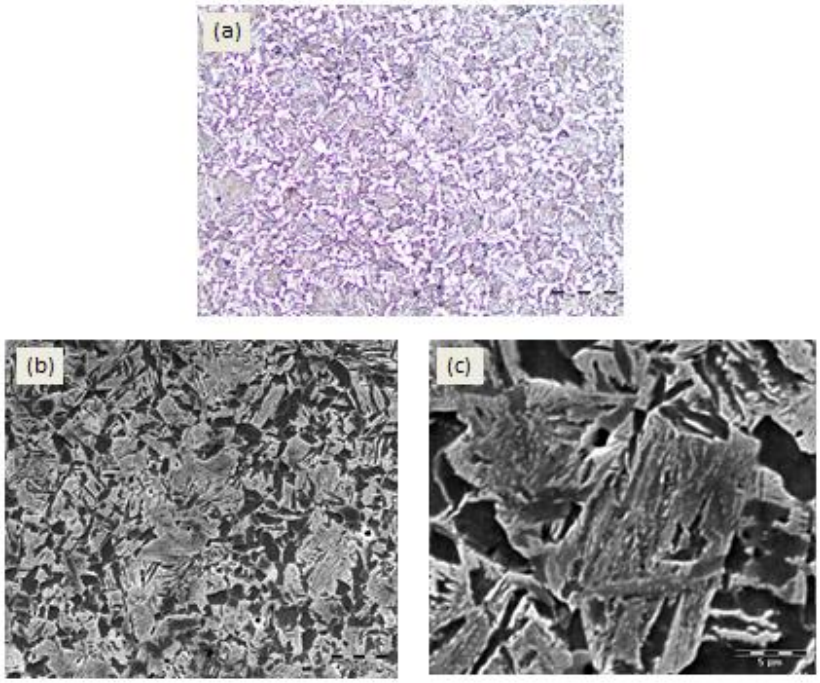

Figure 8-4: Micrograph of sample from Trial 1A, Coil 2 (X 20) Etchant: 2% Nital (a) Optical Microscope, X200; (b) SEM, X1000; (c) SEM, X5000

Sample 4

Figure 8-5 (a) shows a lighter phase, which is ferrite which can be identified as the irregularly shaped white grains. A darker phase which could possibly be pearlite or bainite can also be seen. Figure 8-5 (b) shows 2 phases, namely pearlite and ferrite. Pearlite exhibits the typical lamellae of Fe_3C and ferrite platelets. Figure 8-5 (c) shows grains of ferrite (darker phase) and fine pearlite, with the lamellae of Fe_3C and ferrite platelets being closely packed.

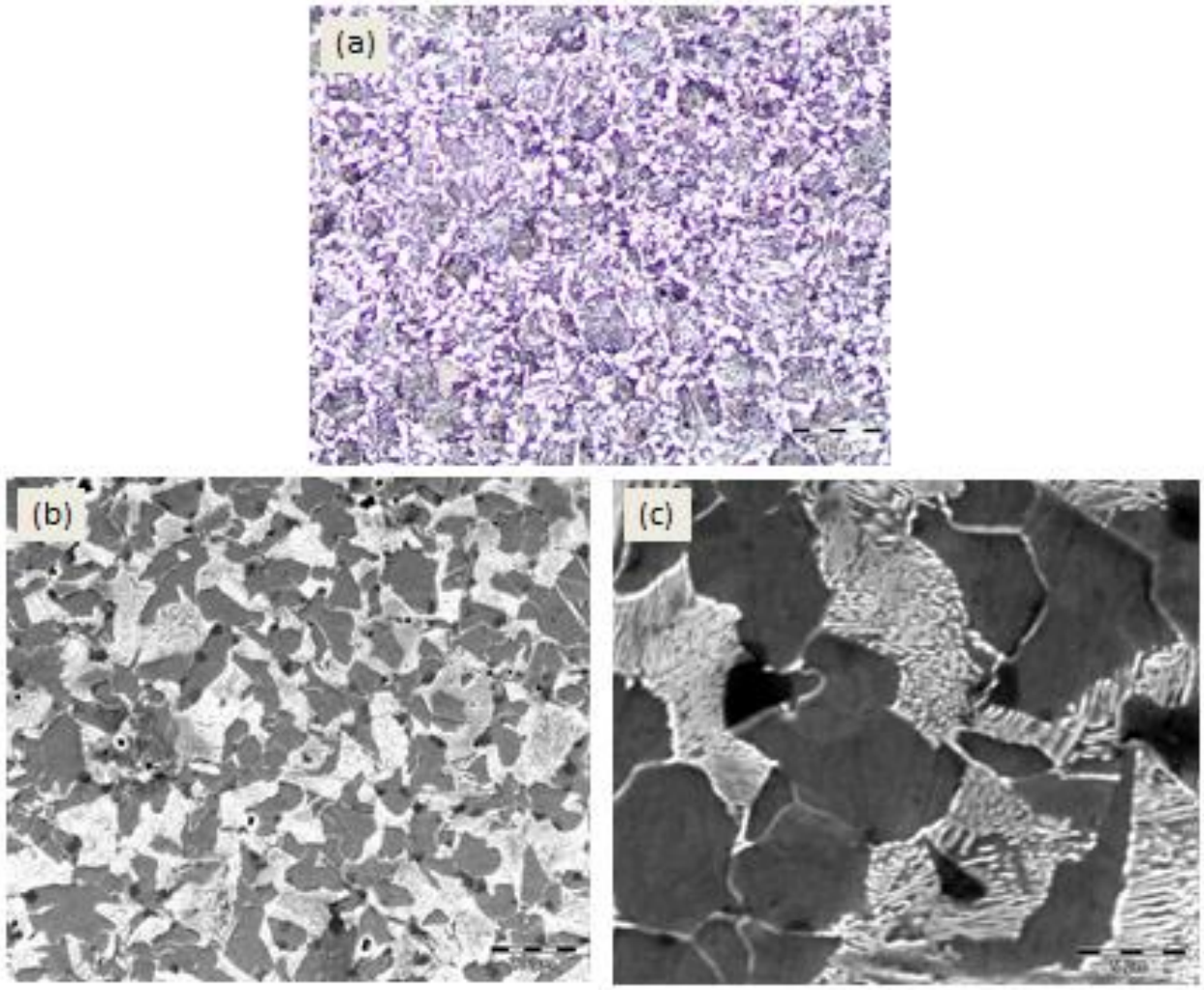

Figure 8-5: Cross-sectional area of sample from Trial 1A, Coil 4 (X 20) Etchant: 2% Nital
(a) Optical Microscope, X200; (b) SEM, X1000; (c) SEM, X5000

Sample 10

Figure 8-6 (a) shows a lighter phase, which is ferrite which can be identified as the white grains. A darker phase which could possibly be pearlite or bainite can also be seen. Figure 8-6 (b) shows a bainitic and ferritic phase. Figure 8-6 (c) shows upper bainite (lighter phase) surrounded by the ferrite phase (darker phase). The cementite platelets and ferrite needles which are characteristic of bainite islands can also be seen.

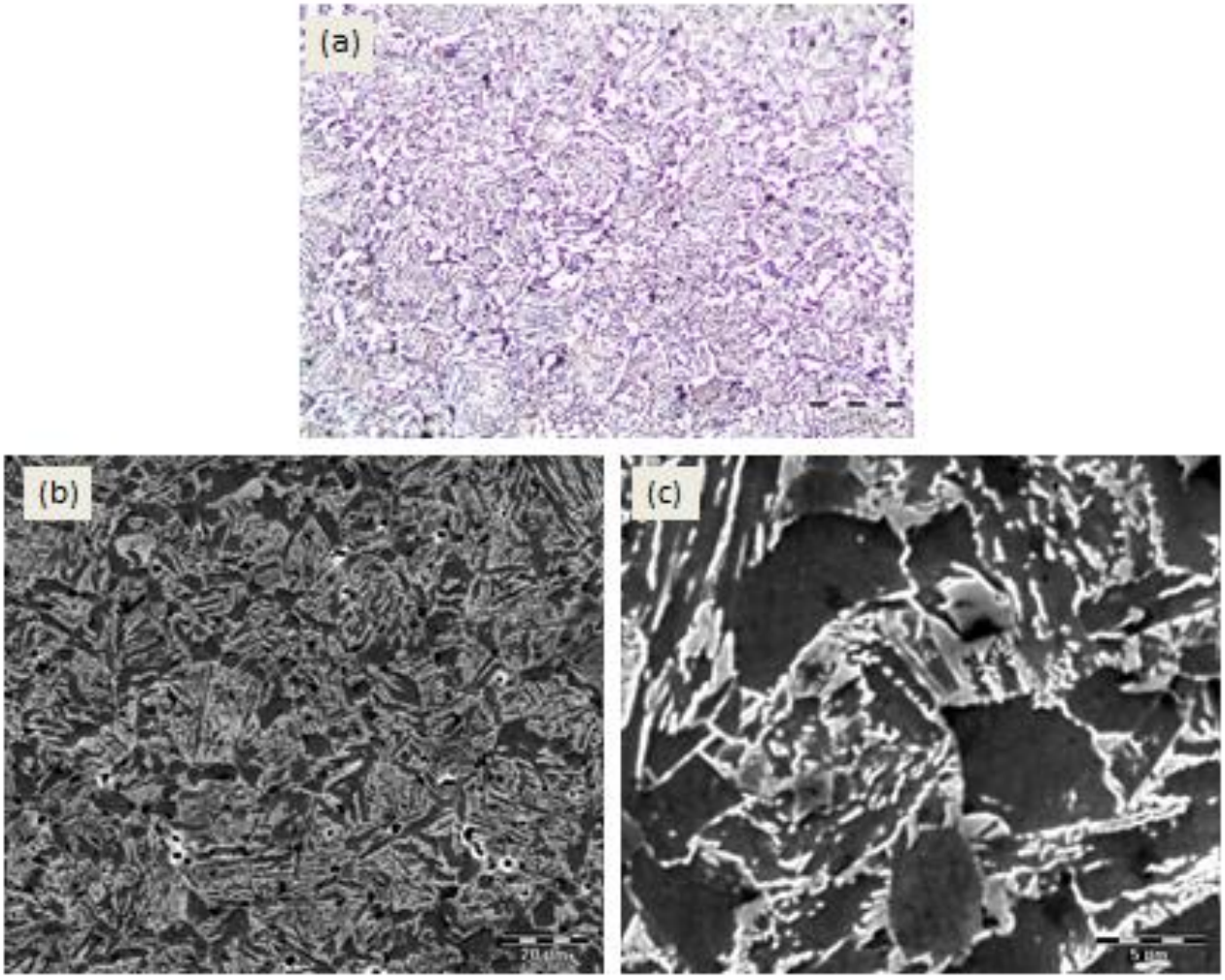

Figure 8-6: Cross-sectional area of sample from Trial 1B, Coil 10 (X 20) Etchant: 2% Nital
(a) Optical Microscope, X200; (b) SEM, X1000; (c) SEM, X5000

Sample 14

Figure 8-7 (a) shows a lighter phase, which is ferrite which can be identified as the white grains. A darker phase which could possibly be pearlite or bainite can also be seen. Figure 8-7 (b) shows 2 phases, namely pearlite (lighter phase) and ferrite (darker phase). Pearlite exhibits the typical lamellae of Fe_3C and ferrite platelets. Figure 8-7 (c) shows grains of fine pearlite, with closely packed lamellae of Fe_3C and ferrite platelets. These pearlite grains are surrounded by ferrite grains.

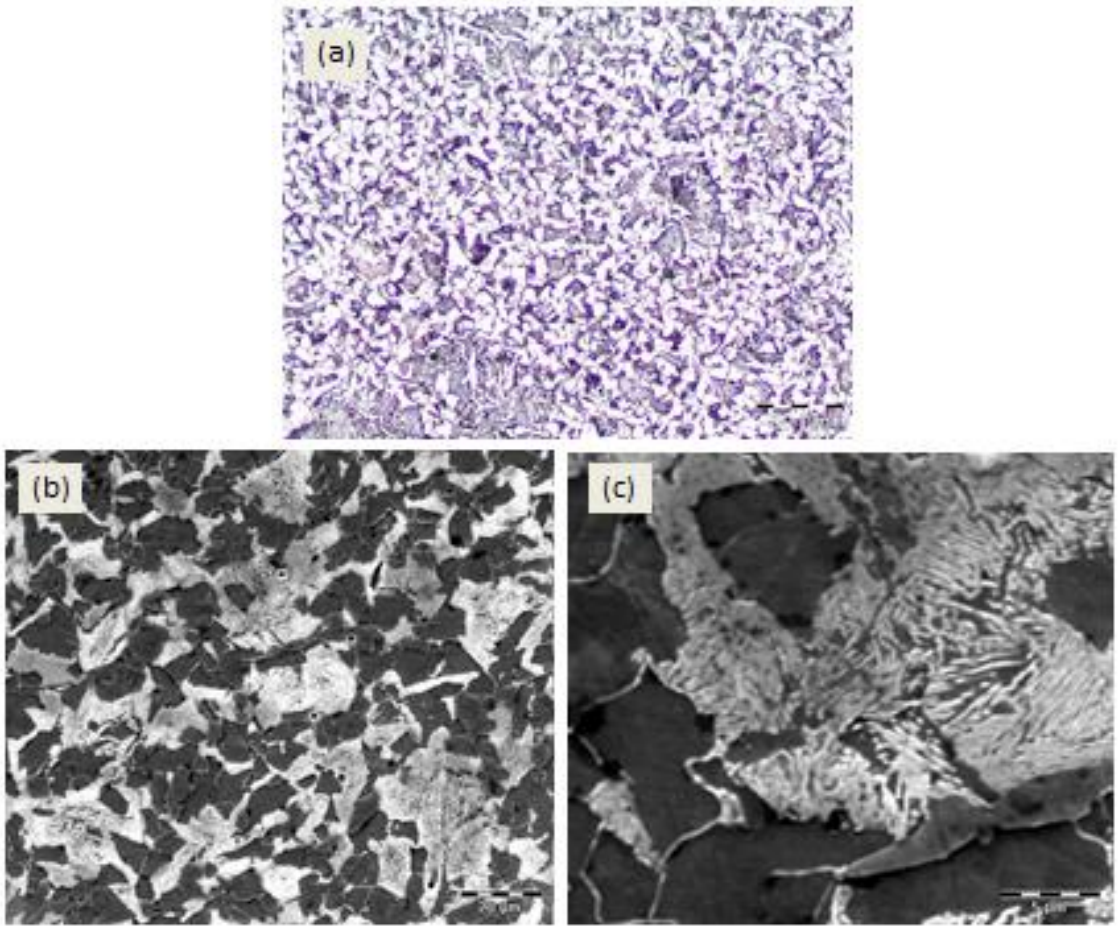

Figure 8-7: Cross-sectional area of sample from Trial 1B, Coil 14 (X 20) Etchant: 2% Nital
(a) Optical Microscope, X200; (b) SEM, X1000; (c) SEM, X5000

8.1.4.2. Phase Analysis

A phase analysis using "analySIS docu", which is an imaging software by Olympus Soft Imaging Solutions, was performed on samples from coils 2, 4, 10 & 14 to determine the percentages of the phases present in the microstructure. The phase percentages and the phase maps are shown in Figure 8-8.

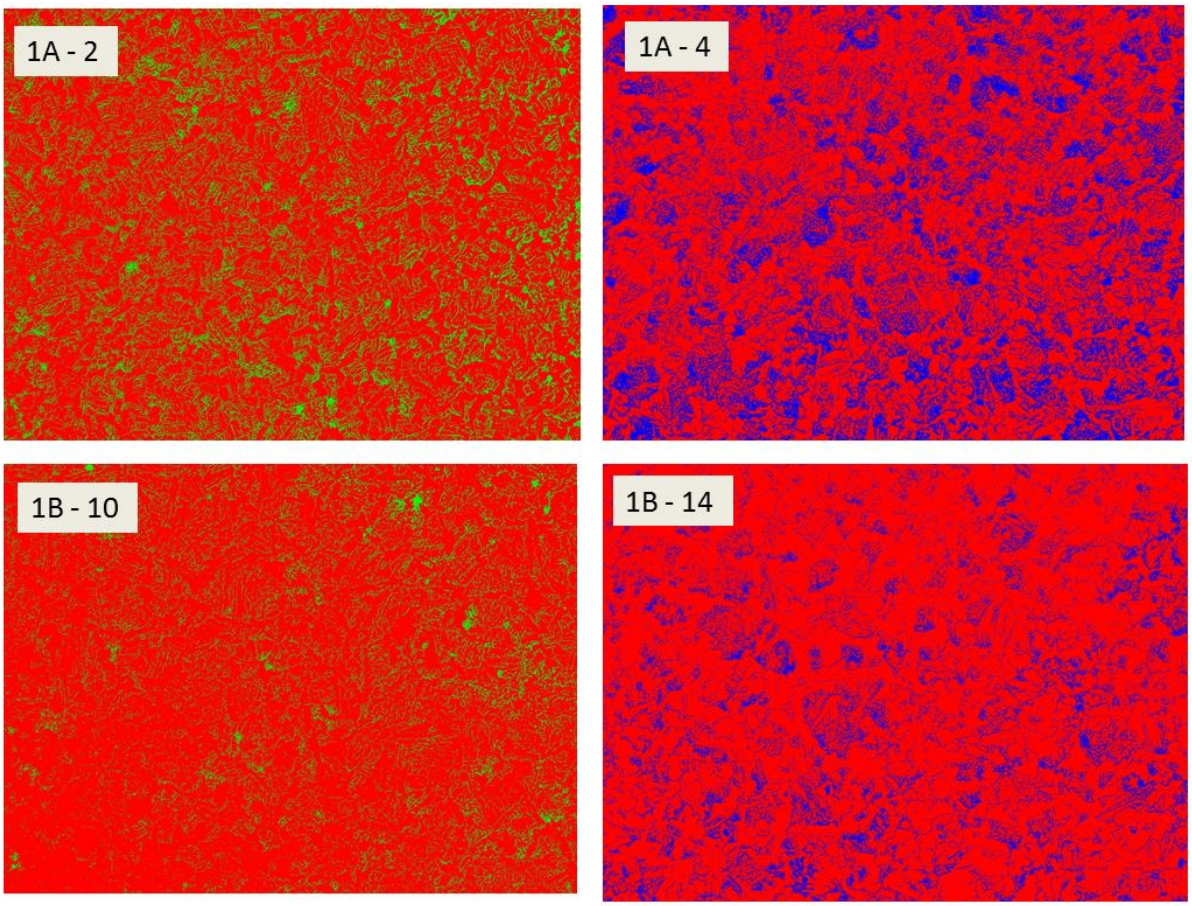

Sample	% Ferrite	% Pearlite	% Bainite
1A-2	82.91	-	17.09
1A-4	75.54	24.46	-
1B-10	90.21	-	9.79
1B-14	87.37	12.63	-

Figure 8-8: Phase analysis of Trial 1A & 1B samples

The samples from trial 1B possess a higher % ferrite and lower % pearlite and % bainite compared to that of trial 1A. There is one sample that contains ferrite and bainite and another sample that contains ferrite and pearlite for both trial 1A and 1B.

8.1.4.3. Grain size

The grain size of the samples from trial 1A and 1B were determined using the Heyn Lineal Intercept Procedure (ASTM E112, Section 5.3.1.), where four 6 inch lines were super-imposed onto the microstructure images of samples 2, 4, 10 and 14 that are presented in Appendix C. The intercept data, the grain size calculation values and the average grain size are tabulated in Table 8-7.

Table 8-7: Grain size calculation data for samples from trial 1A and 1B

Sample	Intercepts per line				Average Intercepts	Line length/ Avg	d (um)
	L1	L2	L3	L4			
1A-2	49	54	58	47	52.00	2.97	14.83
1A-4	49	46	50	43	47.00	3.28	16.40
1B-10	44	53	43	38	44.50	3.47	17.33
1B-14	36	33	28	36	33.25	4.64	23.19

The grain sizes of the samples from trial 1B are larger than those of samples from trial 1A. The grain sizes of the samples from trial 1A vary by 1.57 µm whereas the grain sizes of the samples from trial 1B vary by 5.86 µm.

8.2. Trial 2

The input material for trial 2A and 2B consisted of billets, cast number 9311627, with the 'original' chemical composition described in Table 6-2. This material was rolled using 2 cooling programs, namely CP3 and CP4, described in Table 6-3. The use of the original chemical composition with cooling program CP3 and CP4, constituted Trial 2A and 2B respectively. The billets for trial 2 were rolled into 12mm reinforcing bars. A 12mm sized bar was selected as it is one of the larger sizes available at the rod mill and it would produce lower tensile properties compared to a small rod due to the strain hardening effects during rolling. A summary of trial 2 is presented in Table 8-8.

Table 8-8: Summary of Trial 2

Trial No	Chemical Composition	Cooling Program	Size (mm)	Cast No
2A	Original	CP 3	12	9311627
2B	Original	CP 4		

8.2.1. Chemical Analysis

The chemical composition for Cast 9311627 was determined by using an Optical Emission Spectrometer (OES) and a LECO Combustion analyzer for C and S. The chemical composition for cast 9311627 is shown in Table 8-9.

Table 8-9: Chemical analysis (mass percent) of cast 9311627- Trial 2

C	Mn	P	S	Si	Cu	Ni	Cr	Mo	V	Al
0.25	1.36	0.015	0.012	0.44	0.11	0.04	0.05	0.01	0.05	0.006

The chemical analysis conformed to the BS 4449: 1997 460B specification; however it was out of the aim specification listed in Table 6-2. The Mn composition was 4.64 % higher than the specified maximum of 1.30%.

The chemical analysis of trial 2A and 2B are presented in Table 8-10. The deviation of chemical composition amongst samples belonging to one cast can be attributed to experimental error or poor sampling and preparation methods during LECO and OES Analysis or segregation that occurred at the caster.

Table 8-10: Chemical Analysis (mass percent) for Trial 2A and 2B

Trial	Coil No	C*	Mn	P	S*	Si	Cu	Ni	Cr	Mo	V	Al	CE
2A	1	0.25	1.44	0.015	0.007	0.46	0.12	0.05	0.05	0.01	0.05	0.005	0.52
	2	0.23	1.28	0.015	0.010	0.41	0.11	0.05	0.04	0.01	0.05	0.004	0.48
	3	0.24	1.28	0.016	0.010	0.41	0.11	0.05	0.04	0.01	0.05	0.004	0.48
	4	0.26	1.33	0.013	0.015	0.43	0.10	0.07	0.05	0.01	0.05	0.008	0.51
	5	0.23	1.28	0.016	0.009	0.41	0.11	0.05	0.04	0.01	0.05	0.005	0.48
	6	0.25	1.29	0.015	0.010	0.41	0.11	0.05	0.04	0.01	0.05	0.004	0.49
	7	0.25	1.35	0.013	0.015	0.44	0.11	0.06	0.05	0.01	0.05	0.009	0.51
	8	0.25	1.36	0.014	0.015	0.45	0.12	0.06	0.04	0.01	0.05	0.010	0.51
2B	9	0.25	1.37	0.013	0.015	0.44	0.12	0.06	0.04	0.01	0.05	0.010	0.51
	10	0.26	1.32	0.014	0.015	0.43	0.10	0.07	0.05	0.02	0.05	0.006	0.52
	11	0.27	1.34	0.016	0.015	0.44	0.10	0.07	0.05	0.02	0.05	0.005	0.53
	12	0.27	1.32	0.014	0.014	0.44	0.10	0.07	0.05	0.02	0.05	0.006	0.52
	13	0.24	1.57	0.017	0.006	0.48	0.13	0.06	0.05	0.01	0.05	0.006	0.54
	14	0.24	1.56	0.017	0.006	0.47	0.13	0.06	0.05	0.01	0.05	0.005	0.54
	15	0.27	1.32	0.014	0.014	0.43	0.09	0.07	0.05	0.02	0.05	0.005	0.52

*LECO Analysis

8.2.2. Rod Mill Cooling Data

A description of the acquiring of water box temperatures is presented in section 8.1.2. The aim temperatures for WB1 and WB2 are 1000℃ and 980℃ respectively with a tolerance of ± 20℃. The cooling data of WB 1 and WB 2 are presented in Table 8-11.

Table 8-11: Temperature Data for Trial 2A and 2B

Trial	Coil No	Actual WB Temperatures (°C)	
		WB1	WB2
2A	1	1017	962
	2	1030	977
	3	1007	962
	4	1009	978
	5	1010	958
	6	1015	984
	7	1012	958
	8	1009	963
2B	9	1007	979
	10	1006	952
	11	1011	981
	12	1007	952
	13	1015	956
	14	1025	985
	15	1016	958

The cooling data of WB 1 and WB 2 are presented in Figures 8-9 and 8-10.

Water Box 1

The recommended WB 1 temperature for trial 2A and 2B were both 1000 ℃. During rolling, a 20℃ temperature tolerance is acceptable. This provides a temperature range with a maximum and minimum WB temperature. The temperature ranges for trial 2A and 2B were both 1020 ℃ - 980℃.

From Figure 8-9, it can be seen that cooling temperatures for WB 1 were mostly within tolerance for trial 2A and 2B, with only 1 coil each having a temperature slightly higher than the maximum recommended temperature.

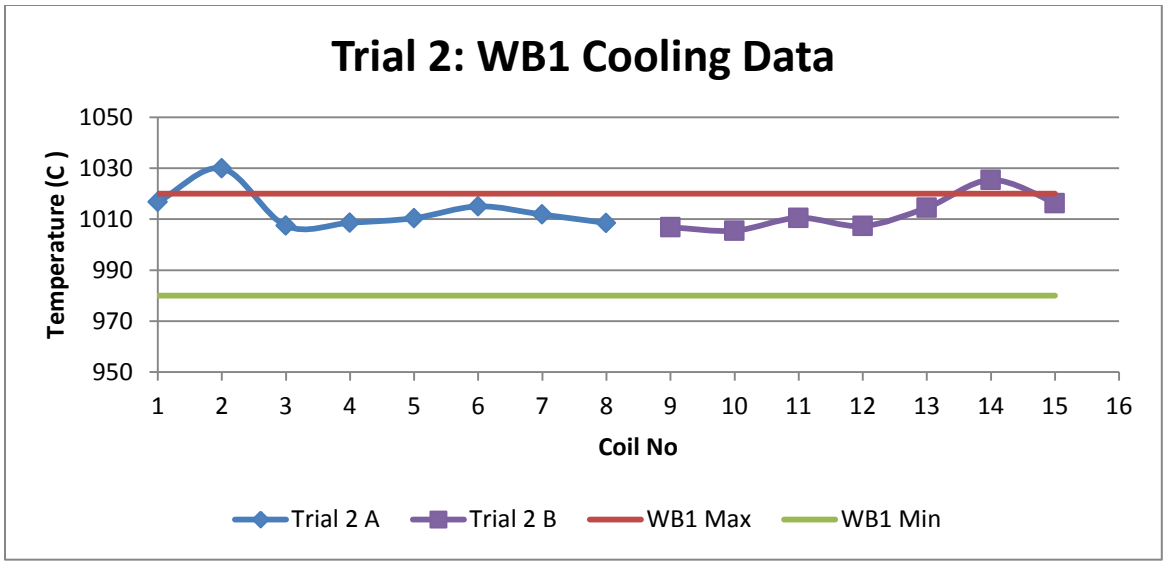

Figure 8-9: Trial 2 Water Box 1 Cooling Data

Water Box 2

The recommended WB 2 temperature for trial 2A and 2B were both 980 ℃. During rolling, a 20℃ temperature tolerance is acceptable. This provides a temperature range with a maximum and minimum WB temperature. The temperature ranges for trial 2A and 2B were both 1000 ℃ - 960 ℃.

From Figure 8-10, it can be seen that cooling temperatures for WB 2 were within tolerance for trial 2A but trial 2B had 3 coils with WB 2 temperatures slightly lower than the minimum recommended temperature.

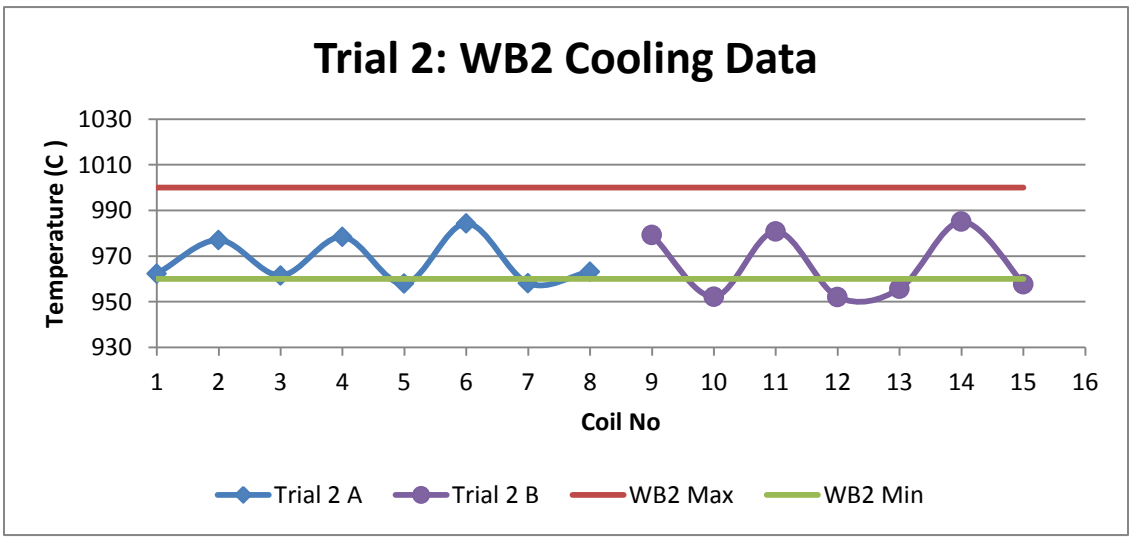

Figure 8-10: Trial 2 Water Box 2 Cooling Data

8.2.3. Mechanical Testing

8.2.3.1. Tensile Test

The yield strength results of trial 2A and 2B are presented in Table 8-12. These samples were tested using the same equipment and specifications as described in section 8.1.3.1.

Table 8-12: Yield Strength Results for Trial 2A and 2B

Trial	Coil No	%A	% Agt	UTS (MPa)	YS (MPa)
2A	1	23.88	16.59	730.8	489.1
	2	25.50	16.20	687.5	475.5
	3	24.84	16.57	695.9	484.7
	4	25.33	15.87	736.8	520.0
	5	26.24	16.17	685.9	467.0
	6	25.84	17.04	688.9	470.0
	7	26.12	14.50	725.9	509.1
	8	26.17	15.95	736.8	506.0
2B	9	24.58	16.01	734.9	497.6
	10	25.21	16.19	727.3	402.7
	11	24.50	15.86	736.2	513.1
	12	26.34	15.95	715.6	393.7
	13	24.92	14.56	742.9	494.6
	14	25.38	16.23	749.2	519.2
	15	26.00	17.37	720.8	498.6

The yield strength results for trial 2A and 2B are depicted in Figure 8-11. It can be seen that 100% of the material (15 samples) for trial 2A and 2B were below 600 MPa.

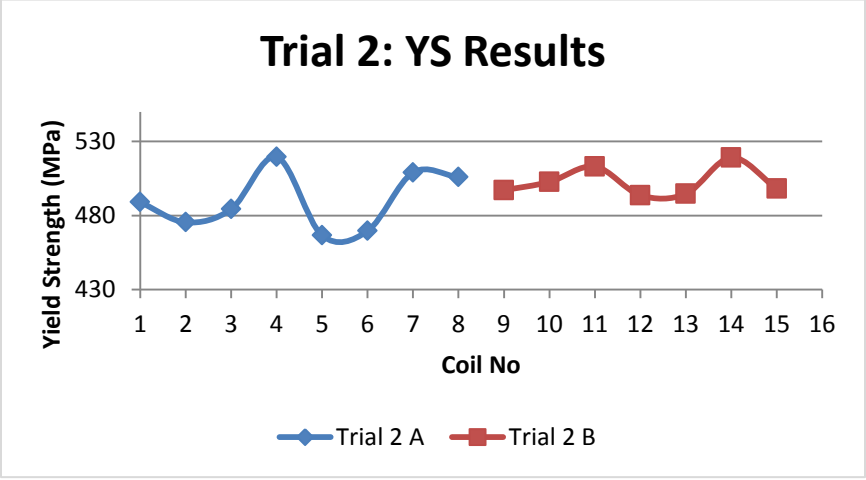

Figure 8-11: Yield Strength results for Trial 2

8.2.3.2. Bend Test

The bend test results of trial 2A and 2B are presented in Table 8-13. These samples were tested using the same equipment and specifications as described in section 8.1.3.2. It can be seen that 100% (15 samples) of the material for trial 2A and 2B passed the bend test.

Table 8-13: Bend Test Results for Trial 2A and 2B

Trial	Coil No	Sample 1	Sample 2
2A	1	Pass	Pass
	2	Pass	Pass
	3	Pass	Pass
	4	Pass	Pass
	5	Pass	Pass
	6	Pass	Pass
	7	Pass	Pass
	8	Pass	Pass
2B	9	Pass	Pass
	10	Pass	Pass
	11	Pass	Pass
	12	Pass	Pass
	13	Pass	Pass
	14	Pass	Pass
	15	Pass	Pass

8.2.4. Metallurgical Testing

8.2.4.1. Microstructural Analysis

Transverse sections were cut from 4 random samples (Coils 2, 4, 10 & 14) for metallographic examination. A metallographic assessment was performed according to the description in 8.1.4.1. with the same magnifications and corresponding labeling of figures.

Sample 2, 4, 10 and 14

The microstructures of samples from samples 2, 4, 10 and 14 have similar traits and the results for these samples will be grouped. Figures 8-12, 8-13, 8-14 and 8-15 (a) shows a lighter phase, which is ferrite which can be identified as the irregularly shaped white grains. A darker phase which could possibly be pearlite or bainite can also be seen. Figures 8-12, 8-13, 8-14 and 8-15 (b) show two phases, namely pearlite and ferrite. Pearlite exhibits the typical lamellae of Fe_3C and ferrite platelets. Figures 8-12, 8-13, 8-14 and 8-15 (c) show grains of fine pearlite, with the lamellae of Fe_3C and ferrite platelets being closely packed. These pearlite grains are surrounded by ferrite grains. The samples from trial 2B (samples 10 & 14) seem to have a finer grained structure compared to that of trial 2A (samples 2 & 4).

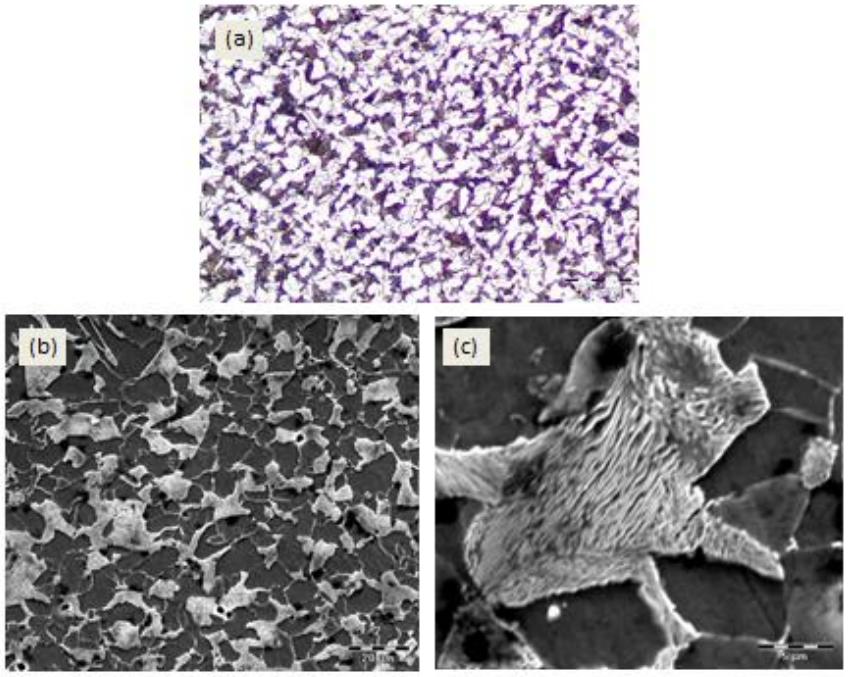

Figure 8-12: Cross-sectional area of sample from Trial 2A, Coil 2 (X 20) Etchant: 2% Nital (a) Optical Microscope, X200; (b) SEM, X1000; (c) SEM, X5000

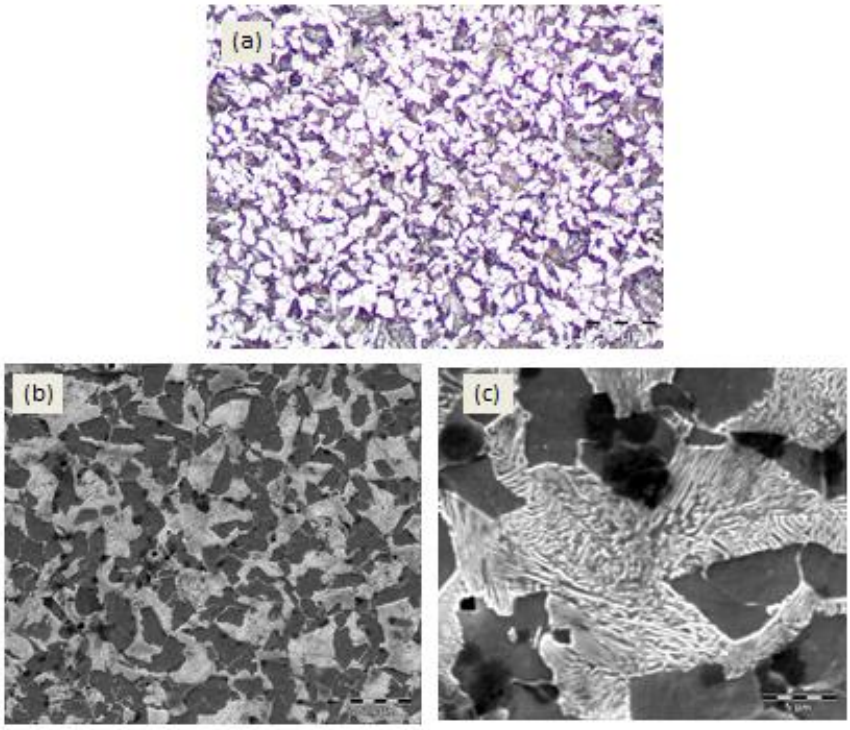

Figure 8-13: Cross-sectional area of sample from Trial 2A, Coil 4 (X 20) Etchant: 2% Nital (a) Optical Microscope, X200; (b) SEM, X1000; (c) SEM, X5000

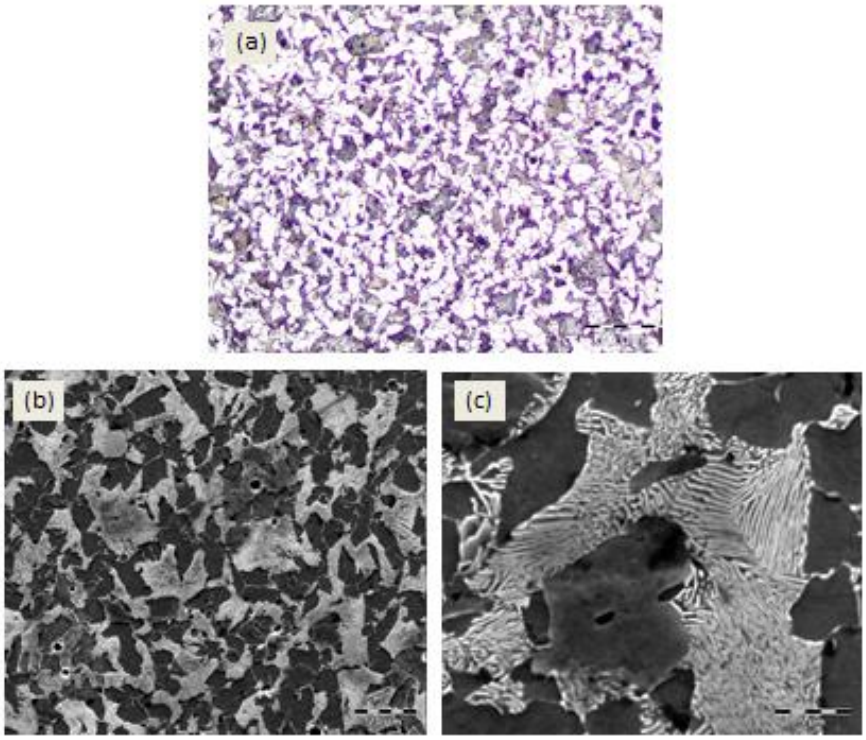

Figure 8-14: Cross-sectional area of sample from Trial 2B, Coil 10 (X 20) Etchant: 2% Nital (a) Optical Microscope, X200; (b) SEM, X1000; (c) SEM, X5000

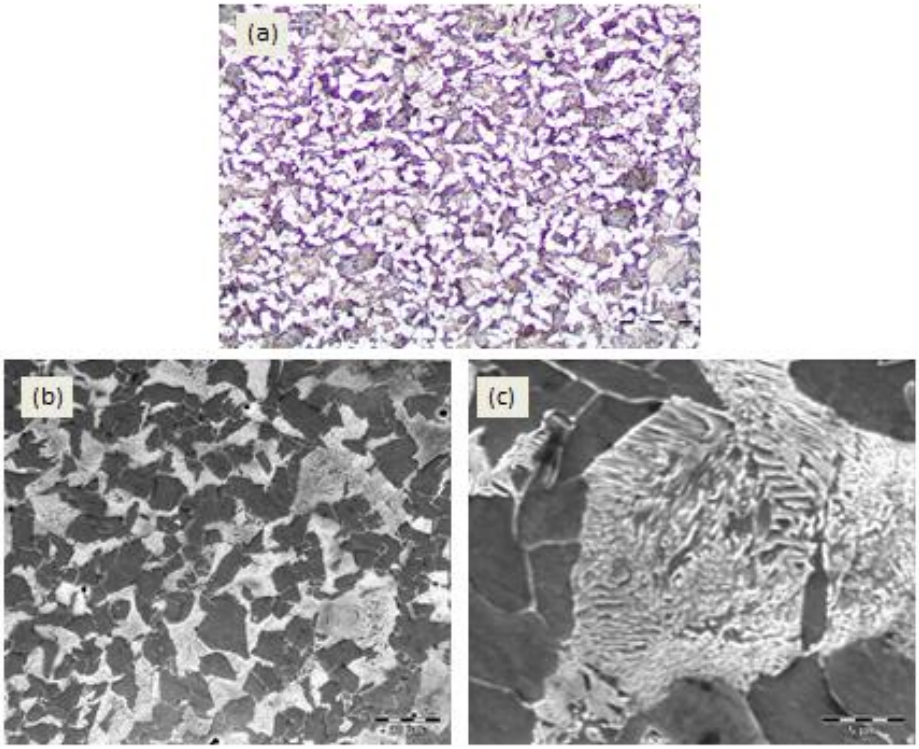

Figure 8-15: Cross-sectional area of sample from Trial 2B, Coil 14 (X 20) Etchant: 2% Nital (a) Optical Microscope, X200; (b) SEM, X1000; (c) SEM, X5000

8.2.4.2. Phase Analysis

A phase analysis was performed on samples from coils 2, 4, 10 & 14 according to the description in 8.1.4.2. The phase percentages and the phase maps are shown in Figure 8-16. It can be seen that the samples from trial 2B possess a higher % ferrite and lower % pearlite compared to that of trial 2A.

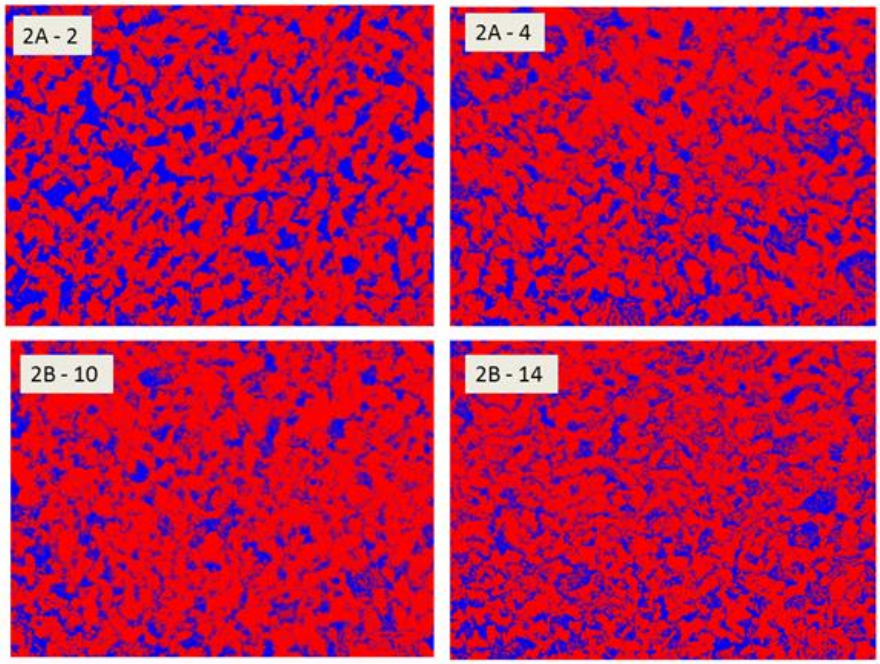

Sample	% Ferrite	% Pearlite	% Bainte
2A-2	70.05	29.95	-
2A-4	73.9	26.1	-
2B-10	78.4	21.6	-
2B-14	74.37	25.63	-

Figure 8-16: Phase analysis of Trial 2A & 2B samples

8.2.4.3. Grain size

The grain size of the samples from trial 2A and 2B were determined according to the procedure described in 8.1.4.3. The intercept data, the grain size calculation values and the average grain size are tabulated in Table 8-14. The grain sizes of the samples from trial 2A and 2B vary by ± 3µm. The largest grain size for the abovementioned trials is 23.19 µm (sample 2A-4).

Table 8-14: Grain size calculation data for samples from trial 2A and 2B

Sample	Intercepts per line				Average Intercepts	Line length/ Avg	d (um)
	L1	L2	L3	L4			
2A-2	37	37	38	37	37.25	4.14	20.70
2A-4	38	33	30	32	33.25	4.64	23.19
2B-10	35	34	36	37	35.50	4.34	21.72
2B-14	42	46	41	42	42.75	3.61	18.04

8.3. Trial 3

The input material for trial 3A and 3B consisted of billets, cast number 9311629, with the optimized chemical composition described in Table 6-2. This material was rolled using 2 cooling programs, namely CP1 and CP5, described in Table 6-3. The use of the optimized chemical composition with cooling program CP1 and CP5, constituted Trial 3A and 3B respectively. The billets for trial 3 were rolled into 6mm reinforcing bars. A 6mm sized bar was selected as it is one of the smaller sizes available at the rod mill and it would produce higher tensile properties compared to a large rod due to the strain hardening effects during rolling. Higher tensile properties are preferable for this trial as it will give an indication of whether the maximum yield strength attained is less than 600 MPa. A summary of trial 3 is presented in Table 8-15.

Table 8-15: Summary of Trial 3

Trial No	Chemical Composition	Cooling Program	Size (mm)	Cast No
3A	Optimized	CP 1	6	9311629
3B	Optimized	CP 5		

8.3.1. Chemical Analysis

The chemical composition for Cast 9311429 was determined by using an Optical Emission Spectrometer (OES) and a LECO Combustion analyzer for C and S. The chemical composition for cast 9311429 is shown in Table 8-16.

Table 8-16: Chemical analysis (mass percent) of cast 9311629- Trial 3

C	Mn	P	S	Si	Cu	Ni	Cr	Mo	V	Al
0.24	1.23	0.014	0.012	0.44	0.10	0.05	0.06	0.02	0.05	0.005

The chemical analysis conforms to the BS 4449: 1997 460B specification; however it is out of the aim specification for the 'optimized' chemical composition listed in Table 6-2. The C composition is 4.35 % higher than the specified maximum of 0.23%.

The chemical analysis of trial 3A and 3B are presented in Table 8-17. The deviation of chemical composition amongst samples belonging to one cast can be attributed to experimental error or poor sampling and preparation methods during LECO and OES Analysis or segregation that occurred at the caster.

Table 8-17: Chemical Analysis (mass percent) for Trial 3A and 3B

Trial	Coil No	C*	Mn	P	S*	Si	Cu	Ni	Cr	Mo	V	Al	CE
3A	1	0.23	1.22	0.012	0.010	0.44	0.10	0.05	0.06	0.02	0.05	0.005	0.47
	2	0.23	1.23	0.013	0.010	0.44	0.10	0.05	0.06	0.02	0.05	0.005	0.47
	3	0.28	1.25	0.013	0.009	0.46	0.10	0.05	0.06	0.02	0.05	0.005	0.53
	4	0.25	1.22	0.014	0.013	0.43	0.10	0.06	0.06	0.02	0.05	0.005	0.49
	5	0.23	1.21	0.012	0.013	0.43	0.10	0.06	0.06	0.02	0.05	0.005	0.47
	6	0.23	1.20	0.012	0.014	0.42	0.10	0.05	0.06	0.02	0.05	0.005	0.47
	7	0.23	1.22	0.013	0.013	0.43	0.10	0.06	0.06	0.02	0.05	0.005	0.47
3B	10	0.23	1.23	0.013	0.010	0.44	0.10	0.05	0.06	0.02	0.05	0.005	0.47
	11	0.25	1.24	0.019	0.015	0.42	0.08	0.05	0.07	0.02	0.05	0.005	0.49
	13	0.25	1.24	0.019	0.015	0.43	0.08	0.05	0.07	0.02	0.05	0.005	0.49
	14	0.25	1.25	0.019	0.016	0.43	0.08	0.05	0.07	0.02	0.05	0.004	0.49
	15	0.24	1.23	0.012	0.008	0.45	0.10	0.05	0.06	0.02	0.05	0.005	0.48

*LECO Analysis

8.3.2. Rod Mill Cooling Data

A description of the acquiring of water box temperatures is presented in section 8.1.2. The aim temperatures for WB1 and WB2 are 970℃ and 950℃ respectively with a tolerance of ±20℃. The cooling data of WB 1 and WB 2 are presented in Table 8-18.

Table 8-18: Temperature Data for Trial 3A and 3B

Trial	Coil No	Actual WB Temperatures (°C)	
		WB1	WB2
3A	1	981	949
	2	983	955
	3	988	950
	4	983	955
	5	993	946
	6	984	957
	7	1000	953
	8	980	952
3B	9	996	960
	10	989	966
	11	987	968
	12	988	979
	13	987	967
	14	991	969
	15	1002	975

The cooling data of WB 1 and WB 2 are presented if Figures 8-11 and 8-12.

Water Box 1

The recommended WB 1 temperature for trial 3A and 3B were both 970 ℃. During rolling, a 20℃ temperature tolerance is acceptable. This provides a temperature range with a maximum and minimum WB temperature. The temperature ranges for trial 3A and 3B were 990 ℃ – 950℃.

From Figure 8-17, it can be seen that cooling temperatures for WB 1 were mostly within tolerance for trial 3A, with 2 coils having temperatures slightly higher than the maximum recommended temperature. The cooling temperatures for WB 1 for trial 3B were all within tolerance.

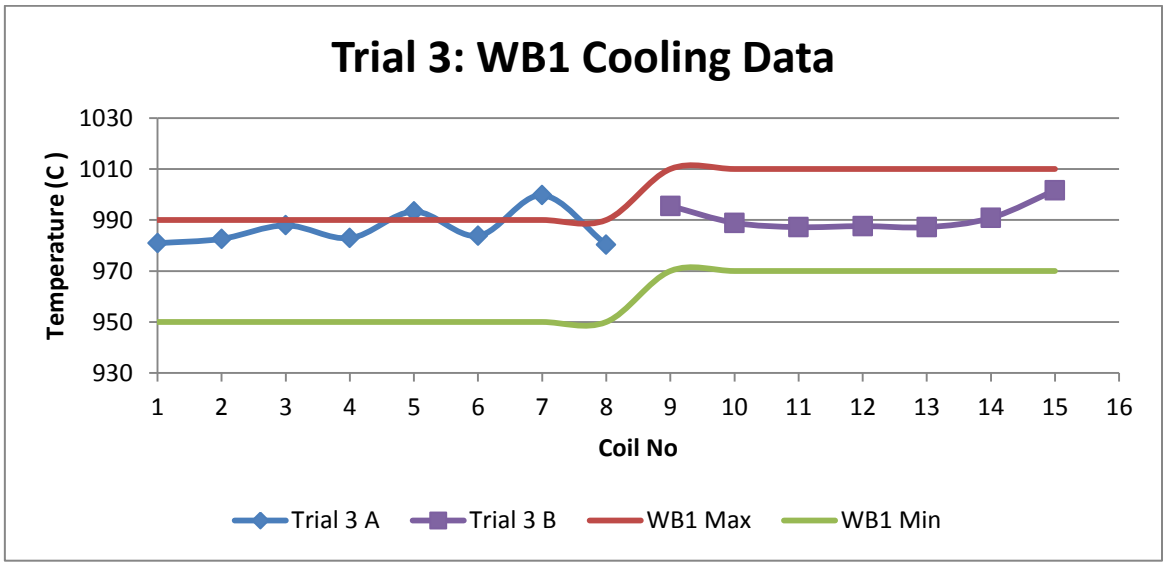

Figure 8-17: Trial 3 Water Box 1 Cooling Data

Water Box 2

The recommended WB 2 temperature for trial 3A and 3B were both 950 ℃. During rolling, a 20 ℃ temperature tolerance is acceptable. This provides a temperature range with a maximum and minimum WB temperature. The temperature ranges for trial 3A and 3B are 970 ℃ – 930℃.

From Figure 8-18, it can be seen that cooling temperatures for WB 2 were within tolerance for both trial 3A and 3B.

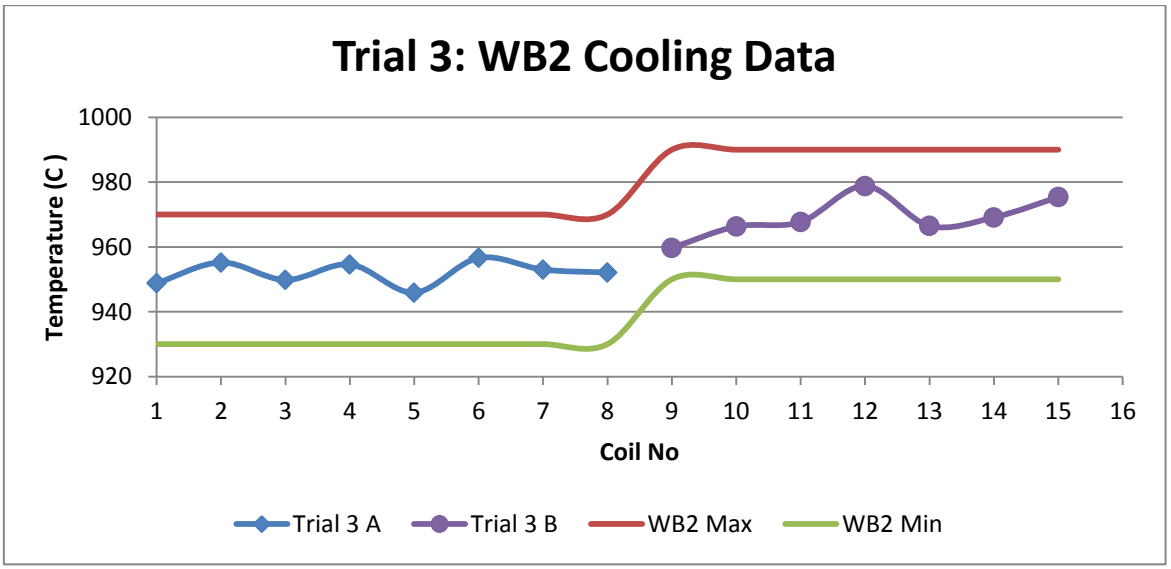

Figure 8-18: Trial 3 Water Box 2 Cooling Data

8.3.3. Mechanical Testing

8.3.3.1. Tensile Test

The yield strength results of trial 3A and 3B are presented in Table 8-19. These samples were tested using the same equipment and specifications as described in section 8.1.3.1.

Table 8-19: Yield Strength Results for Trial 3A and 3B

Trial	Coil No	%A	% Agt	UTS (MPa)	YS (MPa)
3A	1	26.12	11.15	798.5	528.7
	2	27.34	9.48	793.5	552.0
	3	26.10	9.71	798.3	540.4
	4	27.45	12.20	769.2	534.2
	5	27.97	9.40	762.0	524.3
	6	26.65	11.98	777.8	535.4
	7	25.62	10.41	763.9	525.3
	8	27.82	9.73	767.8	534.1
3B	9	26.17	11.70	737.9	544.6
	10	25.83	11.84	751.1	535.1
	11	26.12	10.77	761.0	551.4
	12	26.67	10.31	764.7	549.4
	13	26.00	8.47	782.0	566.8
	14	26.67	10.72	778.4	552.6
	15	26.65	10.93	735.5	539.9

The yield strength results for trial 3A and 3B are depicted in Figure 8-19. It can be seen that 100% of the material for trial 3A and 3B (15 samples) were below 600 MPa.

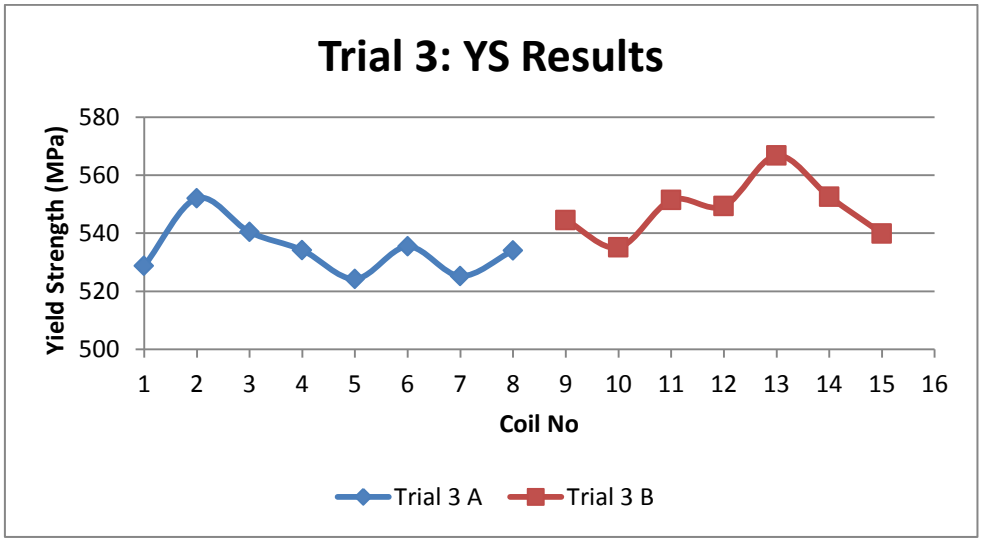

Figure 8-19: Yield Strength results for Trial 3

8.3.3.2. Bend Test

The bend test results of trial 3A and 3B are presented in Table 8-20. These samples were tested using the same equipment and specifications as described in section 8.1.3.2. It can be seen that 100% of the material for trial 3A and 3B (15 samples) passed the bend test.

Table 8-20: Bend Test Results for Trial 3A and 3B

Trial	Coil No	Sample 1	Sample 2
3A	1	Pass	Pass
	2	Pass	Pass
	3	Pass	Pass
	4	Pass	Pass
	5	Pass	Pass
	6	Pass	Pass
	7	Pass	Pass
	8	Pass	Pass
3B	9	Pass	Pass
	10	Pass	Pass
	11	Pass	Pass
	12	Pass	Pass
	13	Pass	Pass
	14	Pass	Pass
	15	Pass	Pass

8.3.4. Metallurgical Testing

8.3.4.1. Microstructural Analysis

Transverse sections were cut from 4 random samples (Coils 2, 4, 10 & 14) for metallographic examination. A metallographic assessment was performed according to the description in 8.1.4.1. with the same magnifications and corresponding labeling of figures.

Sample 2

Figure 8-20 (a) shows a lighter phase which is ferrite as it can be identified as the white grains which is characteristic of 0.2% C steel. A darker phase which could possibly be pearlite or bainite can also be seen. Figure 8-20 (b) shows a bainitic (lighter phase) and ferritic phase (darker phase). Figure 8-20 (c) shows upper bainite surrounded by the ferrite phase. Small cementite platelets and ferrite needles can be seen in the bainite phase.

Sample 4

Figure 8-21 (a) shows a lighter phase which is ferrite and a darker phase, which could possibly be pearlite or bainite. Figure 8-21 (b) shows a bainitic (lighter phase) and ferritic phase (darker phase). Figure 8-21 (c) shows upper bainite surrounded by the ferrite phase. Small cementite platelets and ferrite needles can be seen in the bainite phase; however they are more feathery than that seen in sample 2. There is more ferrite present in this bainitic phase. The bainitic phase in this sample looks similar to pearlite but no parallel pearlite lamellae could be seen.

Sample 10 and 14

Figures 8-22 and 8-23 (a) shows a lighter phase which is ferrite and a darker phase, which could possibly be pearlite or bainite. Figures 8-22 and 8-23 (b) shows a pearlitic (darker phase) and ferritic phase (lighter phase). Figures 8-22 and 8-23 (c) shows pearlite in a ferrite matrix. The pearlite of sample 10 (Figure 8-22 (c)) is coarser that that of sample 14 (Figure 8-23 (c)), which means that the lamellae spacing is larger.

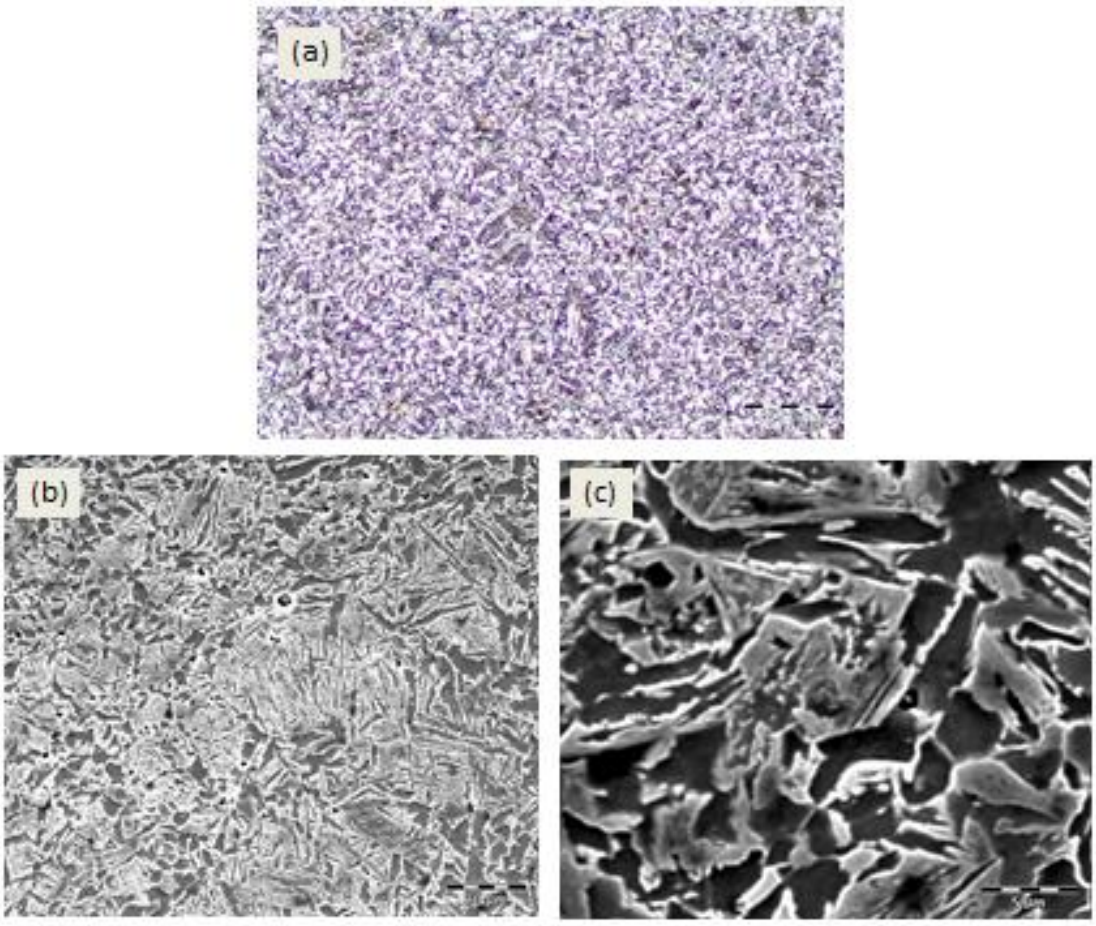

Figure 8-20: Cross-sectional area of sample from Trial 3A, Coil 2 (X 20) Etchant: 2% Nital
(a) Optical Microscope, X200; (b) SEM, X1000; (c) SEM, X5000

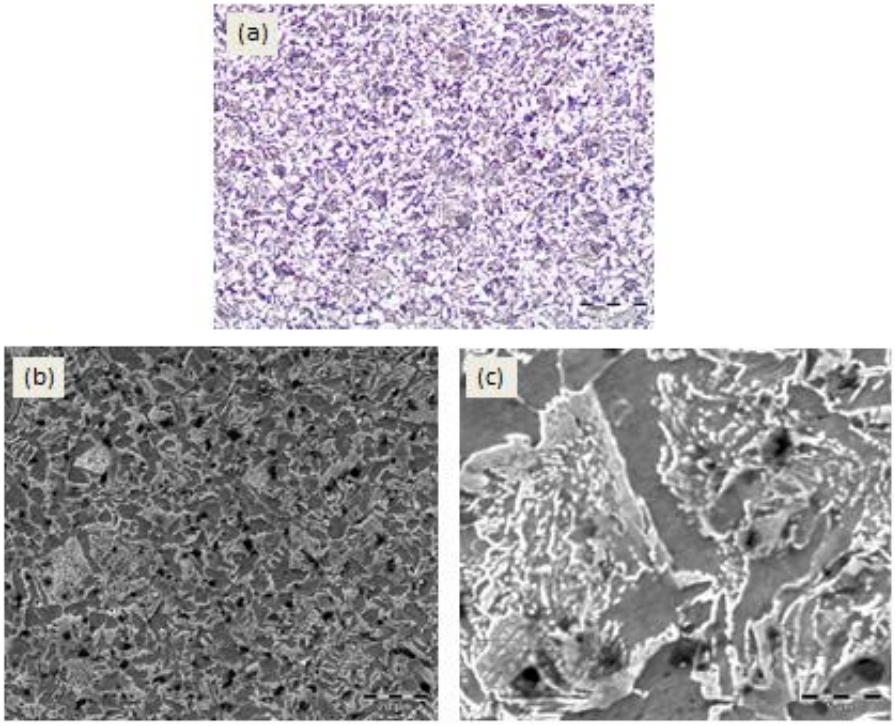

Figure 8-21: Cross-sectional area of sample from Trial 3A, Coil 4 (X 20) Etchant: 2% Nital
(a) Optical Microscope, X200; (b) SEM, X1000; (c) SEM, X5000

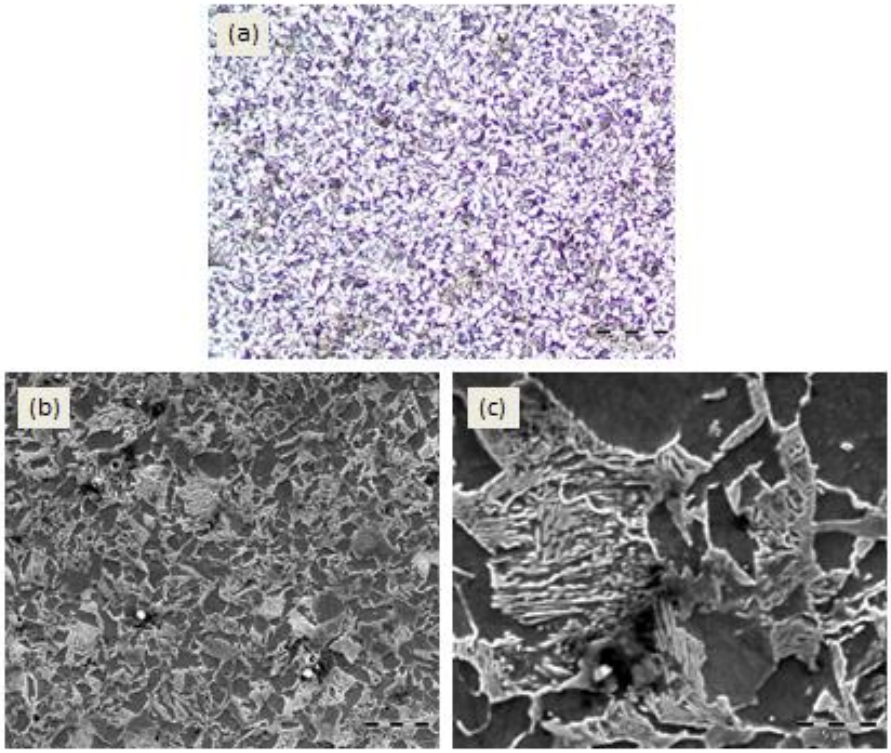

Figure 8-22: Cross-sectional area of sample from Trial 3B, Coil 10 (X 20) Etchant: 2% Nital
(a) Optical Microscope, X200; (b) SEM, X1000; (c) SEM, X5000

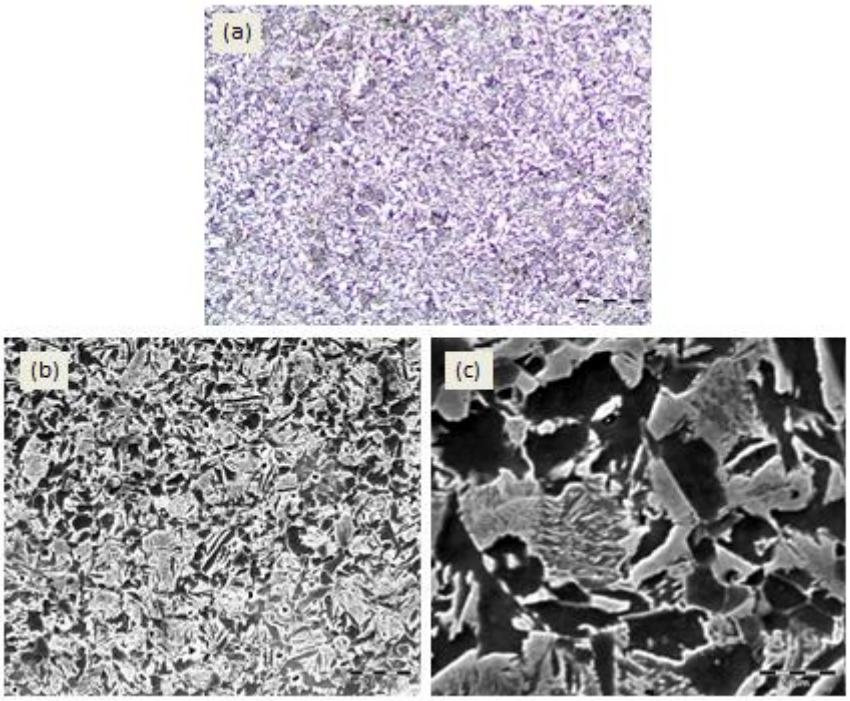

Figure 8-23: Cross-sectional area of sample from Trial 3B, Coil 14 (X 20) Etchant: 2% Nital (a) Optical Microscope, X200; (b) SEM, X1000; (c) SEM, X5000

8.3.4.2. Phase Analysis

A phase analysis was performed on samples from coils 2, 4, 10 & 14 according to the description in 8.1.4.2. The phase percentages and the phase maps are shown in Figure 8-24. The samples from trial 3B possess a slightly higher % ferrite compared to that of trial 3A. The samples from trial 3A consist only of ferrite and pearlite whereas the samples from trial 3B consist only of ferrite and pearlite.

8.3.4.3. Grain size

The grain size of the samples from trial 3A and 3B were determined according to the procedure described in 8.1.4.3.The intercept data, the grain size calculation values and the average grain size is tabulated in Table 8-21. The grain sizes of the samples from trial 3A vary by 3.01 µm whereas the grain sizes of the samples from trial 3B vary by 1.25 µm.

Table 8-21: Grain size calculation data for samples from trial 2A and 2B

Sample	Intercepts per line				Average Intercepts	Line length/ Avg	d (um)
	L1	L2	L3	L4			
3A-2	75	77	53	65	67.50	2.28	11.42
3A-4	54	61	53	46	53.50	2.88	14.41
3B-10	52	50	48	53	50.75	3.04	15.19
3B-14	56	52	54	53	53.75	2.87	14.34

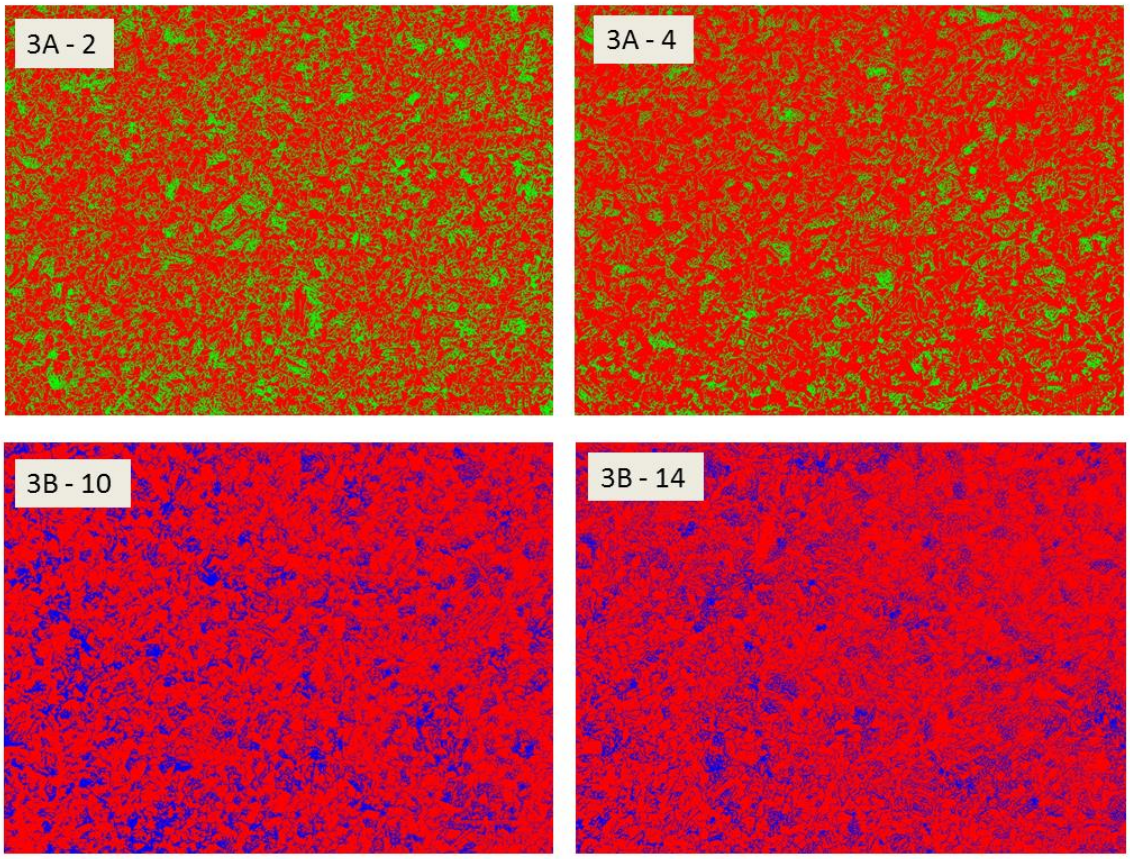

Ferrite
Bainite
Pearlite

Sample	% Ferrite	% Pearlite	% Bainite
3A-2	71.4	-	28.6
3A-4	80.05	-	19.95
3B-10	78.49	21.51	-
3B-14	80.66	19.34	-

Figure 8-24: Phase analysis of Trial 3A & 3B samples

9. DISCUSSION

9.1. Chemical Analysis

The chemical analysis of the material of all 6 trials conform to the BS 4449: 1997 460B specification. A summary of the chemical analysis of the casts used in trials 1A, 1B, 2A, 2B, 3A and 3B are presented in Table 9-1.

Table 9-1: Chemical Analysis (Mass %) Summary of Trial 1, 2 & 3

Details	%C	%Mn	%P	%S	%Si	%Cu	%Ni	%Cr	%Mo	%V	%Al	CE	Avg YS (MPa)
Original	*0.23 – 0.25*	*1.20 – 1.30*	0 - 0.04	0 - 0.05	0.4- 0.5	0- 0.25	0- 0.25	0- 0.25	0 - 0.1	0.05- 0.06	0 - 0.07	0.51 max	-
Optimized	*0.21 – 0.23*	*1.15 – 1.25*	0 - 0.04	0 - 0.05	0.4- 0.5	0- 0.25	0- 0.25	0- 0.25	0 - 0.1	0.05- 0.06	0 - 0.07	0.51 max	-
Trial 1A (Original)	0.25	1.35	0.022	0.013	0.43	0.11	0.10	0.09	0.02	0.05	0.005	0.52	614
Trial 1B (Original)	0.25	1.35	0.022	0.013	0.43	0.11	0.10	0.09	0.02	0.05	0.005	0.52	600
Trial 2A (Original)	0.25	1.36	0.015	0.012	0.44	0.11	0.06	0.05	0.01	0.051	0.006	0.50	490
Trial 2B (Original)	0.25	1.36	0.015	0.012	0.44	0.11	0.06	0.05	0.01	0.05	0.006	0.52	503
Trial 3A (Optimized)	0.24	1.23	0.014	0.012	0.44	0.10	0.05	0.06	0.02	0.05	0.005	0.48	534
Trial 3B (Optimized)	0.24	1.23	0.014	0.012	0.44	0.10	0.05	0.06	0.02	0.05	0.005	0.49	549
Average	**0.25**	**1.31**	**0.017**	**0.012**	**0.43**	**0.106**	**0.07**	**0.07**	**0.02**	**0.05**	**0.005**	**0.51**	**535.2**

Phosphorous and Sulphur Content

The P and S contents fall within the lower ranges of the aim specification. The P and S levels indicate high levels of steel cleanliness. High P and S levels are detrimental to the properties of steel and can cause embrittlement. The lower the S content the fewer sulphide inclusions will be present in the steel. This will have a positive contribution towards the integrity of the internal material structure.

Effect of % Alloy Content on Yield Strength

According to literature, the elements that influence tensile strength are C, Mn, Si, Cu, Ni, Cr and V. The effect of the abovementioned chemical elements on tensile strength is depicted in Figure 9-1.

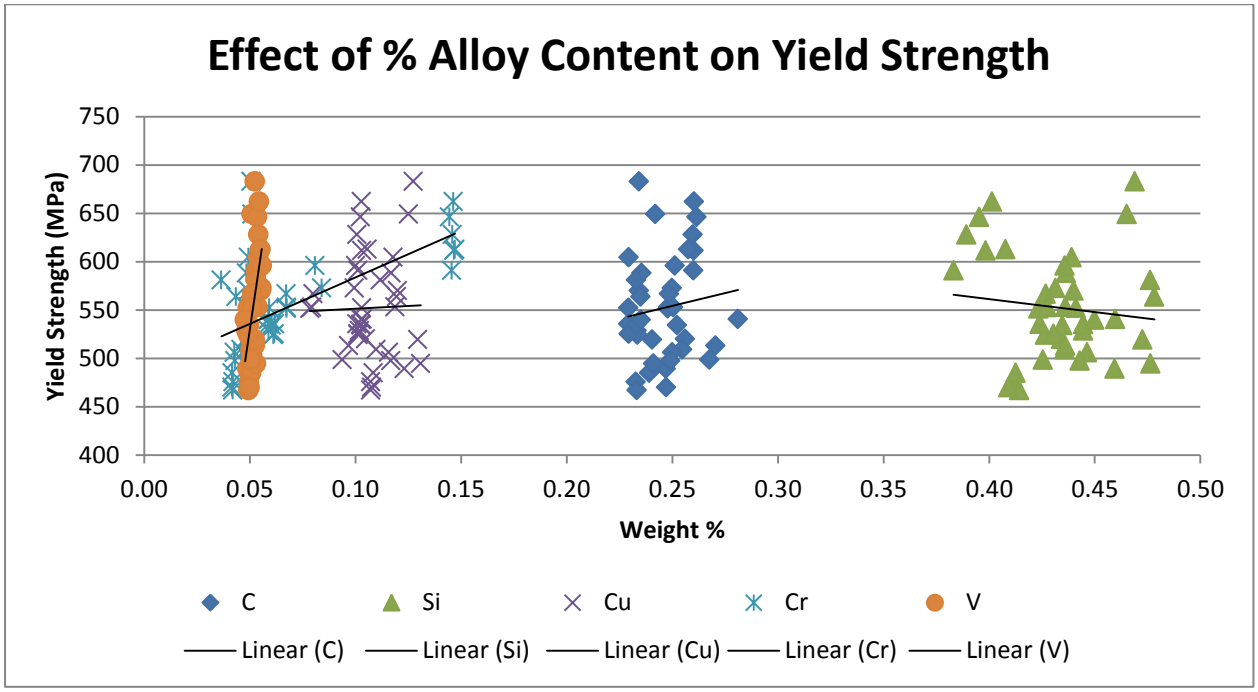

Figure 9-1: Effect of %Alloy Content on Yield Strength

Carbon

The average carbon content of the material used in all 6 trials was 0.246%. This value lies towards the upper range of the carbon aim specification for the 'original' chemical composition and exceeds that of the 'optimized' chemical composition. From the experimental data presented in Figure 9-1 it is evident that the higher the carbon content of the trial material, the higher the mechanical properties will be. This affirms Hypothesis 1 which states that decreasing the C content of the rebar will result in a yield strength below 600 MPa.

As discussed before, when the carbon content is increased the lattice becomes close packed and reduces the movement of dislocations. This causes an increase in the mechanical properties of steel. Carbon has a direct influence on the behaviour of the steel during cooling and the microstructures that are formed, according to Avner (1997).

Silicon

The average silicon content of the material used in all 6 trials is 0.43%. The experimental data presented in Figure 9-1 is very scattered and does not show a clear relationship between Si and the yield strength of steel. This data does not correspond with the findings of Totten (2007) stating that Si has an increasing effect on the hardness of steel which will in turn increase the yield strength.

Vanadium
The average vanadium content of the material used in all 6 trials is 0.05%. The experimental data presented in Figure 9-1 shows that V has an increasing effect on the yield strength of steel. This corresponds with the findings of Klinkenberg (2005) stating that V has an increasing effect on the yield strength. Davis (2001) stated that the V(C, N) precipitates strengthen the steel by the precipitation strengthening mechanism.

Copper
The average copper content of the material used in all 6 trials is 0.106%. The experimental data presented in Figure 9-1 shows that Cu has an increasing effect on the yield strength of steel. When copper is added to steel it offers strengthening via the precipitation hardening mechanism. Deeley et al (1981) established that copper does not interact with carbon therefore Cu will be dissolved or precipitated in ferrite which will induce a hardening effect on the steel.

Chromium
The average Chromium content of the material used in all 6 trials is 0.066%. It can be deduced from the experimental results that the % Cr in steel is directly proportional to the yield strength. Cr has a strong affinity for carbon and therefore has a great tendency to form chromium-carbides, which strengthen the steel further. Cr is also a nitride forming elements and has an increasing effect on the hardness of steel. (Key to Metals, 2010)

Nickel
The average Nickel content of the material used in all 6 trials is 0.071%. Nickel increases the strength of steel by the solid solution strengthening mechanism. The effect of % Ni on the yield strength of steel can be seen in Figure 9-2. The higher the Ni content, the higher the yield strength of the steel will be.

Manganese
The average manganese content of the material used in all 6 trials is 1.31%. The experimental data presented in Figure 9-3 shows that Mn has a slight increasing effect on the yield strength of steel. This affirms Hypothesis 1 which states that decreasing the Mn content of the rebar will result in a yield strength below 600 MPa. This also corresponds with the findings of Totten (2007) stating that Mn has an increasing effect on the hardness and yield strength of steel. The strengthening mechanisms that Mn participates in are solid solution strengthening, strain hardening and precipitation hardening when Mn_3C precipitates are formed.

The effect of CE on Yield Strength
Figure 9-4 depicts the effect of CE on Yield Strength of the steel samples. There is a slight correlation between CE and yield strength. As the CE increases, the yield strength of the samples increases. This affirms the theoretical prediction of the proportionality of CE to yield strength. CE is mostly dependent on % C and % Mn in steel, but other residual elements such as also play a role in the CE content as discussed in section 5.1.3.

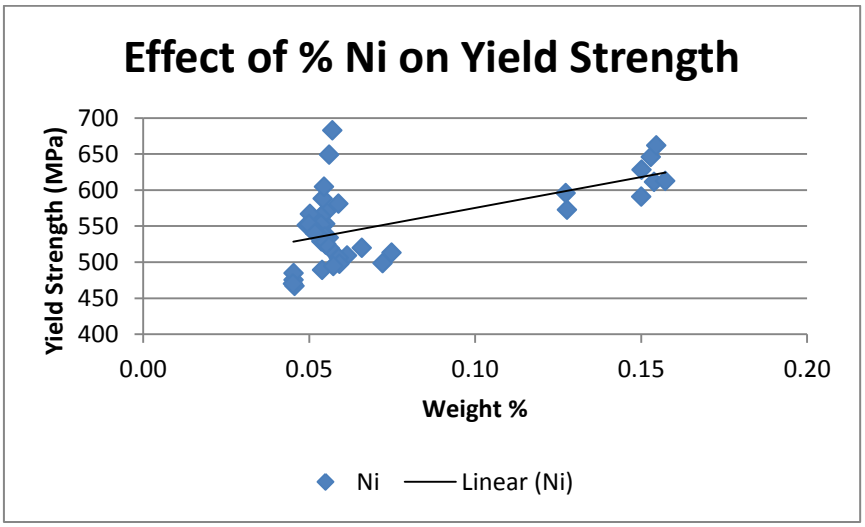

Figure 9-2: Effect of %Ni on Yield Strength

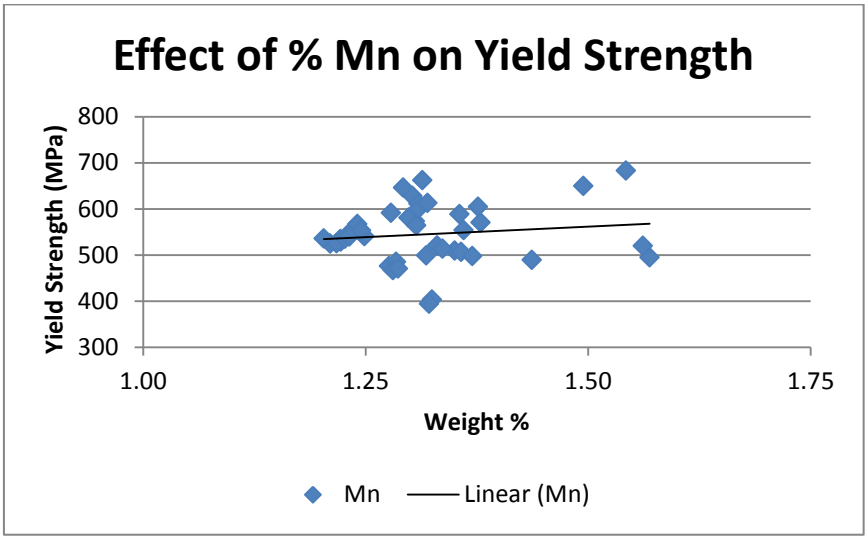

Figure 9-3: Effect of %Mn on Yield Strength

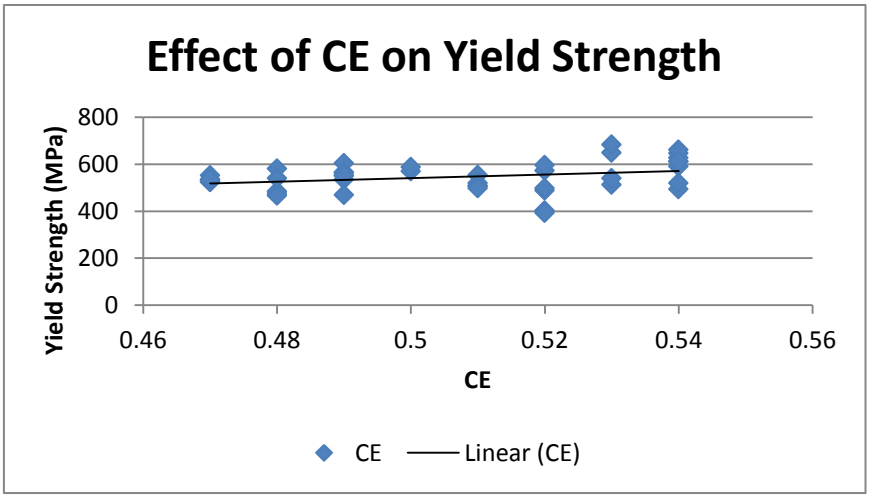

Figure 9-4: The Effect of CE on Yield Strength

9.2. Rod Mill Cooling Data

9.2.1. Effect of Water Box Temperature on Yield Strength

The effect of WB temperature on yield strength is shown in Figure 9-5. An indirectly proportional relationship exists between both WB 1 and WB 2 temperatures and yield strength. This relationship corresponds with the findings of Mekkawy et al (*1990*) stating that a decrease in the finish-rolling temperature results in an increase in the yield strength and a corresponding decrease in ductility of steel due to the formation of bainite in the microstructure.

An increase in water box temperature results in a decrease in cooling rate. It is evident from the experimental results that a decrease in cooling rate results in a decrease in yield strength. These findings affirm Hypothesis 2 which states that decreasing the cooling rate of the rebar at Rod Mill will result in a yield strength below 600 MPa.

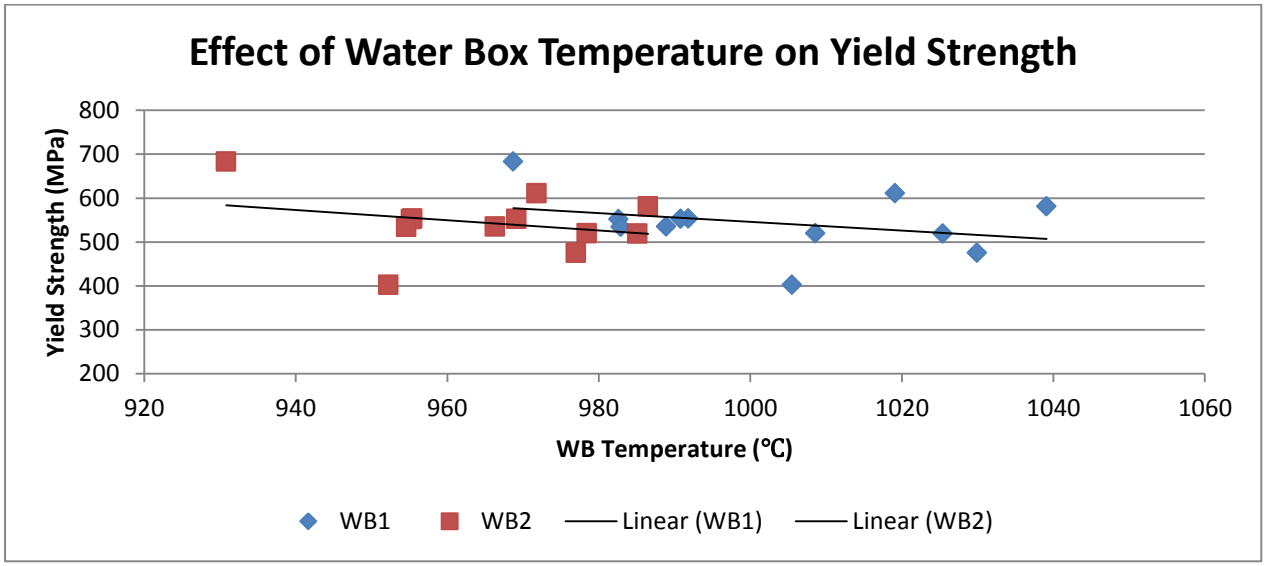

Figure 9-5: The Effect of WB temperature on Yield Strength

A summary of the Rod Mill cooling data of trials 1A, 1B, 2A, 2B, 3A and 3B are presented in Table 9-2. It can be seen that Rod Mill had difficulties obtaining WB1 temperatures within the given temperature range. During trial 2B, Rod Mill had difficulties obtaining WB2 temperatures within the given temperature range.

Table 9-2: Rod Mill Cooling Data Summary of Trial 1A, 1B, 2A, 2B, 3A and 3B

		% of coils (Trial A)				% of coils (Trial B)			
Trial	WB	Within Spec	Above Max	Below Min	AVG YS (MPa)	Within Spec	Above Max	Below Min	AVG YS (MPa)
Trial 1	WB 1	62.5	37.5	-	614	-	100	-	600
	WB 2	100	-	-		100	-	-	
Trial 2	WB 1	87.5	12.5	-	490	87.5	12.5	-	503
	WB 2	100	-	-		57.1	-	42.9	
Trial 3	WB 1	87.5	12.5	-	534	100	-	-	549
	WB 2	100	-	-		100	-	-	

Due to the small sizes of the rods used during the trial, the speed of the rods moving through the mill is very high, approximately 21 m/s. The time difference between the rod passing WB1 and WB2 is approximately 4 seconds. In the water boxes, the high temperature rod passes through water sprays, whereby it is cooled to the recommended water box temperature. The flow of water affects the temperature of the rod when it leaves the water box. Fine control of the rod temperatures proves to be a difficult task due to the high speed of the rod through the water box. Even through the temperature tolerances were exceeded during the trial, the deviation was not excessive. The slight deviations tabulated in Table 9-2 were not high enough to significantly alter the mechanical properties of the trial material.

Another factor that could have influenced the recorded temperature was the point on the bar where the reading was taken. The pyrometer is stationary, whereas the rod is in motion. This causes the temperature to be recorded from different points of the rod's surface. The rod has a deformed surface, as shown in Figure 9-6. The surface cooling of the rod is not uniform due to the irregular surface. Furthermore, the temperature distribution through the rod is not uniform. The temperature of the core is higher than the surface temperature, due to air cooling and water cooling taking place on the surface. The heat from the core then radiates outwards. The rate of heat flow from the core to the surface also depends on the thickness of the rod, which is not uniform, as can be seen from Figure 9-6.

During production, the water flow to the water boxes is altered to achieve the aim WB temperature. The water cooling is therefore not 100% consistent during the trial, but it is still controlled. This can cause material, rolled under the same conditions, to have mechanical properties that differ.

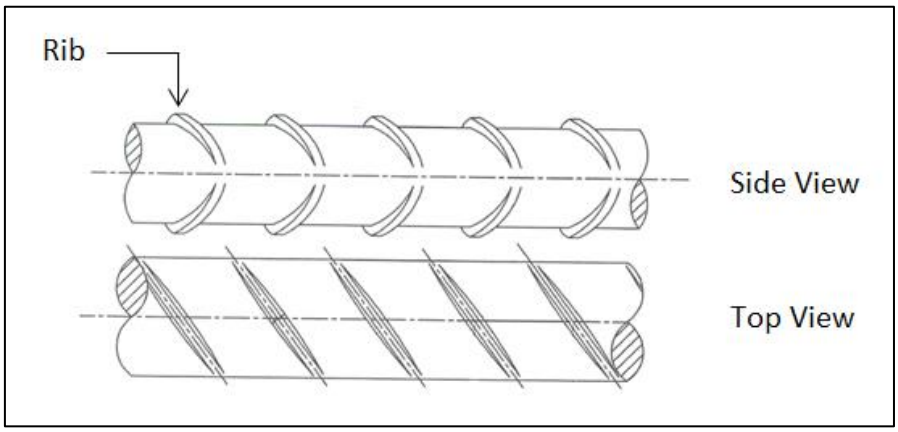

Figure 9-6: Schematic of a Deformed Reinforcing Bar (ArcelorMittal Newcastle Works)

If temperature deviation from the water box temperature tolerance is too low, with temperatures larger than 30℃, it will result in the rod being over-quenched. This results in the formation of bainite and martensite. As discussed earlier, the presence of bainite and martensite in the microstructure contributes to an increase in hardness and in turn the yield strength. The bar will have a finer austenite grain due to being over-quenched, which also contributes to higher mechanical properties.

If temperature deviation from the water box temperature tolerance is excessively high, with temperatures larger than 30℃, it will result in the rod being under-quenched. This results in the formation of ferrite and pearlite. As discussed earlier, the presence of ferrite and pearlite in the microstructure contributes to a decrease in hardness and in turn the yield strength. The bar will have a coarser austenite grain due to being under-quenched, which also contributes to lower mechanical properties.

9.2.2. Effect of Cooling Rate on Yield strength

The cooling rate for each trial could not be determined due to an insufficient number of pyrometers being present on the plant. The only temperatures that could be obtained were the WB1 and WB2 temperatures. Due to the unavailability of cooling data, the cooling rates of the trials were ranked in order of severity.

The cooling rate of the samples belonging to trial 1 and 2 were grouped together since they consist of the same chemical analysis and rod diameter. Samples from trial 3 were analyzed separately since the chemical analysis and rod diameter were different to those of the samples from trial 1 and 2. The cooling programs were ranked in descending order where the cooling program with a ranking of 1 has the highest cooling rate and the cooling program with a ranking of 4 has the lowest cooling rate. The ranking of trial cooling rates with corresponding average yield strengths are presented in Table 9-3.

Table 9-3: Ranking of Trial Cooling Rates

Trial	Rank	Cooling Program	WB1 Aim (°C)	WB2 Aim (°C)	Cooling Fans	Lids	YS (MPa)
1A	1	CP 1	970	950	100%	No	613.5
1B	2	CP 2	990	970	50%	No	600.4
2A	3	CP 3	1000	980	None	No	490.2
2B	4	CP 4	1000	980	None	Yes	474.2
3A	1	CP 1	970	950	100%	No	534.3
3B	2	CP 5	970	950	50%	No	548.5

The effect of cooling rate on yield strength for each trial can be seen in Figures 9-7 and 9-8 for trials 1 & 2 and trial 3 respectively. It is evident that the slower the cooling rate the lower the yield strength is. This applies to the data from all 3 trials. This also reinforces the Hall-Petch relationship and confirms the first aspect of Hypothesis 2 which states that decreasing the cooling rate of the rebar at Rod Mill will result in a yield strength below 600 MPa. The cooling rate influences the grain size and the microstructural constituents of the material. The effect of cooling rate on these variables will be discussed in sections 9.4.2. and 9.5.2 respectively.

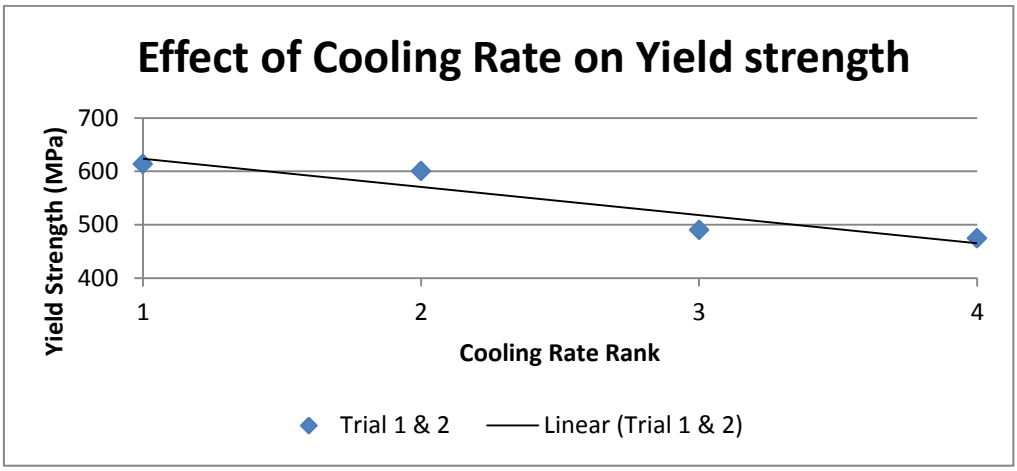

Figure 9-7: Effect of cooling Rate on Yield Strength (Trial 1 & 2)

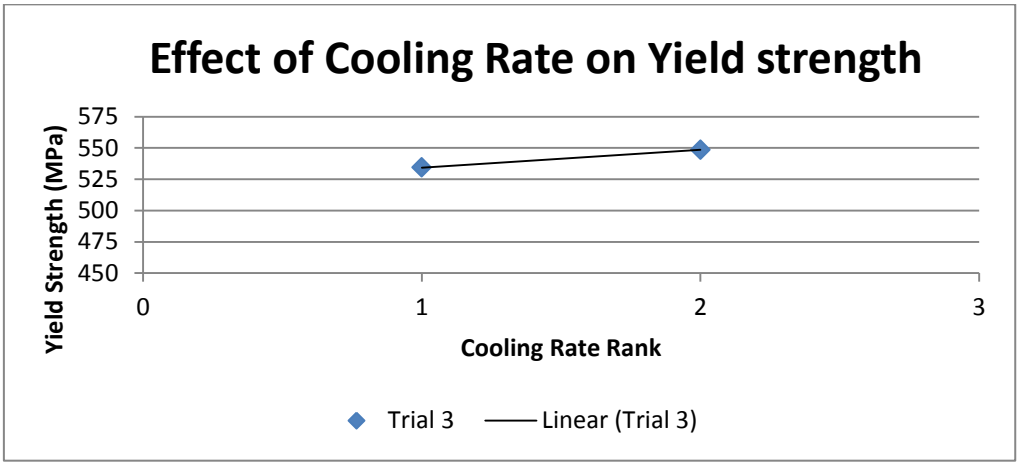

Figure 9-8: Effect of cooling Rate on Yield strength (Trial 3)

9.3. Mechanical Testing

9.3.1. Yield Strength

A summary of the Yield Strength Results of trials 1A, 1B, 2A, 2B, 3A and 3B are presented in Table 9-4. It can be seen that trial 1 had a 50% success rate, whereas trials 2 and 3 had a 100% success rate, due to all the coils achieving a yield strength below 600 MPa.

Table 9-4: Yield Strength Results Summary of Trial 1A, 1B, 2A, 2B, 3A and 3B

		% of coils	
Trial	Average YS (MPa)	< 600 MPa	> 600 MPa
Trial 1A	614	50	50
Trial 1B	600	50	50
Trial 2A	490	100	-
Trial 2B	503	100	-
Trial 3A	534	100	-
Trial 3B	549	100	-

Trial 1:
The average yield strength of trial 1A and 1B was 614 and 600 MPa respectively which does not comply with the aim of achieving a yield strength below 600MPa. The high Mn content of the material used in trial 1A and 1B could be a contributing factor to the high yield strength attained. The yield strength results obtained in trial 1B are lower than that of trial 1A due to the reduced cooling that was imposed. This consisted of an increase in the aim temperature of WB1 and WB2 and the reduction of cooling fan utilization to 50%. The increase in the water box temperatures resulted in a coarse austenite grained structure, which has lower mechanical properties than a fine grained structure. A lower cooling rate was achieved due to the reduction in cooling fan utilization, which also contributed to the lower yield strength. These results correspond to the theory regarding the effect of cooling rate on tensile properties.

Trial 2:
The average yield strength of trial 2A and 2B was 490 and 503 MPa respectively, which complies with the aim of achieving a yield strength below 600MPa. The yield strength results obtained in trial 2A are lower than that of trial 2B. The aim temperature of WB1 and WB2 was the same; however the use of cooling lids was imposed on trial 2B. The yield strength results of trial 2B should have been lower than that of trial 2A due to the use of cooling lids, but this was not the case. The utilization of cooling lids retards the cooling rate by trapping the hot air in the vicinity of the coil, reducing the temperature gradient and thereby the cooling rate. The higher yield strength of trial 2B can be attributed to the cooling that it underwent in the water boxes. The WB temperatures of trial 2A were higher than that of trial 2B. Lower water box temperatures yield higher mechanical properties, due to the fine grained structure attained.

Trial 3:
The average yield strength of trial 3A and 3B is 534 and 549 MPa respectively, which complies with the aim of achieving a yield strength below 600MPa. The yield strength of trial 3B should have been lower than that of trial 3A due to the reduced utilization of the cooling fans, however, that was not the case. A possible explanation of the higher yield strength can be attributed to slight differences that could have occurred during cooling, as explained in section 7.2.

9.3.2. Bend Test

The bend test gives an indication of the ductility of the material. A summary of the bend test results of trials 1A, 1B, 2A, 2B, 3A and 3B are presented in Table 9-5. It can be seen that all samples passed the bend test except for 25% of trial 1A. The reason for this is the high yield strength of trial 1A, 614 MPa. If the yield strength exceeds 600 MPa, the material loses its ductility and breaks during bending.

Table 9-5: Bend Test Results Summary of Trial 1A, 1B, 2A, 2B, 3A and 3B

		% of coils	
Trial	Average YS (MPa)	Pass	Fail
Trial 1A	614	75	25
Trial 1B	600	100	-
Trial 2A	490	100	-
Trial 2B	503	100	-
Trial 3A	534	100	-
Trial 3B	549	100	-

Effect of % Elongation on Yield Strength

% Elongation is a direct indication of ductility. The effect of % elongation on yield strength is depicted in Figure 9-9. It can be seen that an inversely proportional relationship exists between % elongation and yield strength. This corresponds with the Young's Modulus Equation which has an inversely proportional relationship between yield strength and strain. This also affirms Hypothesis 3 which states that the ductility of steel will increase with a decrease in yield strength.

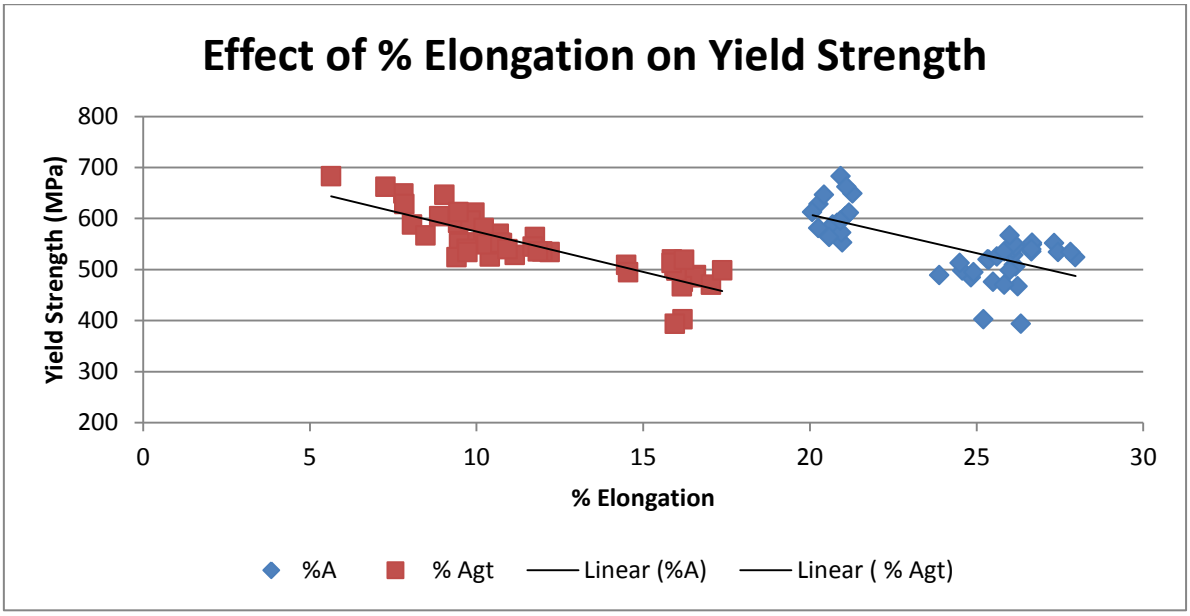

Figure 9-9: Effect of % Elongation on Yield Strength

9.4. Grain Size

9.4.1. Effect of Grain Size on Yield Strength

The effect of Grain Size on Yield Strength is shown in Figure 9-10. It can be seen that there is an indirectly proportional relationship between grain size and yield strength which corresponds to the Hall- Petch equation. The larger the grain size, the lower the yield strength will be. This is affected by the cooling rate because the lower the cooling rate, the larger the grain size will be. This will be discussed in greater detail in Section 9.4.2.

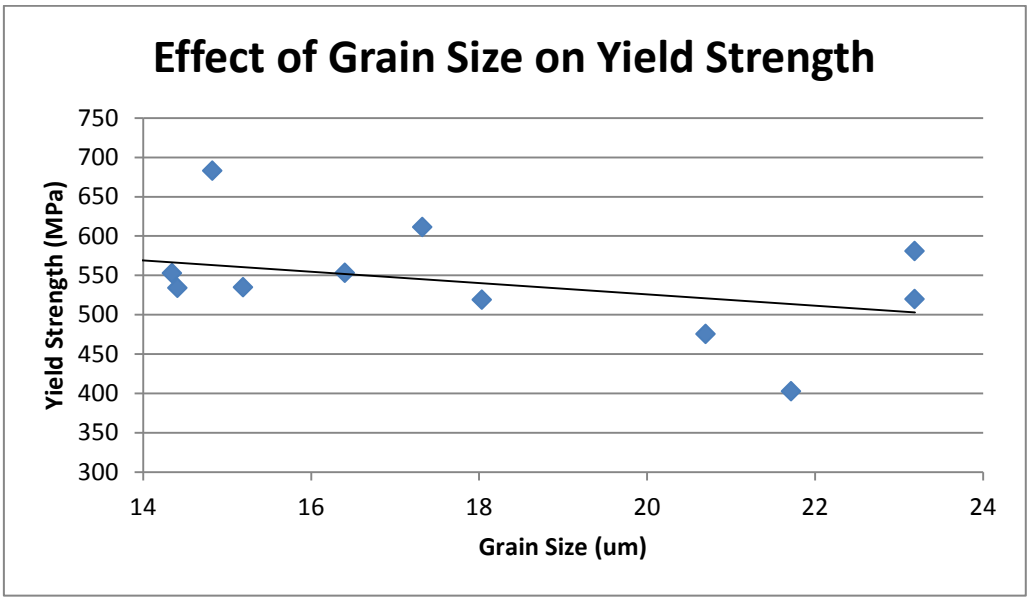

Figure 9-10: Effect of Grain Size on Yield Strength

9.4.2. Effect of Cooling Rate on Grain Size

The ranked cooling rates with corresponding average grain size and % Microstructural constituents are tabulated in Table 9-6. The ranking of cooling rates was discussed in section 9.2.2.

Table 9-6: Ranked Cooling Rates with corresponding Average Grain Size and % Microstructural Constituents

Trial	Rank	Cooling Program	Average Grain Size (µm)	% Ferrite	% Pearlite	% Bainite
1A	1	CP 1	15.62	79.23	24.46	8.545
1B	2	CP 2	20.26	88.79	12.63	4.895
2A	3	CP 3	21.94	71.98	28.03	0
2B	4	CP 4	19.88	76.39	23.62	0
3A	1	CP 1	12.92	75.73	0	24.28
3B	2	CP 5	14.77	79.58	20.43	0

The effect of cooling rate on grains size for each trial can be seen in Figures 9-11 and 9-12 for trials 1 & 2 and trial 3 respectively. It is evident from the data of all 3 trials that the slower the cooling rate the larger the grain size is. This coincides with the theory discussed in section 5.4.2. and confirms the second aspect of Hypothesis 2 which states that decreasing the cooling rate of the rebar at Rod Mill will result in a yield strength below 600 MPa due to an increase in grain size.

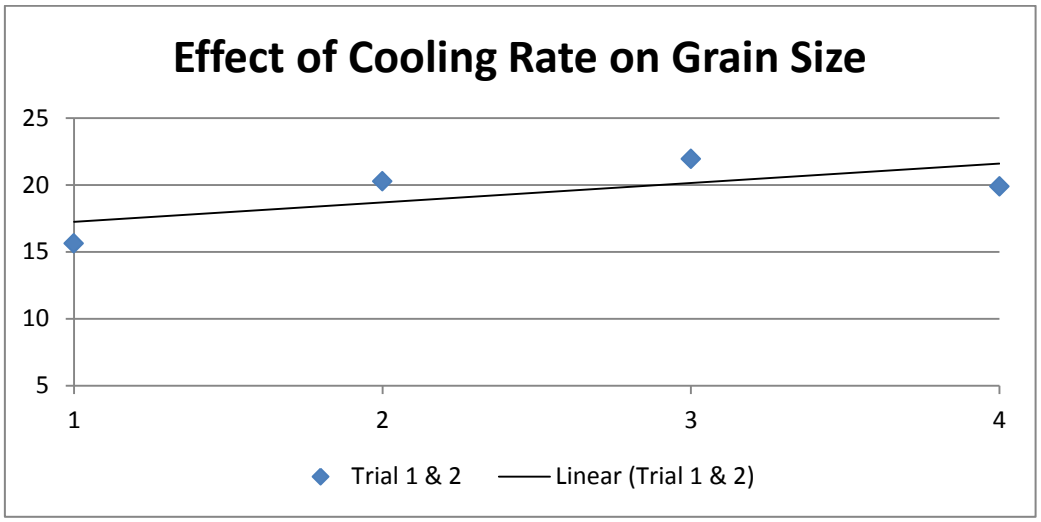

Figure 9-11: Effect of Cooling Rate on Grain Size (Trial 1 & 2)

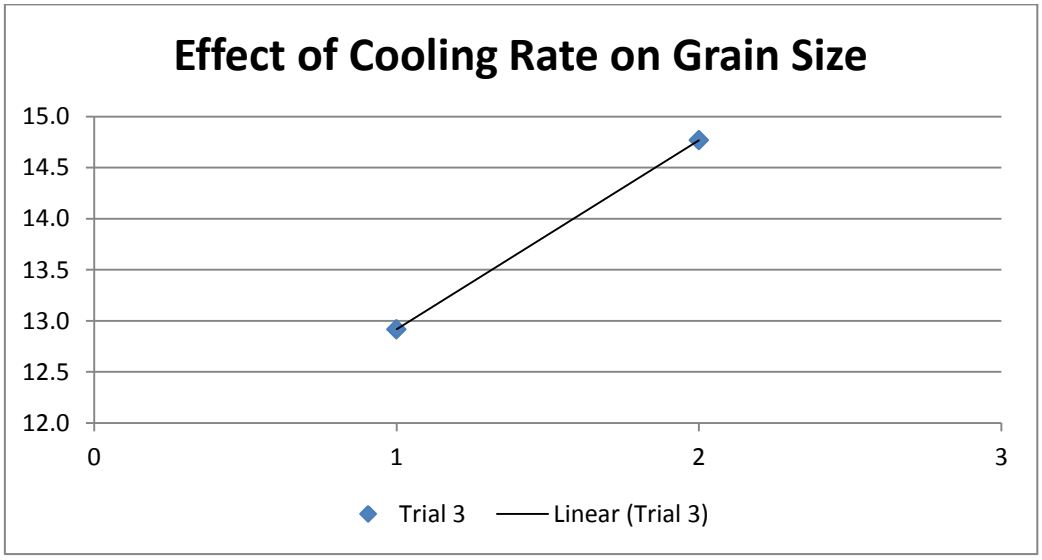

Figure 9-12: Effect of Cooling Rate on Grain Size (Trial 3)

9.5. Phase Analysis

9.5.1. Effect of Microstructural Constituents on Yield Strength

The phase analysis of the samples belonging to trial 1 and 2 were grouped together and samples from trial 3 were analyzed separately due to the reasons discussed in section 9.2.2. Ferrite serves as the matrix of the microstructure since it occupies most of the content. The effect of Microstructural Constituents on Yield Strength for trial 1 and 2 are depicted in Figure 9-13 and that of trial 3 is depicted in Figure 9-14. It can be seen that the % pearlite and % bainite in trial 1 and 2 have a directly proportional relationship to yield strength. The % bainite in trial 3 also has a directly proportional relationship to yield strength. This corresponds with the work done by Avner (1997) stating that the higher increasing amounts of pearlite or bainite will result in a higher yield strength and bainitic microstructures will have a higher tensile strength than that of pearlite microstructures. The % pearlite in trial 3 has an indirectly proportional relationship to yield strength which does not correspond with the aforementioned findings.

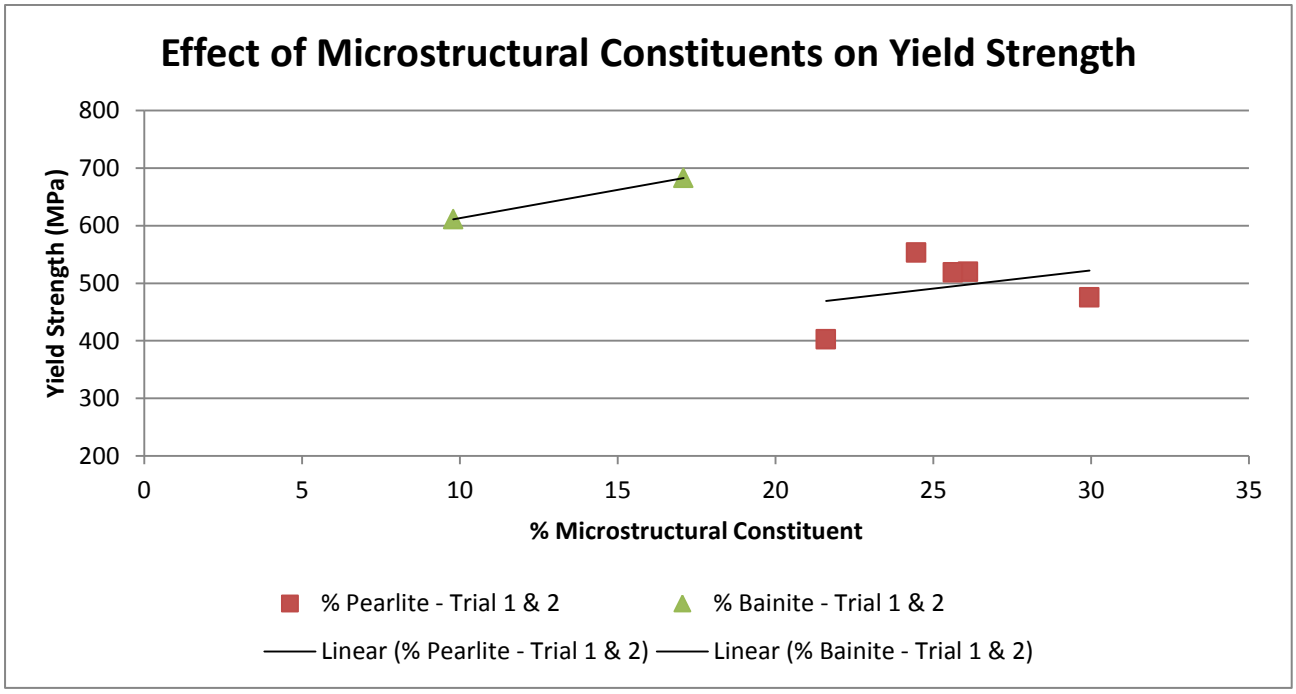

Figure 9-13: Effect of Microstructural Constituents on Yield Strength (Trial 1 & 2)

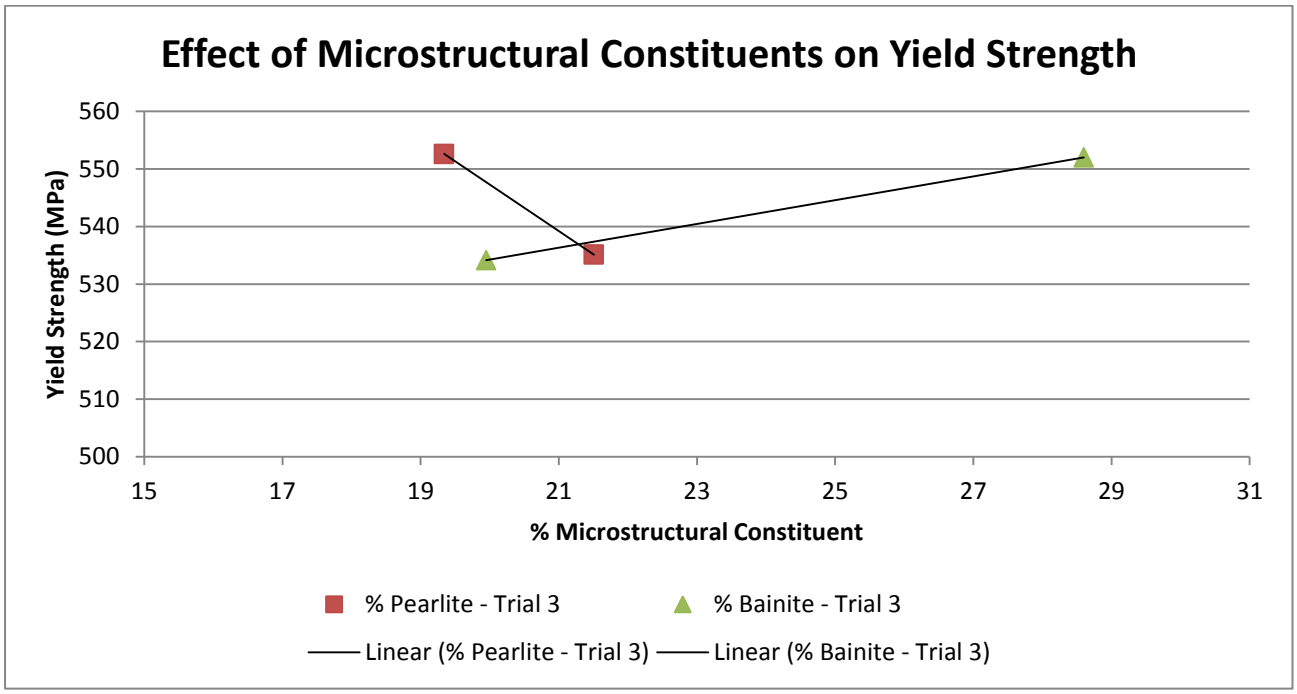

Figure 9-14: Effect of Microstructural Constituents on Yield Strength (Trial 3)

9.5.2. The Effect of Cooling Rate on the % Microstructural Constituents

The effect of cooling rate on the % Microstructural Constituents of the steel samples for each trial can be seen in Figures 9-15 and 9-16 for trials 1 & 2 and trial 3 respectively. It is evident from the data of all 3 trials that the slower the cooling rate the larger the pearlite fraction and the lower the bainite fraction. This coincides with the findings of Çalik (2009), discussed in Section 5.4.2. and confirms the final aspect of Hypothesis 2 which states that decreasing the cooling rate of the rebar at Rod Mill will result in a yield strength below 600 MPa due to a decrease in % bainite in the microstructure. This evidence also corresponds with the Isothermal Transformation Diagram of a hypo-eutectoid steel (Figure 5-16, Avner) and the summary of the effect of cooling rate on the microstructural constituents formed (Figure 5-15).

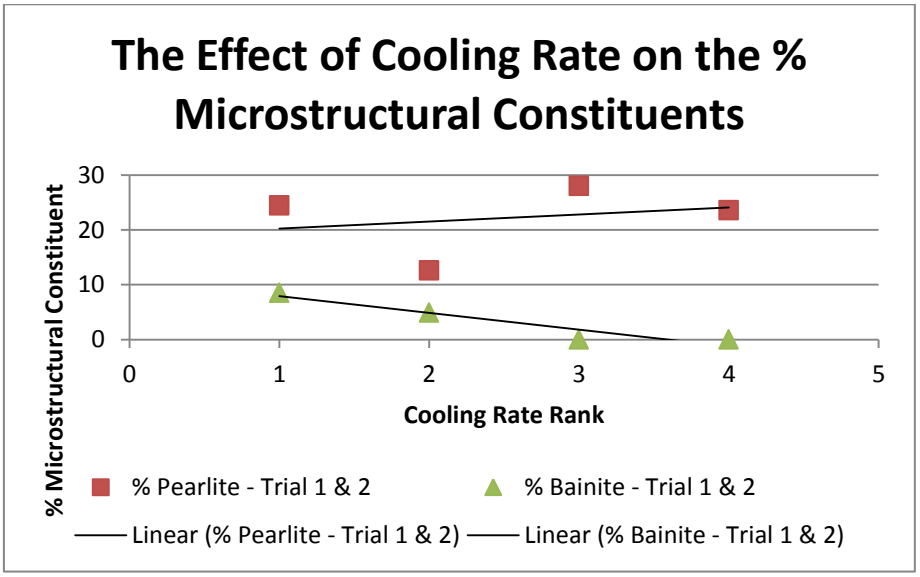

Figure 9-15: The Effect of Cooling Rate on the % Microstructural Constituents (Trial 1 & 2)

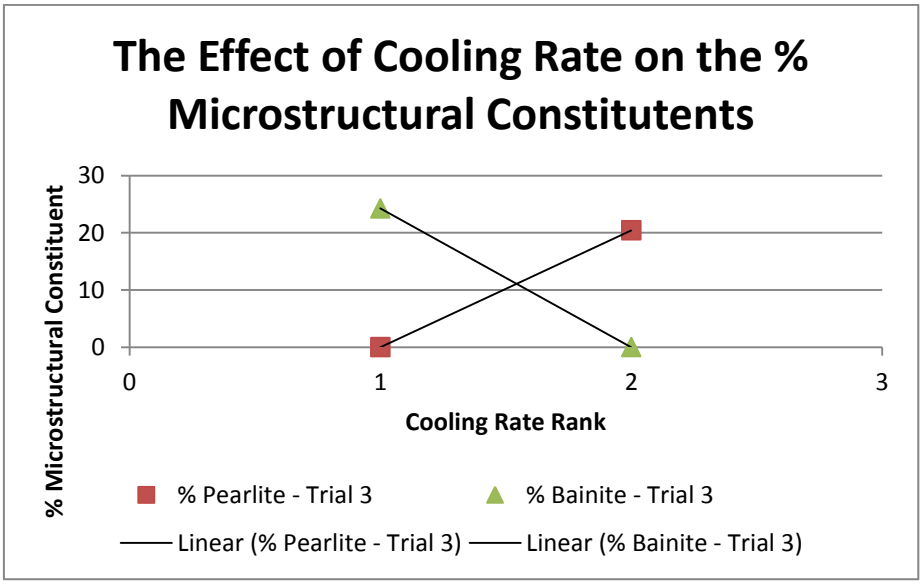

Figure 9-16: The Effect of Cooling Rate on the % Microstructural Constituents (Trial 3)

10. CONCLUSION

- The higher the C, Mn, Cu, Ni and Cr content of the steel, the higher the yield strength will be.
- The higher the carbon equivalent of the steel, the higher the yield strength will be. This is mostly due to the contributions of the abovementioned alloying elements.
- The higher the water box temperatures, the higher the yield strength will be.
- The lower the cooling rate, the lower the yield strength will be. This is closely related to grain size and the formation of microstructural constituents.
- The higher the % elongation (ductility), the lower the yield strength will be.
- The larger the grain size, the lower the yield strength will be.
- The higher the cooling rate, the smaller the grain size will be.
- The higher the % pearlite and % bainite the higher the yield strength will be.
- The higher the cooling rate, the lower the % pearlite will be.
- The higher the cooling rate, the higher the % bainite will be.
- The higher the utilization of the cooling fans, the higher the yield strength. This is due to an increased cooling rate which produces finer grains and a harder microstructure consisting of bainite and pearlite.

11. RECOMMENDATION

It is recommended that trial 3A should be implemented as the standard practice for the following reasons:

- The yield strength results of trial 3A were below 600 MPa
- All coils from trial 3A passed the bend test and are deemed as ductile material.
- The optimized chemical composition used in trial 3A has lower C and Mn contents. This results in a reduction of yield strength as well as a cost saving on alloy additions.
- 100% utilization of cooling fans should be implemented as it produced more favourable results compared to 50% utilization.

The details of trial 3A are presented in Table 11-1.

Table 11-1: Summary of Trial 3A

Chemical Composition	WB1 Temp (℃)	WB2 Temp (℃)	Cooling Fans	Lids
Optimized	970	950	100%	None

12. REFERENCES

American Society of Testing and Materials E112 (ASTM E112), (2004) *Standard Test Methods for*
Determining Average Grain Size.

Attallah M. M. (2002) Lab Session 6 - Cast Iron. The American University in Cairo
[Online] [Accessed 07-04-2014] http://members.tripod.com/mat_manf/426/lab6.htm

Avner S.H. (1997) *Introduction to Physical Metallurgy*, 2nd Edition. India: McGraw-Hill Education Pvt Limited. pp. 260 - 275

Bhadeshia, H. K. D. H. (2001) *Bainite in steels: Transformations, Microstructure and Properties*. Second Edition. IOM Communications Ltd, London

Brush Wellman Inc. (2010). Strain Hardening & Strength. Technical Tidbits. Issue 17. Brush Wellman Inc.

Buahombura, P. (2009) *High Strength Low Alloy Steel (HSLA); Ultra Low Carbon Steel; Advanced High Strength Steel*, School of Metallurgical Engineering, Suranaree University of Technology, Suranaree.

Cabibbo M, Fabrizi A, Merlin M, Garagnani GL. (2008) *Effect of Thermo-Mechanical Treatments on the Microstructure of Micro-Alloyed Low-Carbon Steels*. Journal of Materials Science, Volume 43, Issue 21, pp. 6857-6865

Callister, W.D. Jr. (2003) *Materials Science and Engineering an Introduction,* 6th Edition. John Wiley & Sons, Inc. p 332

Çalik A, (2009). *Effect of cooling rate on hardness and microstructure of AISI 1020, AISI 1040 and AISI 1060 Steels.* International Journal of Physical Sciences Volume 4, pp. 514-518.

Chen S. Y., Xu J, Zhang X, Yang Y. T. (2013). *The Effect of Finish Rolling Temperature on Microstructure and Mechanical Properties of Vanadium Containing Ferritic Stainless Steel.* Advanced Materials Research (Volumes 690 - 693). pp. 176-181. Trans tech Publications, Switzerland.

Cline RS, Heitmann WE, Bhattacharya D (1986) *Micro-alloyed Steel Bars and Forgings.* JOM, Volume 38, Issue 5, pp. 26- 30. Springer-Verlag

Das S, Ghosh A, Chatterjee S, Rao PR (2003) *The Effect of Cooling Rate on Structure and Properties of a HSLA Forging.* Scripta materialia, Elsevier

Davenport E. S., Bain E. (1961) *Trans*, AIME, Volume 209, p 684

Davis J.R. (2001) *Alloying: Understanding the Basics.* USA: ASM International, pp. 193 – 202

Deeley P. D., Kundig K. J. A., Spendelow H. R. (1981) *Ferroalloys & Alloying Additives Handbook*.
Shieldalloy Corp., - Technology & Engineering

Dieter G.E. (1988). *Mechanical Metallurgy*. Mc Graw Hill. pp. 301-303

Effect of Temperature on Tensile Properties. (2012) Engineering Archives. [Online] [Accessed 07-04-2014]
http://www.engineeringarchives.com/les_mom_effectoftemperatureontensileproperties.html

EVRAZ East Metals (2013) *High Strengths at low Costs with Nitrovan ® Vanadium*

Gensamer M., Pearsall E.B., Pellini W. S., Low Jr J. R., (1942) *The Mechanical Properties of the Isothermal Decomposition Products of Austenite*. Transactions of the American Society for Metals, Vol. 30, Dec 1942, pp. 983–1020

Ghosh A, Chatterjee A (2008) *Iron Making and Steelmaking: Theory and Practice.* New Delhi, India: PHI Learning Pvt. Ltd. pp. 264 - 305

Hall EO (1951) *The Deformation and Ageing of Mild Steel: III Discussion Of Results*, Proceedings of the Physical Society. Section B, Vol. 64, pp. 747-753 - iopscience.iop.org

Held JF, Lauer BA (1983), *Development of Micro-alloyed Medium Carbon Hot Rolled Bar Products.* vanitec.org

Jones J. A. T. (2013). *Electric Arc Furnace Steelmaking.* American Iron and Steel Institute. [Online] [Accessed 13-12-2013]
http://www.steel.org/en/Making%20Steel/How%20Its%20Made/Processes/Processes%20Info/Electric%20Arc%20Furnace%20Steelmaking.aspx

Key to Metals (1999-2010). *Constant temperature transformation TTT curves.* Key to Metals [Online] [Accessed 07-04-2014] http://www.keytometals.com/Articles/Art17.htm

Key to Metals (1999-2010). *Influence of Alloying Elements on Steel Microstructure.* Key to Metals. [Online] [Accessed 09-04-2014] http://www.keytometals.com/Articles/Art50.htm

Klinkenberg C. (2005). *Niobium in Micro-alloyed Structural & Engineering Steel*. , Iron & Steel, Vol 40 (S)

Korchynsky M (2001) *A New Role for Micro-alloyed Steels – Adding Economic Value*. Proceedings of Vanitec International Symposium - vanitec.org

Mekkawy M. F. El-fawakhry K. A., Mishreky M. L. and Eissa M. M. (1990) *Effect of finishing rolling temperature on microstructure and strength of V- and Ti- Micro-alloyed steels.* Egypt. Scandinavian Journal of Metallurgy

Niwa, S., Machida, I., Kato, T., Nychara N., Tanaka Y. (1981) *Research and Development of Micro-alloyed Medium Carbon Steels.* SAE Technical Paper 810426

Panigrahi BK , Srikanth S, Sahoo G (2009) *Effect of Alloying Elements on Tensile Properties, Microstructure, and Corrosion Resistance of Reinforcing Bar Steel.* Journal Of Materials Engineering and Performance, Volume 18, Issue 8, pp. 1102-1108. Springer- US

Parker SP (2003), *McGraw-Hill Dictionary of Scientific & Technical Terms*, 6th Edition, The McGraw-Hill Companies, Inc.

Paules J. R. (1991) *Developments in HSLA steel products.* JOM, Volume 43, Issue 1, pp. 41 - 44. Springer-Verlag

Petch N. J. (1953) *The Cleavage Strength of Polycrystals*, J. Iron Steel Inst., 174, pp. 25-28.

Petch N. J. (1959) *Fracture*. John Wiley & Sons, New York p. 54.

Petch N. J. (1986) *The influence of grain boundary carbide and grain size on the cleavage strength and impact transition temperature of steel.* Acta Metallurgica, Elsevier.

Pollack H. (1988) *Materials Science and Metallurgy*. 4th edition, Prentice-Hall

Reed-Hill R. E. (1973). *Physical Metallurgy Principles*. Second Edition. Van Nostrand-Technology & Engineering. Pp. 661-695

Resilience. (2014) Wikipedia [Online] [Accessed 07-04-2014] http://en.wikipedia.org/wiki/Resilience

Roberts W. L. (1983). *Hot Rolling of Steel.* CRC Press, Technology & Engineering

Rollason, E. C. (1961) Metallurgy for Engineers. Third Edition. Edward Arnold (Publishers) Ltd, London. Pp. 179 – 183.

Shah K. P. (2009) *The Hand Book on Mechanical Maintenance.* Published online: http://practicalmaintenance.net/?p=1567

Shanmugam S, Ramisetti NK, Misra RDK (2007). *Effect of Cooling Rate on the Microstructure and Mechanical Properties of Nb-Micro-alloyed Steels.* Materials Science and Engineering Volumes 460–461, pp. 335–343- Elsevier

Siemens *AG* (2010). *Solutions for Long Product Rolling Mills*. Germany: Siemens *AG*

Silvestre L, Pimenta R, Nogueira M, Queiroz L, Salles H, Jordão A, Ribeiro R, Pimenta M, Conceição J, Rocha L, Buratto F, Fonsec E (2012*). High Strength Steel as a Solution for the Lean Design of Industrial Buildings.* Brazil: Elsevier Editora Ltda

Stress-Strain Diagrams (1995-2014). Pennsylvania State University, Department of Engineering Science and Mechanics

Stuart H (1991) *The Properties and Processing of Micro-alloyed HSLA Steels.* JOM, Volume 43, Issue 1, pp. 35-40. Springer-Verlag

Thompson J. (2013) *Effects Of Low Temperature on Performance of Steel & Equipment*. [Online] [Accessed 08-04-2014] http://www.spartaengineering.com/effects-of-low-temperature-on-performance-of-steel-equipment/

Totten, G. (2007) Steel Heat Treatment: Metallurgy and Technologies. CRC Press, Boca Raton, FL, p.191.

TPP Information Centre (2006). *Yield Strength and Heat Treatment.* [Online] [Accessed 07-04-2014] http://www.tppinfo.com/defect_analysis/yield_strength.html

Yan C, Zhen-yi H, Ping W, Gui-quan Y, Xiang-hua L, Guo-dong W (1963) *Effect of Rolling Process on the Microstructure and Mechanical Properties of Low Carbon V-N Steel*. metal.citic.com

Young Kook Lee, Jin-Myung Hong, Chong Sool Choi, Jae Kon Lee (2005). *Continuous Cooling Transformation Temperatures and Microstructures of Niobium Bearing Micro-alloyed Steels.* Switzerland: Trans Tech Publications

Yun-Chul Jung, Sung-Joon Kim, Yasuya Ohmori. (1998) *The Morphology and growth process of bainitic ferrite in steels*. Metals and Materials, Volume 4, Issue 2, pp. 125-134

13. APPENDIX A: Optical Microscope Images

Trial 1

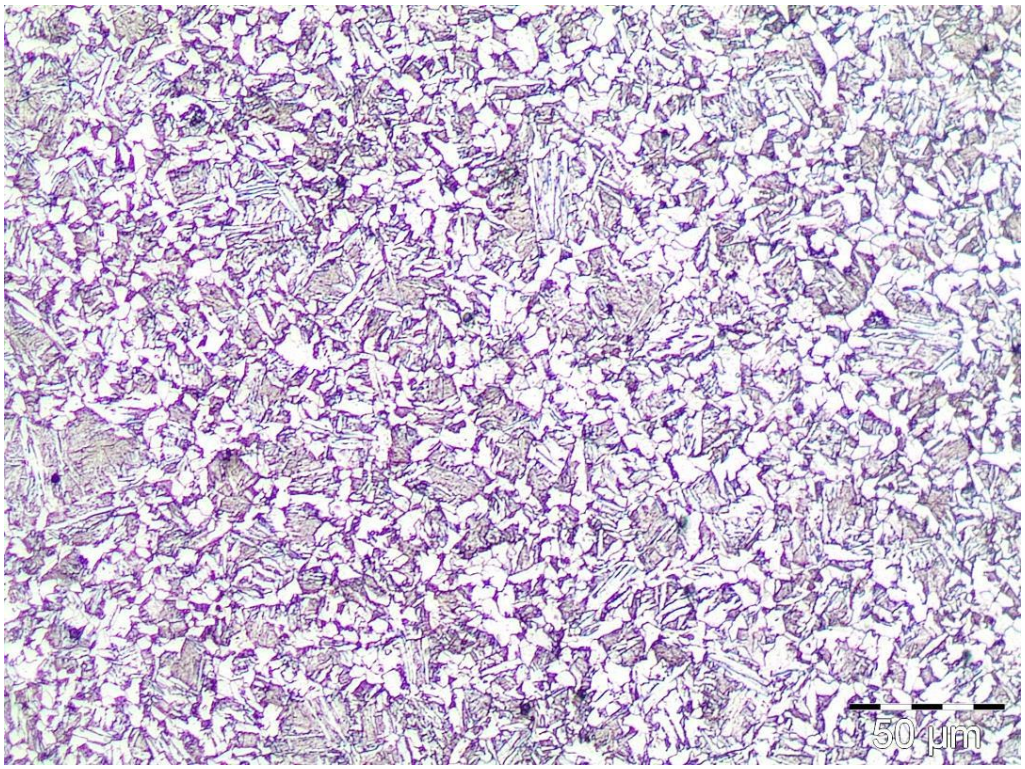

Figure 13-1: Cross-sectional area of sample from Trial 1A, Coil 2 (X 20) Etchant: 2% Nital

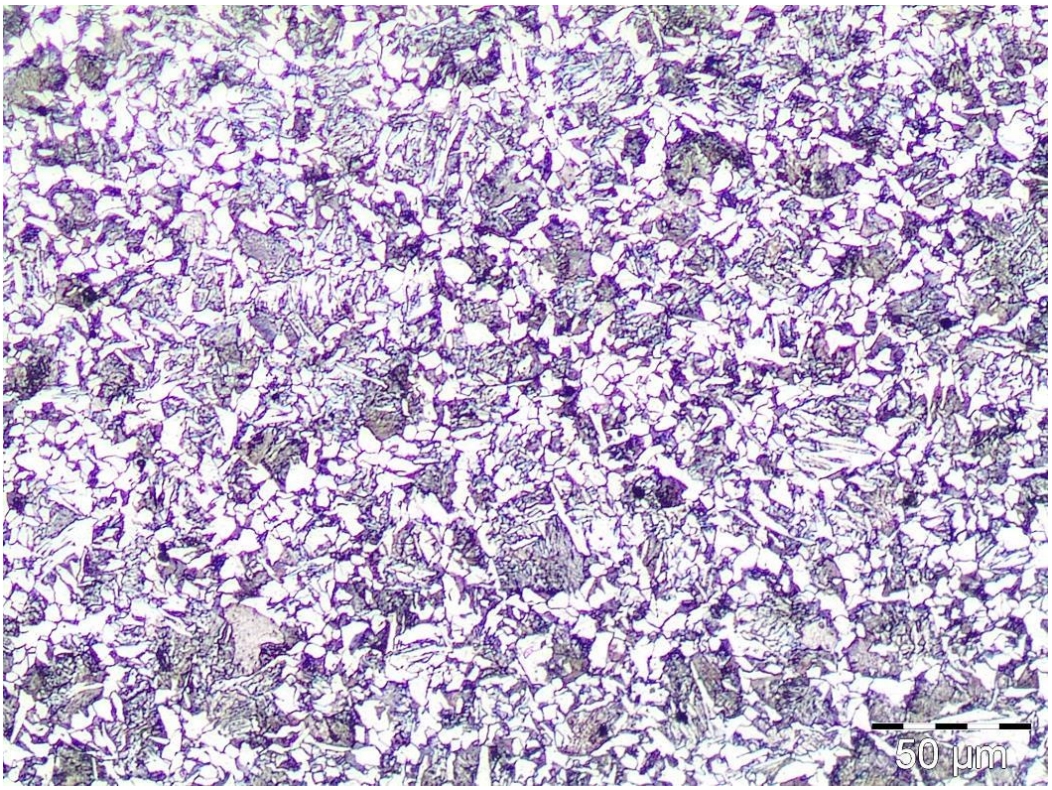

Figure 13-2: Cross-sectional area of sample from Trial 1A, Coil 4 (X 20) Etchant: 2% Nital

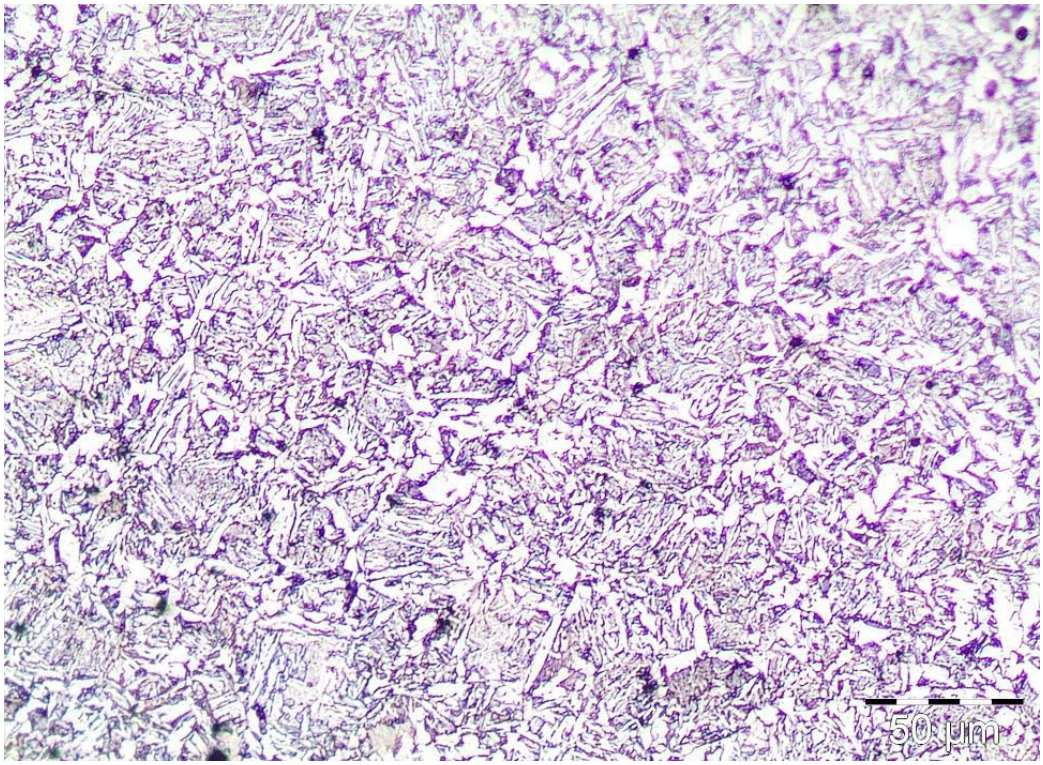

Figure 13-3: Cross-sectional area of sample from Trial 1B, Coil 10 (X 20) Etchant: 2% Nital

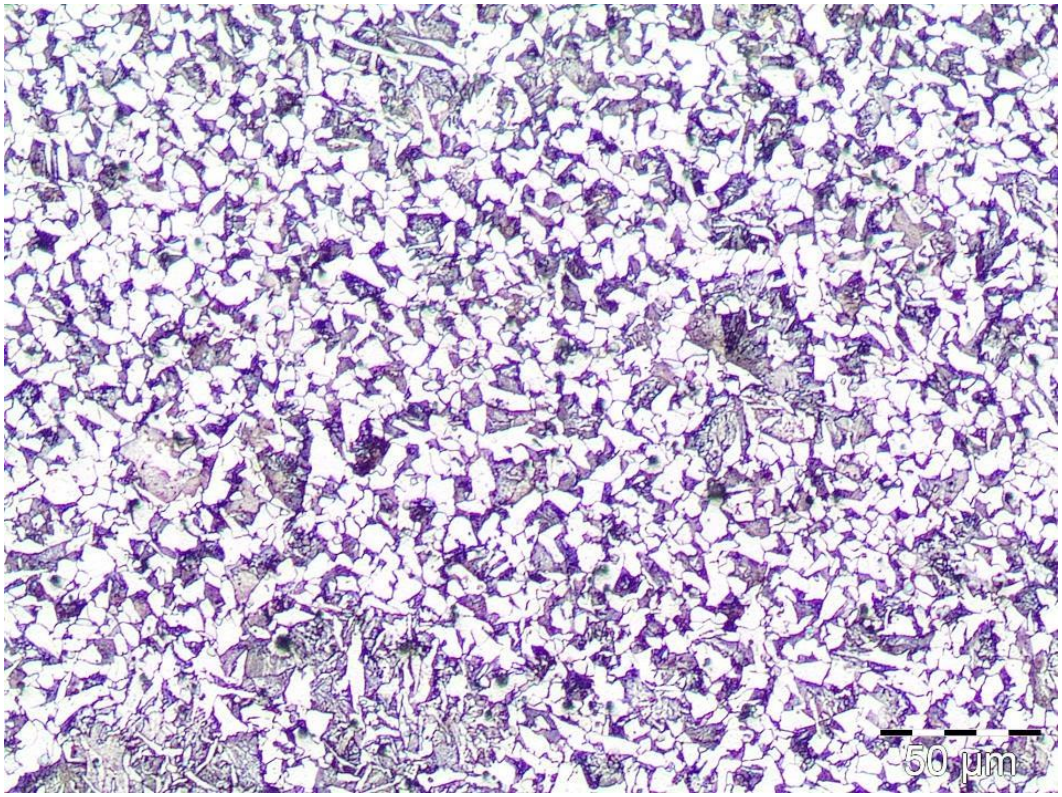

Figure 13-4: Cross-sectional area of sample from Trial 1B, Coil 14 (X 20) Etchant: 2% Nital

Trial 2

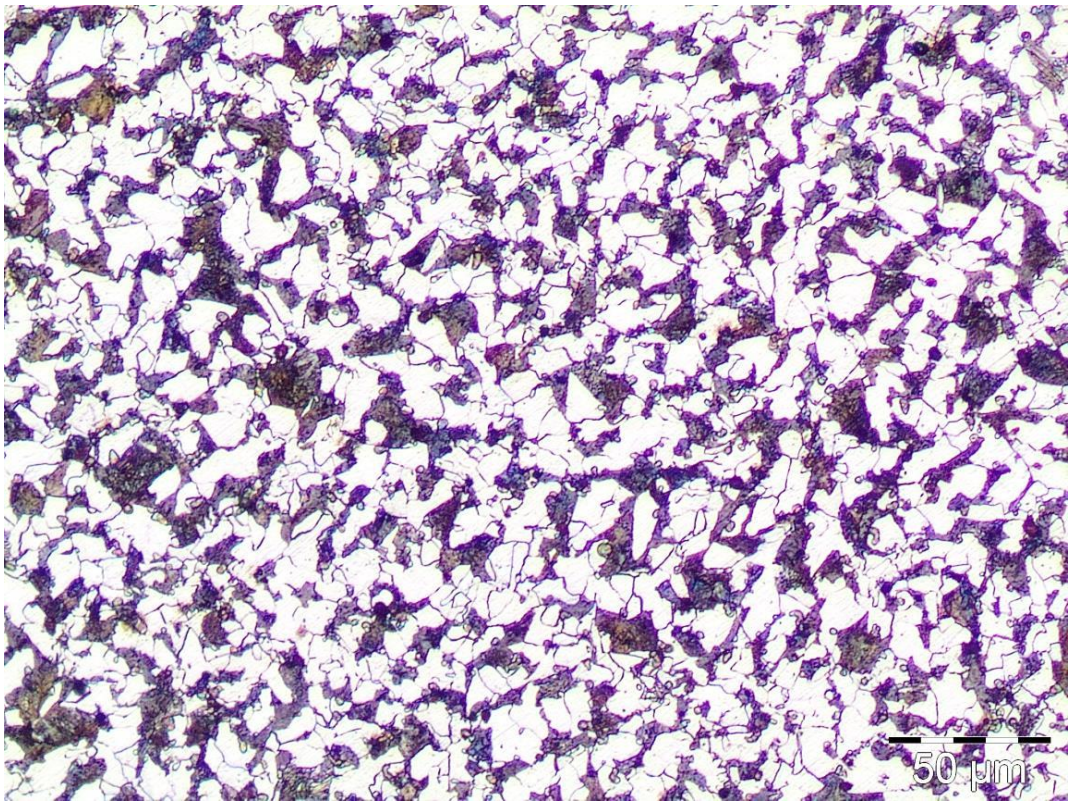

Figure 13-5: Cross-sectional area of sample from Trial 2A, Coil 2 (X 20) Etchant: 2% Nital

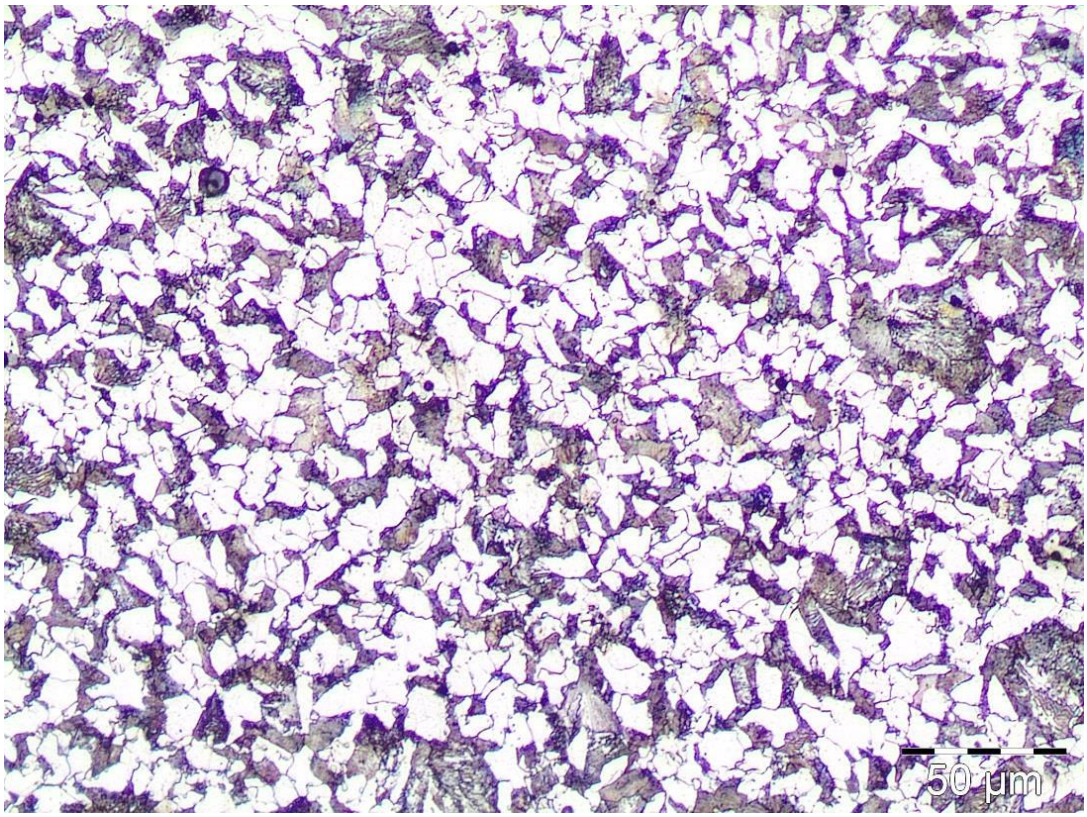

Figure 13-6: Cross-sectional area of sample from Trial 2A, Coil 4 (X 20) Etchant: 2% Nital

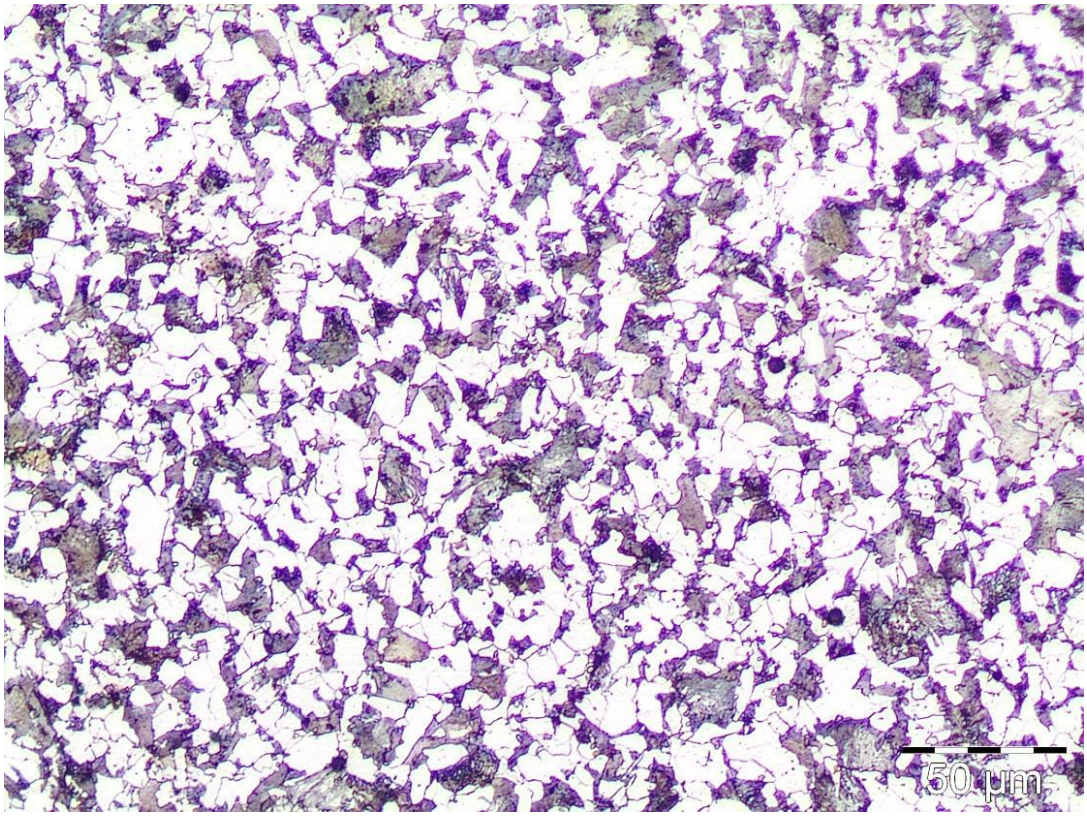

Figure 13-7: Cross-sectional area of sample from Trial 2B, Coil 10 (X 20) Etchant: 2% Nital

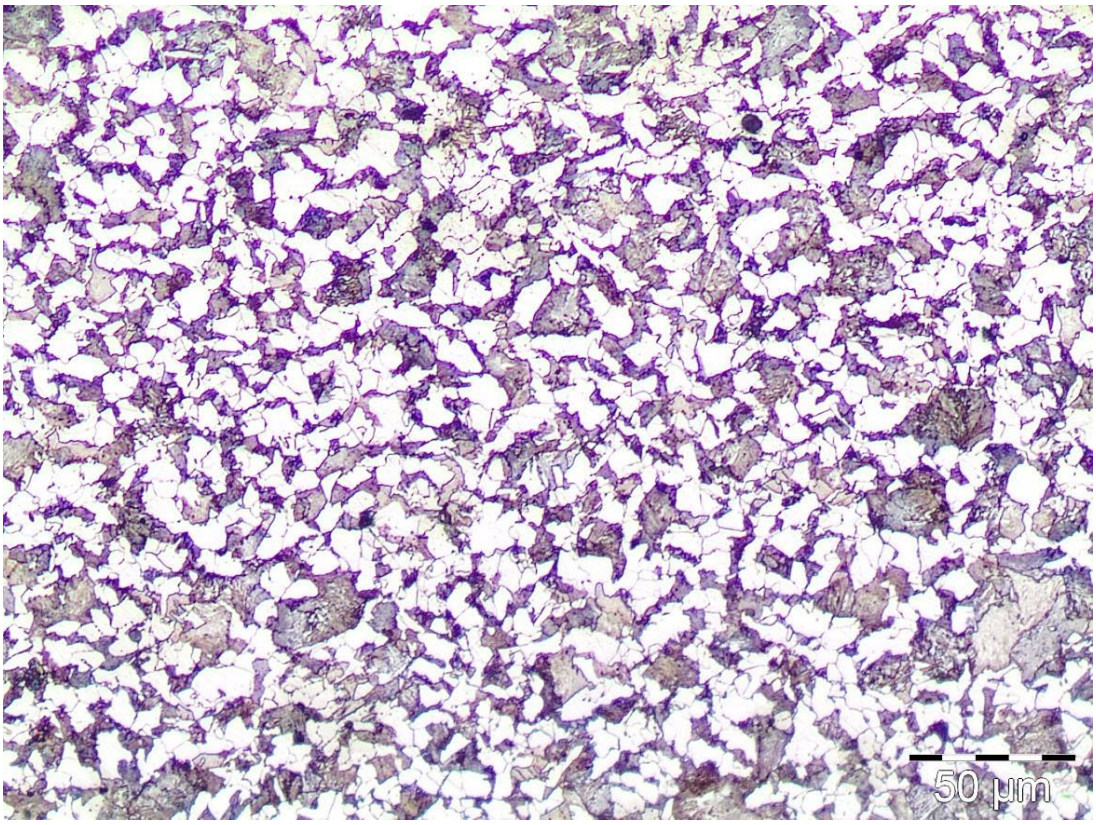

Figure 13-8: Cross-sectional area of sample from Trial 2B, Coil 14 (X 20) Etchant: 2% Nital

Trial 3

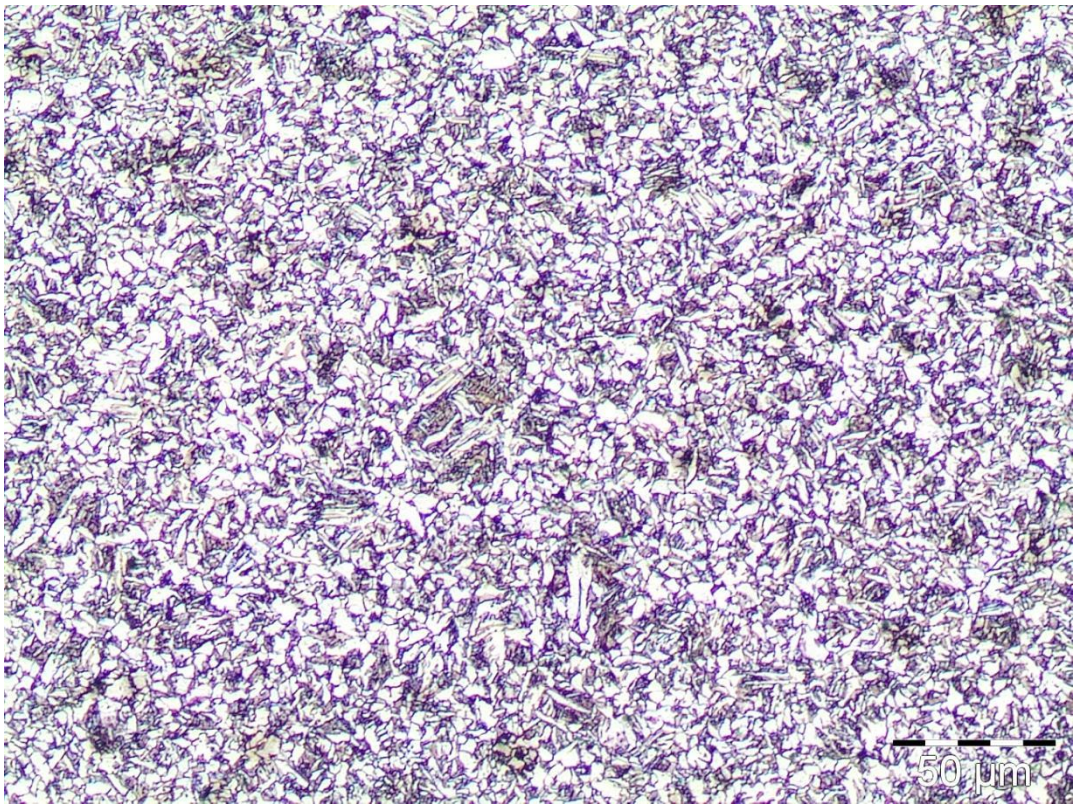

Figure 13-9: Cross-sectional area of sample from Trial 3A, Coil 2 (X 20) Etchant: 2% Nital

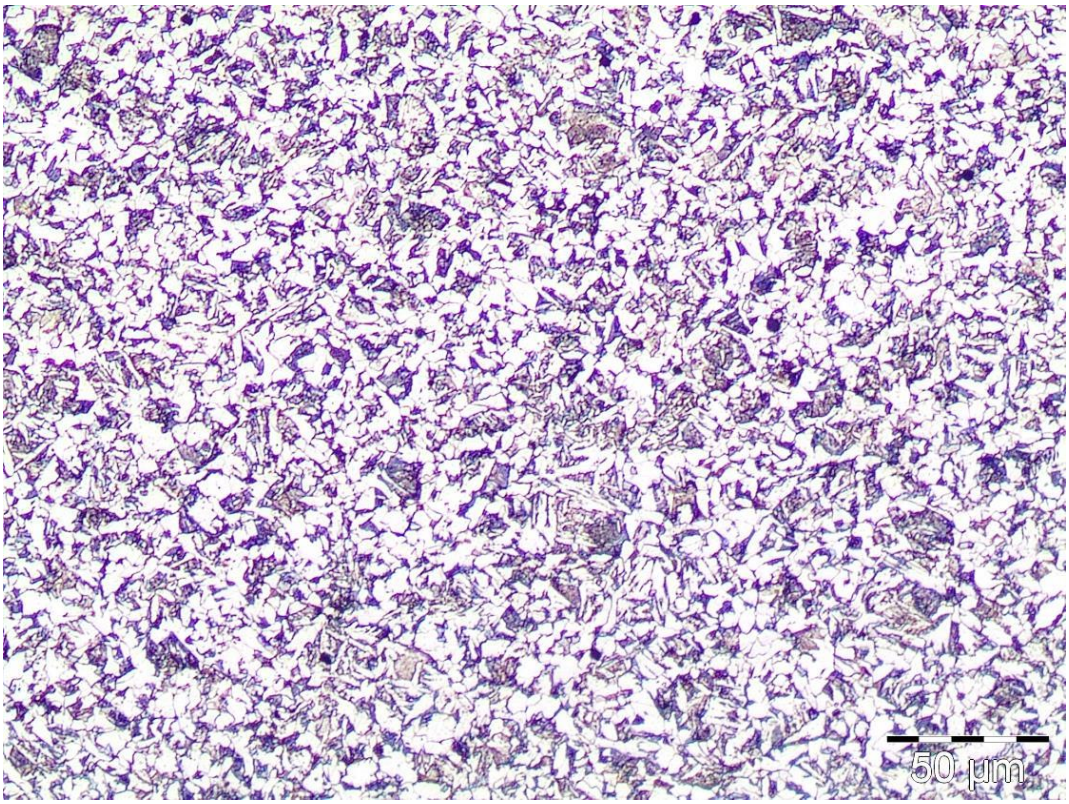

Figure 13-10: Cross-sectional area of sample from Trial 3A, Coil 4 (X 20) Etchant: 2% Nital

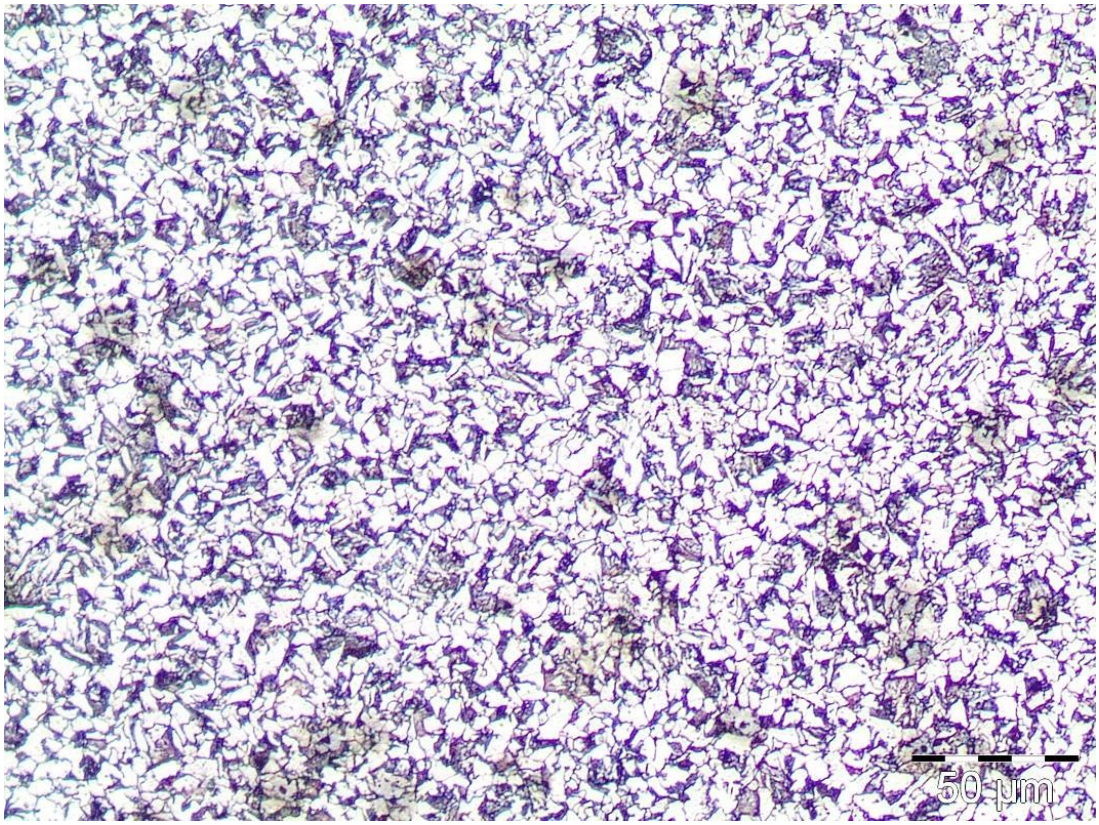

Figure 13-11: Cross-sectional area of sample from Trial 3B, Coil 10 (X 20) Etchant: 2% Nital

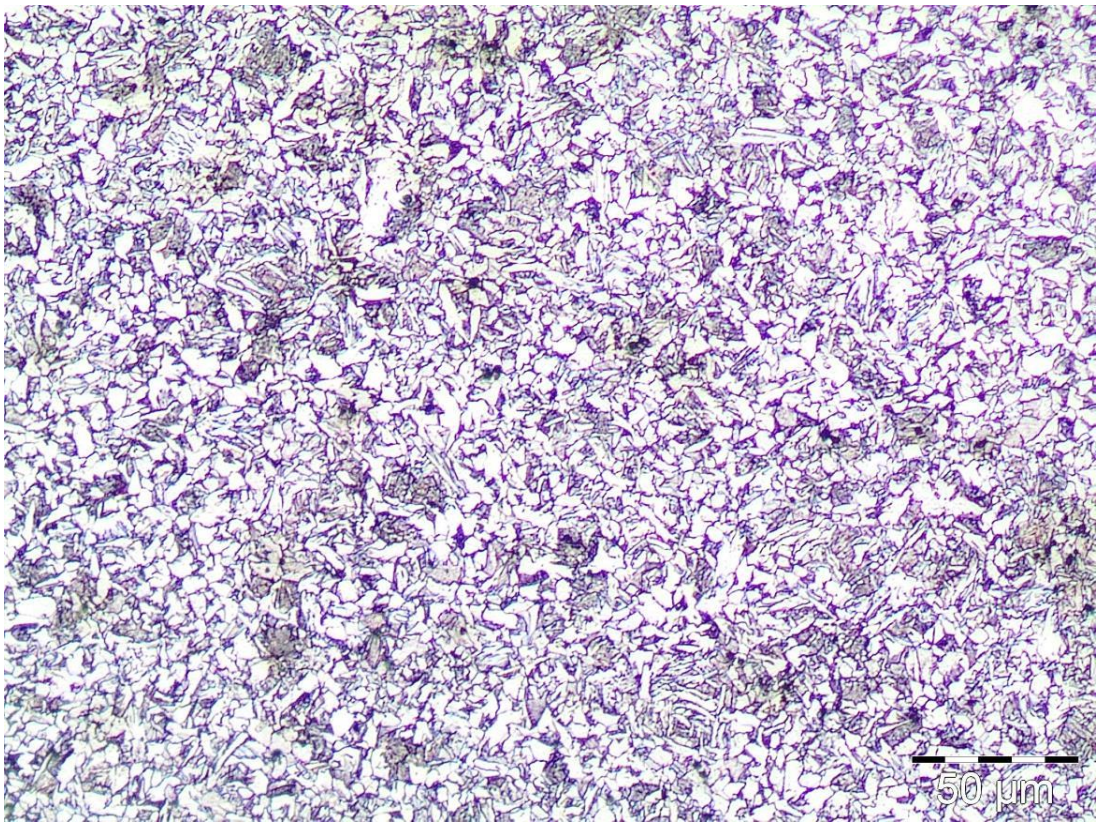

Figure 13-12: Cross-sectional area of sample from Trial 3B, Coil 14 (X 20) Etchant: 2% Nital